

University of Groningen

Modeling and control of power systems in microgrids

Monshizadeh Naini, Pooya

IMPORTANT NOTE: You are advised to consult the publisher's version (publisher's PDF) if you wish to cite from it. Please check the document version below.

Document Version

Publisher's PDF, also known as Version of record

Publication date:

2018

[Link to publication in University of Groningen/UMCG research database](#)

Citation for published version (APA):

Monshizadeh Naini, P. (2018). *Modeling and control of power systems in microgrids*. University of Groningen.

Copyright

Other than for strictly personal use, it is not permitted to download or to forward/distribute the text or part of it without the consent of the author(s) and/or copyright holder(s), unless the work is under an open content license (like Creative Commons).

The publication may also be distributed here under the terms of Article 25fa of the Dutch Copyright Act, indicated by the "Taverne" license. More information can be found on the University of Groningen website: <https://www.rug.nl/library/open-access/self-archiving-pure/taverne-amendment>.

Take-down policy

If you believe that this document breaches copyright please contact us providing details, and we will remove access to the work immediately and investigate your claim.

Downloaded from the University of Groningen/UMCG research database (Pure): <http://www.rug.nl/research/portal>. For technical reasons the number of authors shown on this cover page is limited to 10 maximum.

Modeling and Control of Power Systems in Microgrids

Pooya Monshizadeh



**university of
groningen**

The research described in this dissertation was undertaken at the Johann Bernoulli Institute for Mathematics and Computer Science, University of Groningen, The Netherlands.



connecting innovators

This work was supported by the STW Perspective program “Robust Design of Cyber-physical Systems” under the auspices of the project “Energy Autonomous Smart Microgrids”.

disc dutch institute
of systems
and control

The research reported in this dissertation is part of the research program of the Dutch Institute of Systems and Control (DISC). The author has successfully completed the educational program of the Graduate School DISC.



university of
 groningen

Modeling and Control of Power Systems in Microgrids

PhD Thesis

to obtain the degree of PhD at the
University of Groningen
on the authority of the
Rector Magnificus Prof. E. Sterken
and in accordance with
the decision by the College of Deans.

This thesis will be defended in public on

Tuesday 25 September 2018 at 11:00

by

Pooya Monshizadeh Naini

born on 12 April 1985
in Noshahr, Iran

Supervisors

Prof. A. van der Schaft

Prof. C. De Persis

Assessment Committee

Prof. J. Raisch

Prof. J.M.A. Scherpen

Prof. G. Weiss

ISBN: 978-94-034-0918-4

to my parents,
Ana and Javad

Contents

1	Introduction	1
1.1	Overview and contributions of the thesis	2
1.1.1	Distribution lines	2
1.1.2	Network architecture	3
1.1.3	Modeling synchronous generators	3
1.1.4	Inverters and the problem of low inertia	4
1.1.5	Port-Hamiltonian framework and its applications in power systems	5
1.2	Outline of the thesis	6
1.3	Origins of the chapters	7
1.4	Notation	7
1.5	List of abbreviations	8
2	Preliminaries	9
2.1	Graph Theory	9
2.2	Port-Hamiltonian Systems	11
2.3	Passivity and Shifted Passivity	12
2.4	Stability of Nonlinear Systems	14
3	Power Network Characteristics	19
3.1	Introduction	19
3.2	Measure Definition	21
3.3	Calculating the Network Inductivity/Resistivity Measure ($\Psi_{\text{NIR}}/\Psi_{\text{NRR}}$)	24
3.3.1	Uniform Output Impedances	24
3.3.2	Non-uniform Output Impedances	30
3.4	Kron Reduction in Phasor Domain and the Network Inductivity Ratio	35

3.5	Conclusion	38
4	Power Network Architecture	39
4.1	Introduction	39
4.2	Proposed Architecture and Control Technique	42
4.2.1	Model	42
4.2.2	Controller Design	44
4.2.3	Power Sharing	45
4.3	Implementation	47
4.4	Simulation	48
4.5	Conclusion	49
5	Power Sources I	51
5.1	Introduction	51
5.2	Conventional and Improved Swing Equations	52
5.3	Synchronous Generator Connected to a CPL	53
5.3.1	Stability	53
5.3.2	Shifted Passivity Property	55
5.3.3	Frequency Regulation	57
5.4	Synchronous Generator Connected to an Infinite Bus	59
5.4.1	Stability of the Improved Swing Model	59
5.4.2	Comparison with the Swing Equation	61
5.5	Numerical Simulation	62
5.5.1	CPL: Example 1	62
5.5.2	CPL: Example 2	62
5.5.3	CPL: Example 3	62
5.5.4	SMIB: Different Behavior	63
5.5.5	SMIB: Region of Attraction	63
5.6	Conclusion	64
6	Power Sources II	65
6.1	Introduction	65
6.2	Single Inverter with Capacitive Inertia	67
6.2.1	ICI Model in [69]	67
6.2.2	ICI Model from the Electrical Power Perspective	68
6.2.3	Primary Control	68
6.2.4	Secondary Control	69
6.3	Network of Inverters with Capacitive Inertia	70
6.3.1	Network Model	70
6.3.2	Primary Control	71

Contents


6.3.3	Secondary Control	74
6.4	Numerical Example	77
6.5	Conclusion	78
7	Power Systems in Port-Hamiltonian Framework	81
7.1	Shifted passivity of port-Hamiltonian systems	81
7.1.1	Introduction	82
7.1.2	Problem Formulation	83
7.1.3	Main Results	83
7.1.4	Application to Quadratic Affine Systems	88
7.1.5	Synchronous generator (6 th -order model) connected to a resistor	90
7.1.6	Conclusion	92
7.2	Shifted passivity of power-controlled Hamiltonian systems	93
7.2.1	Introduction	93
7.2.2	Model	94
7.2.3	Main Result: Shifted Passivity	96
7.2.4	Stability Analysis for Constant Inputs	97
7.2.5	Application to DC Networks with Constant Power Loads (CPL)	101
7.2.6	Application to Synchronous Generators connected to a CPL .	106
7.2.7	Conclusion	107
8	Conclusions	109
	Bibliography	113

Chapter 1

Introduction

“As a reader I loathe introductions. Introductions inhibit pleasure, they kill the joy of anticipation, and they frustrate curiosity.”

– Harper Lee, *To Kill a Mockingbird*

RIVEN by environmental and technical motivations, restructuring the classical power networks has been under vast attention during the recent decades. Among the goals are decreasing energy losses by moving towards distributed generation and preventing fault propagation through building up smart *microgrids*. Microgrids are small power network areas which can be seen as single entities from the large power grids. Considering such a network as a building block of the power grid is mainly motivated by preventing blackouts. A microgrid is capable of disconnecting itself from the main grid in case of a fault in the main grid, and reconnecting when the fault is resolved. This leads to an increase in the reliability of the system. Other advantages of microgrids are improving local energy delivery, optimizing energy costs, generating revenue, and reducing carbon emissions.

In classical networks, electrical energy sources were mainly *synchronous generators* (SG). Currently, however, we take advantage of storage systems and renewable energies such as wind, solar, geothermal, etc. . For most of these sources, an interface for power regulation or conversion from Direct Current (DC) to Alternating Current (AC) is necessary. These interfaces are called *power converters* or *inverters*. A microgrid typically includes both synchronous generators and inverters.

In such small-scale networks, the energy consumption and production uncertainty increases to a great extent according to the fewer number of consumers and unpredictable fluctuations in energies captured from nature. This issue calls for an accurate analysis of the control methods, and rethinking about the accuracy of the models that were used in the classical networks. This dissertation investigates control methods and modeling of the power systems in a microgrid.

1.1 Overview and contributions of the thesis

In this thesis, different aspects of the building components of a microgrid is investigated, as introduced briefly through the following lines.

1.1.1 Distribution lines

Many control methods and strategies have been proposed for control of power converters, *e.g.*, *droop controllers* [29, 118, 124], *quadratic droop* [126], *reactive power consensus dynamics* [119], *averaging reactive power controller* [110], and *dispatchable virtual oscillator control* [32]. The performance, stability, and efficiency of these methods highly depend on the power line characteristics. In this regard, different assumptions are made to guarantee the performance of the inverters, *e.g.*, *inductive* [74, 118, 124], *resistive* [60, 145, 146], or *homogeneous* [18, 76, 100, 127] lines. The inductivity of the *lines* can be regarded as the inductivity of the *network* as well, if all the lines share the same ratio between their resistance and inductance values. These networks are called *homogeneous* [22, 24]. However, power loads, together with the output impedances that are inherent elements of the power sources, destroy this *homogeneity*, and hence the definition of the *network inductivity* becomes unclear. In other words, loads and output impedances add new (internal) nodes to the network. Therefore, a model reduction is necessary to eliminate these nodes, and investigate the characteristics of the resulting network. The problem is, as shown in [149], that the obtained description after a model reduction of an RLC network, is not necessarily a description of another RLC network. Despite the crucial importance, few articles have investigated the characteristics of the distribution lines after a model reduction; see, *e.g.*, [22, 24, 138, 149], and in general, the problem of characterizing Schur complements of a complex Laplacian matrix seems largely open [139]. As a (partial) solution to this problem, in the third chapter of this thesis, a measure is proposed to define the inductivity of the resulting network, and it is shown that the impact of the output impedances on the network is highly dependent on the connectivity of the network. In particular, it can be deduced that the more connected the network is, the more output impedance diffuses into the network. Furthermore, through a numerical simulation, it is observed that the optimization of such a measure, leads to a better performance in droop controlled inverters, which are believed to perform better in inductive networks [57, 58, 59, 60, 61]. This shows that, through modifying (virtual) output impedances, one can tune the inductivity of the network to guarantee performance of the droop controlled inverters. The validity of the measure is demonstrated through a comparison with a model reduction in phasor domain. The results show that the overall behavior of the lines of the reduced network, can be predicted by the

proposed measure.

1.1.2 Network architecture

Despite the extensive advances in development of harvesting green energies, and because of the unpredictable nature of the green sources, there is still the need to have synchronous generators present in microgrids; see, *e.g.*, [120, 131, 151]. Hence, the consistency of the power converters with the synchronous generators is of crucial importance, in stability and safe operation of the overall network. A widely accepted approach to deal with this issue is the control scenarios for power converters that mimic the behavior of the synchronous generators [29, 69, 158]. In Chapter 6, a recently proposed inverter control method is discussed, which uses the inherent capacitive elements to mimic the inertia of a synchronous generator [69]. Another way to tackle the problem, as proposed in Chapter 4, is to regard the generator as the master and the inverter as the slaves. This idea originates from the current electrical system, where usually the gas generators are in charge of balancing the power demand and supply, while the power converters inject a determined or maximum capacity of electrical power into the grid, and their frequency follow that of the network. The proposed approach adopts a similar but different scheme, in the sense that the inverters power injection is adjusted by the controllers to respond appropriately to power imbalances. In case of an increase in the loads, the main generator slightly drops the frequency of the generated voltage. Since the rest of the sources are following this frequency, the frequency of the network decreases. The inverters then measure this deviation, and tune their output power until the power imbalance is eliminated, and the frequency goes back to the nominal value (50/60 Hz). In this scheme, these devices act as current-controlled sources instead of the widely used voltage-controlled source. Current-controlled sources, despite their many benefits [35], are rarely investigated in the literature over microgrids. It appears that further research is necessary over the dynamics of these devices, since they are useful tools to deal with the problems that are difficult to resolve by voltage sources.

1.1.3 Modeling synchronous generators

A classical model of synchronous generators, is elaborated in [50], where the dynamics consists of six state variables:¹ two stator fluxes, three rotor fluxes, and the momentum of the rotor (and prime mover). In Chapter 7, using this model,

¹The model consists of eight state variables before the dq transformation.

and through a systematic approach, we derive conditions for the stability of a synchronous generator connected to a resistor. A simplified third order model can be derived from the sixth-order model, which is known as the *First Principle* (FP) [25]². The existence and stability of the equilibrium of a synchronous generator with the FP model, connected to an infinite bus, is investigated in several articles and sufficient conditions have been introduced [10, 23, 101, 102]. However, the stability of two or more synchronous generators connected to each other remains an open problem³.

Due to the complexities in analyzing the interconnection of the FP and higher order models, the so called *Swing Equation* is widely used (also in Chapter 4 of this thesis), which is a first order model that can be derived from the FP model by several simplifying assumptions [25, 143]. An important simplifying, while contradictory approximation is that the frequency is assumed to be identical to the nominal frequency [25]. In Chapter 5, we go back to the mechanical equation of the FP model without considering this assumption, and derive an improved model which is called the *Improved Swing Equation* (ISE). We show passivity properties of this model, and provide a region of attraction for the case where the generator is connected to an infinite bus. While this model is still easy-to-use, simulations demonstrate that, in many cases, the ISE model is a good approximate model and the behavior is very similar to the FP model [148]. Furthermore, unlike the FP model, the stability of a network of generators modeled with the ISE is guaranteed as explained in Chapter 6. Hence, the improved swing equation can act as an approximate model, providing a balance between precision and utility.

1.1.4 Inverters and the problem of low inertia

A major blackout in south Australia in September 2016 has drawn attention to the problem of *low inertia* in inverter dominated networks. In classical networks, the kinetic energy of the large synchronous machines played an important role in stabilizing the network. If there is an imbalance between the generation and load, the kinetic energy of synchronous generators can be released into or absorbed from the network. However, since power converters do not possess any rotational mass, the networks that are dominated by inverters are vulnerable to abrupt changes, and the consequent rapid fluctuations in frequency might lead to power outages, and at larger scales to blackouts. In the report of the Australian Energy Market Operator (AEMO) in December 2016, it is stated that inertia and system strength may have played a role in the system collapse, and amended a secure technical envelope to

²Note that, as it will be seen later, this model is different with the third order model containing three state variables corresponding to the angular velocity, rotor angle, and stator voltage, as in [78, Ch.11].

³This problem is addressed in [152] for two synchronous generators, under the restrictive assumption that the two machines are precisely identical, and are driven by identical prime-movers.

require that a minimum capacity (300MW) of synchronous generating units must be on-line at all times. Obviously, this is an important obstacle in the development and usage of renewable energies.

Although a number of articles have introduced controllers that mimic the inertia of the synchronous generator, known as the *virtual inertia*, this scheme is slow due to delays in power measurements [43]. Hence, there is the need to a physical element in the system that can release or absorb the energy immediately. Capacitors, that are inevitable stabilizing elements on the DC-side of the power converters, can act as this reservoir [5, 146, 147]. Without the need to any programming or control scheme, the capacitors inject or absorb power immediately, when there is a mismatch between the (DC) current injected to and extracted from the capacitor. The main difference is that while any change in the kinetic energy of the synchronous generators is reflected in the frequency of the network, information about the changes in voltage level of the DC-side capacitors remains local. There are two approaches to resolve this problem. First is to transmit the measurement data of the capacitor voltage level through a communication network [147]. However, this method leads to higher costs, larger time delays, and lower reliability. The second approach is to generate a frequency deviation proportional to the difference of the voltage of the capacitor from its nominal value. A third order model of such an inverter is provided in [34, 69], but the network of these inverters is not studied. In Chapter 6, we investigate the network of these converters, propose controllers, and provide a nonlinear stability analysis. Numerical results also show that the method successfully avoids rapid changes in frequency, in response to abrupt load changes. As it is expected, larger capacitors provide larger inertia, and facilitate the stabilization of the network. Note that, as mentioned before, the results also apply to networks of synchronous generators modeled with the improved swing equation.

1.1.5 Port-Hamiltonian framework and its applications in power systems

In any control design, and especially in the nonlinear case, it is widely recognized that physical properties of the system should be exploited [141]. In this regard, Port-Hamiltonian (pH) modeling provides a natural starting point for control of power systems. Recently, a large number of articles have used the pH framework to model, control, and analyze power systems; see, *e.g.*, [9, 13, 33, 50, 69, 90, 91, 117, 118, 130]. Although showing a pH system to be passive and stable around an equilibrium in the origin is straightforward, one of the bottlenecks in using pH systems is to show passivity with respect to a non-zero equilibrium. We refer to this property as *shifted passivity* (see Section 2.3). This property paves the way to design appropriate

controllers, and derive Lyapunov functions for stability analysis. In Chapter 7 of this thesis, we investigate shifted passivity of two classes of pH systems:

- **Conventional pH systems:** Here, using monotonicity properties, we derive sufficient conditions for shifted passivity of pH systems. Using this condition, one is able to design a controller or the necessary damping (in case of lack of passivity) to achieve (global) stability. In case of a quadratic affine Hamiltonian, this condition is not dependent on the state variables. Since many pH systems fall into this category, this is a powerful tool to guarantee stability of physical systems such as synchronous motors and generators. In particular, we show that the results can be exploited to obtain a sufficient condition for stability of a synchronous generator, modeled by the sixth-order model, and connected to a linear resistive element.
- **pH systems with power control input/disturbance:** In a conventional pH system, the control input/disturbance is acting on the *flow*, *i.e.*, the time derivative of the states. However, in many physical systems, only the rate of energy injected or extracted from the system is tunable. In Section 7.2, we propose a pH framework to model such systems and determine a domain within which the system is shifted passive. Using this result, the (non-zero) equilibrium can be regulated with simple PI controllers. Moreover, when the system is connected to a constant power load/source, the stability of the equilibrium can be established. Interestingly, in case that the Hamiltonian is quadratic, an estimate of the region of attraction can be characterized. We apply these results to two cases of interest: i) Electrical DC circuits with constant power loads, and ii) Synchronous generator modeled by the improved swing equation connected to a constant power load. In the latter case, the results are consistent with the results of Chapter 5. Finally, numerical results illustrate that the derived estimates of the region of attraction are good approximations, and bound the least conservative invariant region.

1.2 Outline of the thesis

This thesis is organized as follows. Chapter 2 starts with the preliminaries on graph theory, pH systems, and stability theory. In Chapter 3, we propose a measure for the inductivity of a power network, and, using this measure, investigate how output inductances affect the inductivity of the network. A novel architecture for microgrids is established in Chapter 4, where a synchronous generator (as the master) and a number of inverters (as the slaves) share power without the need to any communication. Chapter 5 introduces the *improved swing equation* model for synchronous

generators and includes stability analysis and frequency regulation. In Chapter 6, inverters with capacitive inertia are studied, and methods for stability and frequency regulation are developed. Finally, Chapter 7 looks into the usage of port-Hamiltonian modeling in power systems.

1.3 Origins of the chapters

Chapter 3 is based on [95] which has been submitted to IEEE Transactions on Power Systems. The origin of Chapter 4 is [92], which has been published in the proceedings of American Control Conference (ACC 2016). Chapters 5 and 6 are based on the papers [93] and [96], which have been published at the 55th and 56th IEEE Conference on Decision and Control (CDC2016, CDC2017), respectively. Finally, Chapter 7 contains two papers, [89] and [94], which both have been submitted for journal publication.

1.4 Notation

For $i \in \{1, 2, \dots, n\}$, by $\text{col}(a_i)$ we denote the column vector $[a_1 \ a_2 \ \dots \ a_n]^\top$. For a given vector $a \in \mathbb{R}^n$, the diagonal matrix $\text{diag}\{a_1, a_2, \dots, a_n\}$ is denoted in short by $\langle a \rangle$. The function $\sin a$ represents the element-wise sine function, *i.e.*, $\sin a = \text{col}(\sin(a_i))$. The symbol $\mathbf{1}$ denotes the vector of ones with an appropriate dimension, and J_n is the identity matrix of size $n \times n$. An $n \times m$ matrix of zeros is denoted by 0_{nm} or $0_{(n) (m)}$. The set of nonnegative real numbers is denoted by $\mathbb{R}_{\geq 0}$.

For differentiable mappings $H : \mathbb{R}^n \rightarrow \mathbb{R}$ and $\mathcal{C} : \mathbb{R}^n \rightarrow \mathbb{R}^n$ we denote the transposed gradient as $\nabla H := \left(\frac{\partial H}{\partial x}\right)^\top$ and the transposed Jacobian matrix as $\nabla \mathcal{C} := \left(\frac{\partial \mathcal{C}}{\partial x}\right)^\top$. The Jacobian $(\nabla \mathcal{C}(\cdot))^\top$ is simply denoted by $\nabla \mathcal{C}(\cdot)^\top$. For a vector $x \in \mathbb{R}^n$, we denote its Euclidean norm by $\|x\|$. For the distinguished vector $\bar{x} \in \mathbb{R}^n$ we define the constant vectors $\bar{H} := H(\bar{x})$ and $\nabla \bar{H} := \nabla H(\bar{x})$; and for the mapping $\mathcal{F} : \mathbb{R}^n \rightarrow \mathbb{R}^{n \times m}$, we define the constant matrix $\bar{\mathcal{F}} := \mathcal{F}(\bar{x})$. The largest and smallest eigenvalues of the square, symmetric matrix A are denoted by $\lambda_M\{A\}$, and $\lambda_m\{A\}$, respectively.

1.5 List of abbreviations

SG	Synchronous Generator
FP	First Principle
ISE	Improved Swing Equation
pH	Port-Hamiltonian
NIR	Network Inductivity Ratio
NRR	Network Resistivity Ratio
VSI	Voltage Source Inverter
CSI	Current Source Inverter
GAS	Globally Asymptotically Stable
PLL	Phase Locked Loop
CPL	Constant Power Load
SMIB	Single Machine Infinite Bus
ICI	Inverters with Capacitive Inertia
RCOF	Rate of Change of Frequency
PWM	Pulse Width Modulation
P_wH	Power-controlled Hamiltonian
ROA	Region of Attraction

Chapter 2

Preliminaries

“Learning to see — accustoming the eye to calmness, to patience, to letting things come up to it; postponing judgment, learning to go around and grasp each individual case from all sides. That is the first preliminary schooling for spirituality: not to react at once to a stimulus, but to gain control of all the inhibiting, excluding instincts.”

– Friedrich Nietzsche, *Twilight of the Idols*



THIS chapter provides the preliminaries for the remainder of this thesis on graph theory, port-Hamiltonian systems, and passivity and stability analysis. The graph theory in Section 2.1 is used to model the interconnection topology of the network studied in chapters 3 and 6. The nodes of the graph correspond to the sources and loads, while the edges of the graph correspond to the power lines interconnecting them. Port-Hamiltonian framework is introduced in 2.2, and is used in Chapter 7, where power systems are modeled as input-state-output port-Hamiltonian systems. Section 2.3 introduces the properties of *passivity* and *shifted passivity* which is employed in Chapters 5 and 7. Finally, Section 2.4 provides tools for the stability analysis of the studied systems which is used in chapters 4-7.

2.1 Graph Theory

This section provides some essentials from the field of graph theory. Graphs are (mathematical) structures to model the pairwise interaction between objects. They are used to model many types of systems in physical, biological, social, and information systems. Examples are power networks, spreading of diseases amongst animal populations, rumor spreading, and social networks. Graph theory provide powerful tools for the modeling, analysis, and design of complex networks.

In this thesis, graphs are used to model the interaction amongst a group of sources and loads. The nodes of the graph correspond to the sources and loads, while the

edges correspond to the power distribution lines. The definitions below are distilled from [16, 52, 86].

Throughout the thesis, a graph is denoted by $\mathcal{G} = (\mathcal{V}, \mathcal{E}, \Gamma)$ consisting of a *node set* \mathcal{V} and an *edge set* $\mathcal{E} \subseteq \mathcal{V} \times \mathcal{V}$. The node set $\mathcal{V} = \{1, \dots, n\}$ has $n = |\mathcal{V}|$ elements, while the edge set has $m = |\mathcal{E}|$ elements. The edge weights are collected in the diagonal matrix Γ , and will be specified later.

There exists an edge $\{i, j\} \in \mathcal{E}$ if and only if the source/load at node i can transfer power to the source/load at node j . Since the graph models the *physical* interconnection structure, except for a minor case study, only *undirected* graphs are considered throughout this thesis. For undirected graphs the edge set \mathcal{E} is an unordered pair of nodes $\{i, j\}$ of vertices $i, j \in \mathcal{V}$. Furthermore, self-loops are not considered (i.e., $\{i, i\} \notin \mathcal{E}$).

For graph \mathcal{G} , there exists an *undirected path* from node n_i to node n_j if there exists a sequence of distinct edges e_1, \dots, e_K such that $e_k \in \mathcal{E}$ for $k = 1, \dots, K$ and $e_1 = \{i, *\}$, $e_K = \{*, j\}$. A graph is *connected* if there exists a path from every node to every other node. A *cycle* is a path that starts and ends with the same node.

Graphs admit a straightforward representation in terms of matrices. For an undirected graph, one can arbitrarily assign an orientation to each edge [86], by assigning a positive sign to one end (the *head*) and a negative sign to the other end (the *tail*). Then the *incidence matrix* $B \in \mathbb{R}^{n \times m}$ associated to \mathcal{G} is defined as

$$b_{ik} = \begin{cases} +1 & \text{if node } i \text{ is the head of edge } e_k, \\ -1 & \text{if node } i \text{ is the tail edge } e_k, \\ 0 & \text{otherwise.} \end{cases}$$

The n rows of B correspond to the nodes of \mathcal{G} , while the m columns correspond to the edges of \mathcal{G} . Another matrix considered here is the *Laplacian matrix*, $\mathcal{L} \in \mathbb{R}^{n \times n}$, which its elements ℓ_{ij} are defined as

$$\ell_{ij} = \begin{cases} \sum_{j=1}^n w_k & \text{if } i = j, \\ -w_k & \text{if } i \neq j, \end{cases}$$

where w_k is the weight of the k th edge with $k \sim \{i, j\}$. The Laplacian matrix can also be expressed as $\mathcal{L} = B\Gamma B^\top$ where $\Gamma := \text{diag}\{w_1, \dots, w_m\}$. Note that the Laplacian matrix is independent of the orientation.

Example 2.1.1 [Incidence and Laplacian matrices]

Consider the undirected graph $\mathcal{G}(\mathcal{V}, \mathcal{E})$ shown in 2.1 with all edge weights equal to 1.

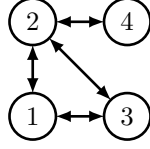


Figure 2.1: Graph for Example 2.1.1.

The node set and edge set are given by given by

$$\mathcal{V} = \{n_1, n_2, n_3, n_4\}$$

$$\mathcal{E} = \{\{n_1, n_2\}, \{n_1, n_3\}, \{n_2, n_3\}, \{n_2, n_4\}\}.$$

Since there is a path from every node to every other node the graph is connected. The incidence matrix B , and Laplacian matrix \mathcal{L} associated to \mathcal{G} are given by

$$B = \begin{bmatrix} -1 & -1 & 0 & 0 \\ 1 & 0 & 1 & -1 \\ 0 & 1 & -1 & 0 \\ 0 & 0 & 0 & 1 \end{bmatrix}, \quad \mathcal{L} = \begin{bmatrix} 2 & -1 & -1 & 0 \\ -1 & 3 & -1 & -1 \\ -1 & -1 & 2 & 0 \\ 0 & -1 & 0 & 1 \end{bmatrix}.$$

2.2 Port-Hamiltonian Systems

The *port-Hamiltonian* framework was introduced in [83] as an energy-based framework for modeling (nonlinear) systems in different domains (mechanical, electrical, etc.). The name comes from two key ingredients of the framework: *power ports* to interconnect (sub)systems and the *Hamiltonian*, which is the total energy stored in the system.

Power ports provide an interface for the sub-models within the model to interact with each other. In physical systems, these interactions are related to the exchange (or flow) of energy (*i.e.*, power) [45]. Each power port has two power-conjugate variables called *flow* and *effort*. The flow vector f belongs to the flow space \mathcal{F} , while the effort vector e belongs to the effort space \mathcal{E} which is the dual of the flow space $\mathcal{E} := \mathcal{F}^*$. The total space of flows and effort $\mathcal{F} \times \mathcal{F}^*$ is called the space of port-variables. On the total space of port-variables power is defined as $P = \langle e|f \rangle$, where $\langle e|f \rangle$ denotes the duality product (*i.e.*, the product of flows and efforts has the dimension of power). In the remainder $\mathcal{F} = \mathbb{R}^n$ and f and e are written as column vectors, which implies that $P = \langle e|f \rangle = e^\top f$.

Let $x \in \mathcal{X}$ denote the state of the system to be modeled, where \mathcal{X} denotes the state space $\mathcal{X} \subseteq \mathbb{R}^n$. The *input-state-output port-Hamiltonian system* can be written into the

following form :

$$\begin{aligned}\dot{x} &= (J(x) - R(x)) \nabla H(x) + G(x)u, \\ y &= G^\top(x) \nabla H(x),\end{aligned}\tag{2.1}$$

with skew-symmetric interconnection matrix $J(x) = -J^\top(x)$, positive semi-definite dissipation matrix $R(x) = R^\top(x) \geq 0$, input matrix $G(x)$, and the continuous and differentiable Hamiltonian $H(x)$ [141]. We will use the dynamics (2.1) in Chapter 7 to model electrical systems, and study their properties.

2.3 Passivity and Shifted Passivity

Passive systems are a class of dynamical systems where the rate at which the energy flows into the system is not less than the increase in storage. In other words, starting from any initial condition, only a finite amount of energy can be extracted from a passive system. This, together with the invariance under negative feedback interconnection, has promoted passivity as a basic building block for control of dynamical and interconnected systems; see [8, 107, 140] for the applications of passivity in control theory.

Passivity has been used as a key tool for stability analysis and design of large scale systems and dynamic networks [107, 129, 140, 153]. The reason for this mainly lies in the intriguing relation of passivity with the physics of the system, and its invariance under negative feedback. These properties promote the physical energy of the system as the cornerstone of Lyapunov functions verifying stability of large scale interconnected passive systems. In a similar vein, passivity can be exploited as a powerful design tool regulating the behavior of a system to a desired one [6, 107, 109, 112, 140].

Passivity of state-space systems is commonly defined as an input-output property for systems whose desired equilibrium state is the origin and the input and output variables are zero at this equilibrium [107, 140, 153]. If several of such systems are interconnected—for instance, a plant with a controller—the origin is an equilibrium point of the overall system whose stability may be assessed using the tools of passivity theory.

Definition 1 [Passivity [141]]

A system $\dot{x} = f(x, u), y = h(x, u)$, where $x \in \mathcal{X}, \mathcal{X} \subseteq \mathbb{R}^n$, and $u, y \in \mathbb{R}^m$, is called *passive* if there exists a differentiable storage function $S : \mathcal{X} \rightarrow \mathbb{R}_{\geq 0}$, satisfying the differential dissipation inequality

$$\dot{S} \leq u^\top y,\tag{2.2}$$

along all solutions $x \in \mathcal{X}$. \square

For physical systems, the right-hand side $u^\top y$ is usually interpreted as the supplied power, and $S(x)$ as the stored energy of the system when being in state x . Hence, a passive system cannot store more energy than it is supplied with.

Remark 2.3.1 [Passivity of pH systems]

It is easily verified that the pH system (2.1) is always passive with respect to port-variables (u, y) with storage function $H(x)$ since

$$\begin{aligned} \dot{H} &= \nabla H(x)^\top \dot{x} \\ &= \nabla H(x)^\top (J(x) - R(x)) \nabla H(x) + \nabla H(x)^\top G(x)u \\ &= -\nabla H(x)^\top R(x) \nabla H(x) + y^\top u \\ &\leq y^\top u. \end{aligned} \tag{2.3}$$

The interpretation of (2.3) is that the increase in stored energy H is always smaller than or equal to the power $y^\top u$ supplied through the control port. \square

In many applications, however, the desired equilibrium is not at the origin and the input and output variables of the system take nonzero values at steady-state. A standard procedure to describe the dynamics in these cases is to generate a so-called incremental model with inputs and outputs the deviations with respect to their value at the equilibrium. A natural question that arises is whether passivity of the original system is inherited by its incremental model, a property that we refer in this thesis as *shifted passivity*.¹ Thus shifted passivity is in fact passivity with respect to the shifted signals, as formalized below.

Definition 2 [Shifted passivity]

Consider the system $\dot{x} = f(x, u)$, $y = h(x, u)$, where $x \in \mathcal{X}$, $\mathcal{X} \subseteq \mathbb{R}^n$, and $u, y \in \mathbb{R}^m$. Define the steady-state relation

$$\mathcal{E} := \{(x, u) \in \mathcal{X} \times \mathbb{R}^m \mid f(x, u) = 0\}.$$

Fix $(\bar{x}, \bar{u}) \in \mathcal{E}$ and the corresponding output $\bar{y} := h(\bar{x}, \bar{u})$. The system is *shifted passive* if the mapping $(u - \bar{u}) \rightarrow (y - \bar{y})$ is passive, *i.e.*, there exists a function $\mathcal{S} : \mathcal{X} \rightarrow \mathbb{R}_{\geq 0}$ such that

$$\dot{\mathcal{S}} \leq (u - \bar{u})^\top (y - \bar{y}) \tag{2.4}$$

along all solutions $x \in \mathcal{X}$. \square

¹This property is called passivity of the incremental model in [68]. Notice that shifted passivity is defined with respect to a given pair $(\bar{x}, \bar{u}) \in \mathcal{E}$. If (2.3) holds for all $(\bar{x}, \bar{u}) \in \mathcal{E}$, then the (shifted) passivity property becomes independent of the steady-state values \bar{u} and \bar{x} [21, 66, 123] where the term “equilibrium-independent passivity” has been used.

Remark 2.3.2 [Shifted passivity and incremental passivity]

Shifted passivity is different from the classical incremental passivity property [38]. In fact, the latter is much more demanding as the word “incremental” refers to two arbitrary input-output pairs of the system, whereas in the former only one input-output pair is arbitrary and the other one is fixed to a constant.

Shifted passivity is defined with respect to a given pair $(\bar{x}, \bar{u}) \in \mathcal{E}$. If (2.4) holds for all (\bar{x}, \bar{u}) , then the (shifted) passivity property becomes independent of the steady-state values \bar{u} and \bar{x} [66]. \square

Interestingly, under certain conditions, pH systems are shifted passive.

Theorem 2.3.3 [Shifted passivity of pH systems [68]]

The pH system (2.1) with a convex Hamiltonian H , is shifted passive, if the interconnection, dissipation, and control input matrices are all *constant*.

Proof. The proof is straightforward using the storage function

$$\mathcal{H}(x) = H(x) - (x - \bar{x})^\top \nabla H(\bar{x}) - H(\bar{x}). \quad (2.5)$$

■

Throughout the thesis, we refer to the storage function (2.5) as the *Shifted Hamiltonian*. As will be shown in chapter 7, showing shifted passivity for the pH systems with state dependent matrices $J(x)$, $R(x)$, or $G(x)$ is nontrivial.

Remark 2.3.4 [Bregman distance]

The shifted function (2.5) is closely related to the notion of availability function used in thermodynamics [7, 8], and the *Bregman distance* with respect to an equilibrium of the system [20]. In Chapters 4, 5, and 6 of this thesis, we use this technique to shift the candidate Lyapunov function V , to a non-zero equilibrium

$$V_s(x) = V(x) - (x - \bar{x})^\top \nabla V(\bar{x}) - V(\bar{x}). \quad (2.6)$$

By construction, V_s is positive definite locally, and takes its minimum at $x = \bar{x}$, if the function V is strictly convex around \bar{x} [20]. \square

2.4 Stability of Nonlinear Systems

This section presents a brief recall of Lyapunov stability theory for nonlinear systems (see [70] for more details). Let $x \in \mathbb{R}^n$ denote the state of the system of interest and consider the time-invariant system

$$\dot{x} = f(x), \quad (2.7)$$

where $f : \mathcal{D} \rightarrow \mathbb{R}^n$ is a locally Lipschitz map from a domain $\mathcal{D} \subset \mathbb{R}^n$ into \mathbb{R}^n . Suppose that x^* is an equilibrium point of (2.7), i.e., $f(x^*) = 0$. Without loss of generality, assume that $x^* = 0$. The stability of the origin $x^* = 0$ is defined as follows.

Definition 3 [Stability [70]]

The equilibrium point $x^* = 0$ of (2.7) is

- **stable** if, for each $\epsilon > 0$ there exists a $\delta_1 = \delta_1(\epsilon) > 0$ such that

$$\|x(0)\| < \delta_1 \Rightarrow \|x(t)\| < \epsilon, \quad \forall t \geq 0.$$

- **unstable** if it is not stable.
- **asymptotically stable** if it is stable and additionally δ_2 can be chosen such that

$$\|x(0)\| < \delta_2 \Rightarrow \lim_{t \rightarrow \infty} x(t) = 0.$$

□

Stability of system (2.7) in the sense of Definition 3 can be assessed using Lyapunov's stability theorem, which is stated next.

Theorem 2.4.1 [Lyapunov's direct method [70]]

Let $x = 0$ be an equilibrium point for (2.7) (without loss of generality) and $\mathcal{D} \subset \mathbb{R}^n$ be an open subset containing $x = 0$. Let $V : \mathcal{D} \rightarrow \mathbb{R}$ be a continuously differentiable function such that

$$V(0) = 0 \text{ and } V(x) > 0 \text{ in } \mathcal{D} - \{0\}, \quad (2.8)$$

$$\dot{V}(x) \leq 0 \text{ in } \mathcal{D}. \quad (2.9)$$

Then, $x = 0$ is *stable*. Moreover, if

$$\dot{V}(x) < 0 \text{ in } \mathcal{D} - \{0\}, \quad (2.10)$$

then $x = 0$ is *asymptotically stable*. Furthermore, if $D = \mathbb{R}^n$, and together with (2.10), V is *radially unbounded*, i.e.,

$$\|x\| \rightarrow \infty \Rightarrow V(x) \rightarrow \infty,$$

then $x = 0$ is *globally asymptotically stable* (GAS).

A continuously differentiable function $V(x)$ satisfying (2.8) and (2.9) is called a *Lyapunov function*. Many (physical) systems fail to meet condition (2.10), because \dot{V} is only negative semi-definite ($\dot{V} \leq 0$) in $\mathcal{D} - \{0\}$. In this case, LaSalle's invariance principle can be invoked to assess the stability of (2.7). In order to state LaSalle's invariance principle, first the definition of an invariant set is needed.

Definition 4 [Invariant Set [70]]

A set \mathcal{M} is said to be *invariant* if

$$x(0) \in \mathcal{M} \Rightarrow x(t) \in \mathcal{M}, \quad \forall t,$$

and *positively invariant* if

$$x(0) \in \mathcal{M} \Rightarrow x(t) \in \mathcal{M}, \quad \forall t > 0.$$

□

LaSalle's invariance principle is now stated as follows.

Theorem 2.4.2 [LaSalle's invariance principle [70]]

Let $\Omega \subset \mathcal{D}$ be a compact set that is positively invariant with respect to (2.7). Let $V : \mathcal{D} \rightarrow \mathbb{R}$ be a \mathcal{C}^1 function satisfying (2.9). Let \mathcal{F} be the set of all points in \mathcal{D} where $\dot{V}(x) = 0$. Let \mathcal{M} be the largest invariant set in \mathcal{F} . Then every solution starting in Ω approaches \mathcal{M} as $t \rightarrow \infty$.

Interestingly, under additional conditions, the corresponding equilibrium of shifted passive systems with constant inputs are stable, as formalized in the following proposition.

Remark 2.4.3 [Stability of shifted passive systems]

Suppose that the system $\dot{x} = f(x, \bar{u})$, $y = h(x, \bar{u})$, is shifted passive with respect to the equilibrium pair (\bar{x}, \bar{u}) , and the storage function is a Lyapunov function, *i.e.*, is positive definite, and have a strict minimum at $x = \bar{x}$. Then the equilibrium (\bar{x}, \bar{u}) of the system $\dot{x} = f(x, \bar{u})$, $y = h(x, \bar{u})$ is stable. □

In many cases, we are interested in determining how far from the equilibrium the trajectory can be and still converge to the equilibrium as time approaches ∞ . This gives rise to the definition of the region (domain) of attraction:

Definition 5 [Region of attraction (ROA)[70]]

Let $\varphi(t; x)$ be the solution of $\dot{x} = f(x)$, that starts at initial state x at time $t = 0$. Assume that there exists an equilibrium \bar{x} , *s.t.* $f(\bar{x}) = 0$. Then, the *region of attraction* of the equilibrium \bar{x} is defined as the set of all points x such that $\varphi(t; x)$ is defined for all $t \geq 0$ and $\lim_{t \rightarrow \infty} \varphi(t; x) = \bar{x}$. □

Finding the exact region of attraction analytically might be difficult or even impossible. However, Lyapunov functions can be used to estimate the region of attraction, that is, to find sets contained in the region of attraction. In particular, if there is a Lyapunov function that satisfies the conditions of asymptotic stability over a domain D


and, if $\Omega_c = \{x \in \mathbb{R}^n | V(x) \leq c\}$ is bounded and contained in D , then Ω_c is positively invariant, and every trajectory starting in Ω_c approaches the equilibrium as $t \rightarrow \infty$ [70].

Chapter 3

Power Network Characteristics: Output Impedance Diffusion Into Lossy Power Lines

“Almost all absurdity of conduct arises from the imitation of those whom we cannot resemble.”

– Samuel Johnson, *The Rambler*

 OUTPUT impedances are inherent elements of power sources in the electrical grids. In this chapter, we give an answer to the following question: What is the effect of output impedances on the inductivity of the power network? To address this question, we propose a measure to evaluate the inductivity of a power grid, and we compute this measure for various types of output impedances. Following this computation, it turns out that network inductivity highly depends on the algebraic connectivity of the network. By exploiting the derived expressions of the proposed measure, one can tune the output impedances in order to enforce a desired level of inductivity on the power system. Furthermore, the results show that the more *connected* the network is, the more the output impedances diffuse into the network. Finally, using Kron reduction, we provide examples that demonstrate the utility and validity of the method.

3.1 Introduction

Output impedance is an important and inevitable element of any power producing device, such as synchronous generators and inverters. Synchronous generators typically possess a highly inductive output impedance according to their large stator coils, and are prevalently modeled by a voltage source behind an inductance. Similarly, inverters have an inductive output impedance, at the nominal frequency,

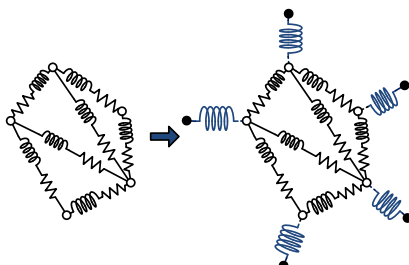


Figure 3.1: Inductive outputs are typically added to the sources in order to assume inductive lines for the resulting network.

due to the low pass filter in the output, which is necessary to eliminate the high frequencies of the modulation signal.

There are numerous motivations to add an impedance to the inherent output impedance of the inverters, one of the most important of which is to enhance the performance of droop controllers in a lossy network. Droop controllers show a better performance in a dominantly inductive network (or analogously in dominantly resistive networks for the case of inverse-droop controllers) [57, 58, 59, 60, 61, 74, 98] (see Figure 3.1). The additional output impedance is also employed to improve stability and correct the load sharing error [61, 80, 103],[79, 99], supply harmonics to nonlinear loads [18],[59], [84], share current among sources resilient to parameters mismatch and synchronization error [31], decrease sensitivity to line impedance unbalances [60, 63],[56], reduce the circulating currents [154], limit output current during voltage sags [150], minimize circulating power [71], and damp the LC resonance in the output filter [74]. In most of these methods, to avoid the costs and large size of an additional physical element, a *virtual output impedance* is employed, where the electrical behavior of a desired output impedance is simulated by the inverter controller block.

Although an inductive output impedance, either resulting from the inherent output filter or the added output impedance, is considered as a means to regulate the inductive behavior of the resulting network, there is a lack of theoretical analysis to verify the feasibility of this method and to quantify the effect of the output impedances on the network inductivity/resistivity. Note that the output impedance cannot be chosen arbitrarily large, since a large impedance substantially boosts the voltage sensitivity to current fluctuations, and results in high frequency noise amplification [74]. Furthermore, there is the fundamental challenge of quantifying inductivity/resistivity of a network, which is nontrivial unless the overall network has uniform line characteristics (homogeneous). This is not the case here as the augmented network will be nonuniform (heterogeneous) even if the initial network is. Note that, to investigate the characteristics of the direct connections between

sources, a model reduction (*e.g.*, Kron) is necessary to eliminate the (internal) nodes added by the output impedances. However the resulting network might not be a description of an RLC network [149].

In this chapter, we examine the effect of the output impedances on a homogeneous power distribution grid by proposing a quantitative measure for the inductivity of the resulting heterogeneous network. Similarly, a dual measure is defined for its resistivity. Based on these measures, we show that the network topology plays a major role in the diffusion of the output impedance into the network. Furthermore, we exploit the proposed measures to maximize the effect of the added output impedances on the network inductivity/resistivity. We demonstrate the validity and practicality of the proposed method on various examples and special cases.

The structure of the chapter is as follows: In Section 3.2, the notions of Network Inductivity Ratio (Ψ_{NIR}) and Network Resistivity Ratio (Ψ_{NRR}) are proposed. In Section 3.3, the proposed measures are analytically computed for various cases of output inductors and resistors. In Section 3.4 the proposed measure is evaluated with the Kron reduction in the phasor domain. Finally, Section 3.5 is devoted to conclusions.

3.2 Measure Definition

Consider an electrical network with an arbitrary topology, where we assume that all the sources and loads are connected to the grid via power converter devices (inverters) [132]. later in Section 3.3, we show how to relax this assumption. The network of this grid is represented by a connected and weighted undirected graph $\mathcal{G}(\mathcal{V}, \mathcal{E}, \Gamma)$, as defined in Section 2.1. Recall that the nodes $\mathcal{V} = \{1, \dots, n\}$ represent the inverters, and the edge set \mathcal{E} accounts for the distribution lines. The total number of edges is denoted by m , *i.e.*, $|\mathcal{E}| = m$, and the edge weights are collected in the diagonal matrix Γ .

We start our analysis with the voltages across the edges of the graph \mathcal{G} . We restrict this analysis to the low/medium voltage networks with short line lengths,¹ where the shunt capacitance of the line (π) model can be neglected [54, Ch.13], [27, App.1], [53, Ch.6]. Let $R_e \in \mathbb{R}^{m \times m}$ and $L_e \in \mathbb{R}^{m \times m}$ be the diagonal matrices with the line resistances and inductances on their diagonal, respectively. We have

$$R_e I_e + L_e \dot{I}_e = B^\top V, \quad (3.1)$$

where $I_e \in \mathbb{R}^m$ denotes the current flowing through the edges. The orientation of the currents is taken in agreement with that of the incidence matrix. The vector $V \in \mathbb{R}^n$

¹A power line is defined as a short-length line if its length is less than 80 km [54].

indicates the voltages at the nodes. Let τ_k denote the physical distance between nodes i and j , for each edge $k \sim \{i, j\}$. We assume that the network is homogeneous, *i.e.*, the distribution lines are made of the same material and possess the same resistance and inductance per length:²

$$r = \frac{R_{e_k}}{\tau_{e_k}}, \quad l = \frac{L_{e_k}}{\tau_{e_k}}, \quad k = \{1, \dots, m\}.$$

Now, let the weight matrix Γ be specified as

$$\Gamma = \text{diag}(\gamma) := \text{diag}(\tau_1^{-1}, \tau_2^{-1}, \dots, \tau_m^{-1}). \quad (3.2)$$

We can rewrite (3.1) as [24]

$$rI_e + \ell\dot{I}_e = \Gamma B^\top V.$$

Hence, $rBI_e + \ell B\dot{I}_e = B\Gamma B^\top V$, and

$$rI + \ell\dot{I} = \mathcal{L}V, \quad (3.3)$$

where $I := BI_e$ is the vector of nodal current injections. As shown in Chapter 2, the matrix $\mathcal{L} = B\Gamma B^\top$ is the Laplacian matrix of the graph $\mathcal{G}(\mathcal{V}, \mathcal{E}, \Gamma)$ with the weight matrix Γ .

Remark 3.2.1 [Homogeneity assumption]

The homogeneity assumption is ubiquitous in the literature of power network analysis (see, *e.g.*, [22, 24, 76, 100, 110, 127, 157]). The main obstacle to investigate the case of a network with arbitrary impedances is that the network dynamics cannot be described by the nodal currents vector I . This is essential to our analysis, which is based on the nodal representation in (3.4). \square

Note that, as the network (3.3) is homogeneous, its inductivity behavior is simply determined by the ratio $\frac{\ell}{r}$. However, clearly, network homogeneity will be lost once the output impedances are augmented to the network. This makes the problem of determining network inductivity nontrivial and challenging. To cope with the heterogeneity resulting from the addition of the output impedances, we need to depart from the homogeneous form (3.3), and develop new means to assess the network inductivity. To this end, we consider the more general representation

$$RI + L\dot{I} = \mathcal{L}V_o, \quad (3.4)$$

²The homogeneity assumption is ubiquitous in the literature of power network analysis; see, *e.g.*, [22, 24, 76, 100, 110, 127, 157].

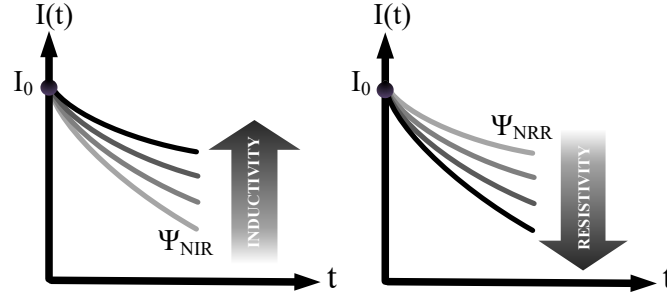


Figure 3.2: Worst cases are selected for inductivity and resistivity measures.

where $V_o \in \mathbb{R}^n$ is the vector of voltages of the augmented nodes (black nodes in Figure 3.1), and $R \in \mathbb{R}^{n \times n}$ and $L \in \mathbb{R}^{n \times n}$ are matrices associated closely with the resistances and inductances of the lines, respectively. We will show that the overall network after the addition of the output impedances, can be described by (3.4). Note that this description cannot necessarily be realized with passive RL elements. Therefore, while the inductivity behavior of the homogeneous network (3.3) is simply determined by the ratio $\frac{\ell}{r}$, the one of (3.4) cannot be trivially quantified.

Recall that in a single RL circuit, the current is damped with the rate $\frac{R}{L}$. The idea here is to promote this rate of convergence of the currents as a suitable metric quantifying the inductivity/resistivity of the network. For the network dynamics in (3.3), the rate of convergence of the solutions is determined by the ratio $\frac{r}{\ell}$. The more inductive the lines are, the slower the rate of convergence is. Now, we seek for a similar property in (3.4). Notice that the solutions of (3) are damped with corresponding eigenvalues of $L^{-1}R$. Throughout the chapter, we assume the following property:

Assumption 3.2.2 [Positive real damping ratios]

The eigenvalues of the matrix $L^{-1}R$ are all positive and real.

It will be shown that Assumption 3.2.2 is satisfied for all the cases considered in this chapter.

Figure 3.2 sketches the behavior of homogeneous solutions of (3.4). Among all the solutions, we choose the fastest one as our measure for inductivity, and the slowest one for resistivity of the network. Opting for these worst case scenarios allows us to guarantee a prescribed inductivity or resistivity ratio by proper design of output impedances. These choices are formalized in the following definitions.

Definition 6 [Network inductivity ratio]

Let $I(t, I_0)$ denote the homogeneous solution of (3.4) for an initial condition $I_0 \in \text{im } B$.

Let the set $M_L \subseteq \mathbb{R}^+$ be given by

$$M_L := \{\sigma \in \mathbb{R}^+ \mid \exists \mu \text{ s.t.} \\ \|I(t, I_0)\| \geq \mu e^{-\sigma t} \|I_0\|, \forall t \in \mathbb{R}^+, \forall I_0 \in \text{im } B\}.$$

Then we define the *Network Inductivity Ratio* (NIR) as

$$\Psi_{\text{NIR}} := \frac{1}{\inf(M_L)}.$$

□

Definition 7 [Network resistivity ratio]

Let $I(t, I_0)$ denote the homogeneous solution of (3.4) for an initial condition $I_0 \in \text{im } B$. Let the set $M_R \subseteq \mathbb{R}^+$ be given by

$$M_R := \{\sigma \in \mathbb{R}^+ \mid \exists \mu \text{ s.t.} \\ \|I(t, I_0)\| \leq \mu e^{-\sigma t} \|I_0\|, \forall t \in \mathbb{R}^+, \forall I_0 \in \text{im } B\}.$$

We define the *Network Resistivity Ratio* (NRR) as

$$\Psi_{\text{NRR}} := \sup(M_R).$$

□

Note that the set M_L is bounded from below and M_R is bounded from above by definition and Assumption 3.2.2. Interestingly, in case of the homogeneous network (3.3), *i.e.*, without output impedances, we have $\Psi_{\text{NIR}} = \frac{\ell}{r}$ and $\Psi_{\text{NRR}} = \frac{r}{\ell}$, which are natural measures to reflect the inductivity and resistivity of an RL homogeneous network.

3.3 Calculating the Network Inductivity/Resistivity Measure ($\Psi_{\text{NIR}}/\Psi_{\text{NRR}}$)

In this section, based on Definitions 1 and 2, we compute the network inductivity/resistivity ratio for both cases of uniform and nonuniform output impedances.

3.3.1 Uniform Output Impedances

In most cases of practical interest, the output impedance consists of both inductive and resistive elements. We investigate the effect of the addition of such output

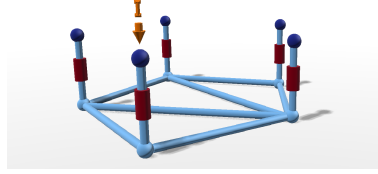


Figure 3.3: The injected currents at the nodes of the original graph pass through the added output impedance.

impedances on the network inductivity ratio. The change in network resistivity ratio can be studied similarly, and thus is omitted here. Consider the uniform output impedances with the inductive part ℓ_o and the resistive component r_o (in series), added to the network (3.3). Note that the injected currents I now pass through the output impedances, as shown in Figure 3.3. Clearly, we have

$$V = V_o - r_o I - \ell_o \dot{I}. \quad (3.5)$$

Having (3.3) and (3.5), the overall network can be described as

$$(r_o \mathcal{L} + r \mathcal{J})I + (\ell_o \mathcal{L} + \ell \mathcal{J})\dot{I} = \mathcal{L}V_o, \quad (3.6)$$

where $\mathcal{J} \in \mathbb{R}^{n \times n}$ denotes the identity matrix, and \mathcal{L} is the Laplacian matrix of \mathcal{G} as before. In view of equation (3.4), the matrices R and L are given by $R = r_o \mathcal{L} + r \mathcal{J}$ and $L = \ell_o \mathcal{L} + \ell \mathcal{J}$, respectively. As both matrices are positive definite, the eigenvalues of the product $L^{-1}R$ are all positive and real, see [67, Ch. 7]. Hence, Assumption 3.2.2 is satisfied. To calculate the measure Ψ_{NIR} for the inductivity of the resulting network, we investigate the convergence rates of the homogeneous solution of (3.6). This brings us to the following theorem:

Theorem 3.3.1 [Computing NIR: Uniform output impedances]

Consider a homogeneous network (3.3) with the resistance per length unit r and inductance per length unit ℓ . Suppose that an output resistance r_o and an output inductance ℓ_o are attached in series to each node. Assume that $\frac{r_o}{\ell_o} < \frac{r}{\ell}$. Then the network inductivity ratio is given by

$$\Psi_{\text{NIR}} = \frac{\ell_o \lambda_2 + \ell}{r_o \lambda_2 + r}, \quad (3.7)$$

where λ_2 is the *algebraic connectivity* of the graph $\mathcal{G}(\mathcal{V}, \mathcal{E}, \Gamma)$.³

³The algebraic connectivity of either a directed or an undirected graph \mathcal{G} is defined as the second smallest eigenvalue of the Laplacian matrix throughout the chapter. Note that the smallest eigenvalue is 0.

Proof. The homogeneous solution is

$$I(t) = e^{-(r_o \mathcal{L} + r \mathcal{J})(\ell_o \mathcal{L} + \ell \mathcal{J})^{-1} t} I_0 .$$

The Laplacian matrix can be decomposed as $\mathcal{L} = U^\top \Lambda U$. Here, U is the matrix of eigenvectors and $\Lambda = \text{diag}\{\lambda_1, \lambda_2, \dots, \lambda_n\}$ where $\lambda_1 < \lambda_2 < \dots < \lambda_n$ are the eigenvalues of the matrix \mathcal{L} . Note that $\lambda_1 = 0$. We have

$$\begin{aligned} I(t) &= e^{-u(r_o \Lambda + r \mathcal{J})u^\top (u(\ell_o \Lambda + \ell \mathcal{J})u^\top)^{-1} t} I_0 \\ &= U e^{-(r_o \Lambda + r \mathcal{J})(\ell_o \Lambda + \ell \mathcal{J})^{-1} t} U^\top I_0 \\ &= \begin{bmatrix} \frac{1}{\sqrt{n}} \mathbf{1} & \tilde{U} \end{bmatrix} e^{-\begin{bmatrix} \frac{r}{\ell} & 0 \\ 0_{(n-1) \times 1} & \tilde{\Lambda} \end{bmatrix} t} \begin{bmatrix} \frac{1}{\sqrt{n}} \mathbf{1}^\top \\ \tilde{U}^\top \end{bmatrix} I_0 , \end{aligned}$$

where $\tilde{\Lambda} = \text{diag}\{\frac{r_o \lambda_2 + r}{\ell_o \lambda_2 + \ell}, \dots, \frac{r_o \lambda_n + r}{\ell_o \lambda_n + \ell}\}$. Noting that U is unitary and by the Kirchoff Law, $\mathbf{1}^\top I_0 = 0$, we have

$$\begin{aligned} I(t) &= \tilde{U} e^{-\tilde{\Lambda} t} \tilde{U}^\top I_0 = \left(\sum_{i=1}^{n-1} e^{-\tilde{\lambda}_i t} \tilde{U}_i \tilde{U}_i^\top \right) \left(\sum_{i=1}^{n-1} \alpha_i \tilde{U}_i \right) \\ &= \sum_{i=1}^{n-1} \alpha_i e^{-\tilde{\lambda}_i t} \tilde{U}_i , \end{aligned}$$

where \tilde{U}_i denotes the i th column of \tilde{U} , and we used again $\mathbf{1}^\top I_0 = 0$ to write I_0 as the linear combination

$$I_0 = \sum_{i=1}^{n-1} \alpha_i \tilde{U}_i .$$

Hence

$$\|I(t)\|^2 = \sum_{i=1}^{n-1} \alpha_i^2 e^{-2\tilde{\lambda}_i t} . \quad (3.8)$$

Having $\frac{r_o}{\ell_o} < \frac{r}{\ell}$, it is straightforward to see that

$$\frac{r_o \lambda_2 + r}{\ell_o \lambda_2 + \ell} \geq \frac{r_o \lambda_i + r}{\ell_o \lambda_i + \ell}, \quad \forall i .$$

and bearing in mind that $\|I_0\|^2 = \sum_{i=1}^{n-1} \alpha_i^2$, we conclude that

$$\|I(t)\| \geq e^{-\frac{r_o \lambda_2 + r}{\ell_o \lambda_2 + \ell} t} \|I_0\| , \quad (3.9)$$

which yields $\Psi_{\text{NIR}} = \frac{\ell_o \lambda_2 + \ell}{r_o \lambda_2 + r}$. Note that (3.9) holds with equality in case I_0 belongs to the span of the corresponding eigenvector of the second smallest eigenvalue of the Laplacian matrix \mathcal{L} . This completes the proof. ■

Theorem 3.3.1 provides a compact and easily computable expression which quantifies the network inductivity behavior. Moreover, the expression (3.7) is an easy-to-use measure that can be exploited to choose the output impedances in order to impose a desired degree of inductivity on the network. The only information required is the line parameters r , and ℓ , and the algebraic connectivity of the network.

Algebraic connectivity is a measure of connectivity of the weighted graph \mathcal{G} , which depends on both the density of the edges and the weights (inverse of the lines lengths). Hence, Theorem 3.3.1 reveals the fact that: *“The more connected the network is, the more the output impedance diffuses into the network.”*

The algebraic connectivity of the network can be estimated through distributed methods [51], [75]. Furthermore, line parameters (resistance and inductance) can be identified through PMUs (Phase Measurement Units) [155] [44] [121]. Therefore, our proposed measure can be calculated in a distributed manner.

Remark 3.3.2 [Magnitude of the resistive output]

In case the resistance part of the output impedance is negligible, *i.e.*, $r_o = 0$, the network inductivity ratio reduces to

$$\Psi_{\text{NIR}} = \frac{\ell_o \lambda_2 + \ell}{r}.$$

In case $\frac{r_o}{\ell_o} > \frac{r}{\ell}$, the network inductivity ratio will be given by

$$\Psi_{\text{NIR}} = \frac{\ell_o \lambda_M + \ell}{r_o \lambda_M + r},$$

where λ_M is the largest eigenvalue of the Laplacian matrix of \mathcal{G} . Furthermore, if $\frac{r_o}{\ell_o} = \frac{r}{\ell}$, then $\tilde{\Lambda} = \frac{r}{\ell} \mathbf{J}$ and $\Psi_{\text{NIR}} = \frac{r}{\ell}$. However, the condition $\frac{r_o}{\ell_o} < \frac{r}{\ell}$ assumed in Theorem 3.3.1 is more relevant since the resistance r_o of the inductive output impedance is typically small. □

As mentioned in Section 3.1, in low-voltage microgrids where the lines are dominantly resistive, the inverse-droop method is employed. In this case, a purely resistive output impedance is of advantage [60].

Corollary 3.3.3 [Computing NRR: Uniform output impedances]

Consider a homogeneous distribution network with the resistance per length unit r ,

inductance per length unit ℓ , and output inductors ℓ_o . Then the network resistivity ratio is given by

$$\Psi_{\text{NRR}} = \frac{r_o \lambda_2 + r}{\ell},$$

where λ_2 is the *algebraic connectivity* of the graph $\mathcal{G}(\mathcal{V}, \mathcal{E}, \Gamma)$.

Proof. The proof can be constructed in an analogous way to the proof of Theorem 3.3.1 and is therefore omitted. ■

Remark 3.3.4 [Plug-and-play capability]

One of the main desired features in microgrids is plug-and-play capability for planning and connection of the new sources. In most cases, a new node connects to the network initially through few edges. This results in a decrease in the algebraic connectivity of the overall network, *e.g.*, as shown in [55], adding a pendant vertex and edge to a graph does not increase the algebraic connectivity. Therefore, for plug-and-play capability, larger output impedances should be employed in the network to compensate the possible drop in the algebraic connectivity, and thus the network inductivity ratio, resulting from attaching new nodes to the network. In some special cases, such as uniform line lengths, the additional required output impedances can be estimated using lower bounds on the algebraic connectivity; see [88] and [36] for more details on algebraic connectivity and its lower and upper bounds in various graphs. □

Case Study: Identical Line Lengths

Recall that the notion of network inductivity ratio allows us to quantify the inductivity behavior of the network, while the model (3.6), in general, cannot be synthesized with RL elements only. A notable special case where the model (3.6) can be realized with RL elements is a complete graph with identical line lengths. Although such case is improbable in practice, it provides an example to assess the validity and credibility of the introduced measures. Interestingly, Ψ_{NIR} matches precisely the inductance to resistance ratio of the lines of the synthesized network in this case:

Theorem 3.3.5 [Verification of NIR in complete graphs with identical line lengths]

Consider a network with a uniform complete graph where all the edges have the length τ . Suppose that the lines have inductance $\ell_e \in \mathbb{R}$ and resistance $r_e \in \mathbb{R}$. Attach an output inductance ℓ_o in series with a resistance r_o to each node. Then the model of the augmented graph can be equivalently synthesized by a new RL network with identical lines, each with inductance $\ell_c := n\ell_o + \ell_e$ and resistance

$r_c := nr_o + r_e$, where n denotes the number of nodes. Furthermore, the resulting network inductivity ratio Ψ_{NIR} is equal to $\frac{\ell_c}{r_c}$.

Proof. The nodal injected currents satisfy $rI + \ell\dot{I} = \mathcal{L}V$. In this network, $r = \frac{r_e}{\tau}$, $\ell = \frac{\ell_e}{\tau}$, and $\mathcal{L} = \frac{n}{\tau}\Pi$ where $\Pi := \mathcal{J} - \frac{1}{n}\mathbb{1}\mathbb{1}^\top$. Hence,

$$r_e I + \ell_e \dot{I} = n\Pi V. \quad (3.10)$$

By appending the output impedance we have $V = V_o - r_o I - \ell_o \dot{I}$. Hence (3.10) modifies to

$$(nr_o\Pi + r_e\mathcal{J})I + (n\ell_o\Pi + \ell_e\mathcal{J})\dot{I} = n\Pi V_o,$$

which results in

$$(n\ell_o\Pi + \ell_e\mathcal{J})^{-1}(nr_o\Pi + r_e\mathcal{J})I + \dot{I} = n(n\ell_o\Pi + \ell_e\mathcal{J})^{-1}\Pi V_o.$$

Since $(n\ell_o\Pi + \ell_e\mathcal{J})^{-1} = \frac{1}{\ell_e + n\ell_o}\mathcal{J} + \frac{\ell_o}{\ell_e(\ell_e + n\ell_o)}\mathbb{1}\mathbb{1}^\top$, we obtain

$$(nr_o\Pi + r_e\mathcal{J})I + (n\ell_o + \ell_e)\dot{I} = n\Pi V_o, \quad (3.11)$$

where we used $\mathbb{1}^\top I = 0$ and $\mathbb{1}^\top \Pi = 0$. Similarly we have

$$I + \ell_c(nr_o\Pi + r_e\mathcal{J})^{-1}\dot{I} = n(nr_o\Pi + r_e\mathcal{J})^{-1}\Pi V_o,$$

and hence $r_c I + \ell_c \dot{I} = n\Pi V_o$. This equation is analogous to (3.10) and corresponds to a uniform complete graph with identical line resistance $r_c = nr_o + r_e$ and inductance $\ell_c = n\ell_o + \ell_e$.

Note that the algebraic connectivity of the weighted Laplacian \mathcal{L} is $\frac{n}{\tau}$. By Theorem 3.3.1, the inductivity ratio is then computed as

$$\Psi_{\text{NIR}} = \frac{\frac{n}{\tau}\ell_o + \ell}{\frac{n}{\tau}r_o + r} = \frac{\ell_c}{r_c}.$$

■

Case Study: Constant Current Loads

So far, we have considered loads which are connected via power converters. The same definitions and results can be extended to the case of loads modeled with constant current sinks. Consider the graph $\mathcal{G}(\mathcal{V}, \mathcal{E}, \Gamma)$ divided into source (S) and load nodes (L), and decompose the Laplacian matrix accordingly as

$$\mathcal{L} = \begin{bmatrix} \mathcal{L}_{SS} & \mathcal{L}_{SL} \\ \mathcal{L}_{LS} & \mathcal{L}_{LL} \end{bmatrix}.$$

We have

$$rI_S + \ell\dot{I}_S = \mathcal{L}_{SS}V_S + \mathcal{L}_{SL}V_L \quad (3.12)$$

$$rI_L + \ell\dot{I}_L = \mathcal{L}_{LS}V_S + \mathcal{L}_{LL}V_L. \quad (3.13)$$

Suppose that the load nodes are attached to constant current loads $I_L = -I_L^*$. Then from (3.13) we obtain

$$-rI_L^* = \mathcal{L}_{LS}V_S + \mathcal{L}_{LL}V_L,$$

and therefore

$$-r\mathcal{L}_{LL}^{-1}I_L^* - \mathcal{L}_{LL}^{-1}\mathcal{L}_{LS}V_S = V_L. \quad (3.14)$$

Substituting (3.14) into (3.12) yields

$$rI_S + \ell\dot{I}_S = \mathcal{L}_{\text{red}}V_S - r\mathcal{L}_{SL}\mathcal{L}_{LL}^{-1}I_L^*.$$

Here the Schur complement $\mathcal{L}_{\text{red}} = \mathcal{L}_{SS} - \mathcal{L}_{SL}\mathcal{L}_{LL}^{-1}\mathcal{L}_{LS}$ is again a Laplacian matrix known as the *Kron-reduced* Laplacian [72], [138]. Bearing in mind that $V_G = V_o - \ell_o\dot{I}_S - r_oI_S$, the system becomes

$$\begin{aligned} (r\mathcal{J} + r_o\mathcal{L}_{\text{red}})I_S + (\ell\mathcal{J} + \ell_o\mathcal{L}_{\text{red}})\dot{I}_S \\ = \mathcal{L}_{\text{red}}V_o - r\mathcal{L}_{SL}\mathcal{L}_{LL}^{-1}I_L^*, \end{aligned} \quad (3.15)$$

and one can repeat the same analysis as above working with \mathcal{L}_{red} instead of \mathcal{L} . Note that (3.15) matches the model (3.4) with the difference of a constant. As this constant term does not affect the homogeneous solution, the network inductivity and resistivity ratios are obtained analogously as before, where the algebraic connectivity is computed based on the Kron reduced Laplacian. \square

3.3.2 Non-uniform Output Impedances

In this section we investigate the case where output inductances with different magnitudes are connected to the network, and we quantify the network inductivity ratio Ψ_{NIR} under this non-uniform addition. The case with non-uniform resistances can be treated in an analogous manner.

For the sake of simplicity, throughout this subsection, we consider the case where the resistive parts of the output impedances are negligible (see Remark 3.3.7 for relaxing this assumption). Let $D = \text{diag}(\ell_{o_1}, \ell_{o_2}, \dots, \ell_{o_n})$, where ℓ_{o_i} is the (nonzero) output inductance connected to the node i . We have

$$rI + \ell\dot{I} = \mathcal{L}V, \quad V = V_o - D\dot{I},$$

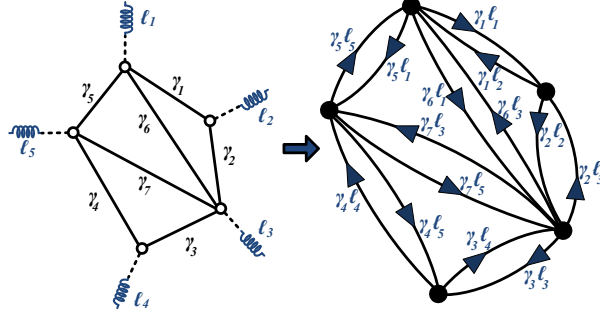


Figure 3.4: Output inductances appear as weights in the corresponding directed graph, with the Laplacian $D\mathcal{L}$.

and hence

$$rI + (\ell\mathcal{J} + \mathcal{L}D)\dot{I} = \mathcal{L}V_o. \quad (3.16)$$

Note that $\mathcal{L}D$ is similar to $D^{\frac{1}{2}}\mathcal{L}D^{\frac{1}{2}}$ and therefore has nonnegative real eigenvalues. In view of equation (3.4), here $R = r\mathcal{J}$ and $L = \ell\mathcal{J} + \mathcal{L}D$. Hence, the matrix $L^{-1}R$ possesses positive real eigenvalues, and Assumption 3.2.2 holds.

The matrix $\mathcal{L}D$ is also similar to $D\mathcal{L}$, which can be interpreted as the (asymmetric) Laplacian matrix of a directed connected graph noted by $\hat{\mathcal{G}}(\mathcal{V}, \hat{\mathcal{E}}, \hat{\Gamma})$ with the same nodes as the original graph $\mathcal{V} = \{1, \dots, n\}$, but with directed edges $\hat{\mathcal{E}} \subset \mathcal{V} \times \mathcal{V}$. As shown in Figure 3.4, in this representation, for any $(i, j) \in \hat{\mathcal{E}}$, there exists a directed edge from node i to node j with the weight $\ell_{o_i}\tau_{ij}^{-1}$ (recall that τ_{ij}^{-1} is the weight of the edge $\{i, j\} \in \mathcal{E}$ of the original graph \mathcal{G}). Hence, the weight matrix $\hat{\Gamma} \in \mathbb{R}^{2m \times 2m}$ is the diagonal matrix with the weights $\ell_{o_i}\tau_{ij}^{-1}$ on its diagonal. Note that the edge set $\hat{\mathcal{E}}$ is symmetric in the sense that $(i, j) \in \hat{\mathcal{E}} \Leftrightarrow (j, i) \in \hat{\mathcal{E}}$, and its cardinality is equal to $2m$. We take advantage of this graph to obtain the network inductivity ratio Ψ_{NIR} , as formalized in the following theorem.

Theorem 3.3.6 [Computing NIR: Non-uniform output impedances]

Consider a homogeneous network with the resistance per length unit r , inductance per length unit ℓ , edge lengths τ_1, \dots, τ_n , and output inductors $\ell_{o_1}, \ell_{o_2}, \dots, \ell_{o_n}$. Then the network inductivity ratio is given by

$$\Psi_{\text{NIR}} = \frac{\lambda_2 + \ell}{r},$$

where λ_2 is the algebraic connectivity of the graph $\hat{\mathcal{G}}(\mathcal{V}, \hat{\mathcal{E}}, \hat{\Gamma})$ defined above.

Proof. Let $\mathcal{L}' = D^{\frac{1}{2}} \mathcal{L} D^{\frac{1}{2}}$. The homogeneous solution to (3.16) is

$$\begin{aligned} I(t) &= e^{-r(\ell\mathcal{J} + \mathcal{L}D)^{-1}t} I_0 \\ &= D^{-\frac{1}{2}} e^{-rD^{\frac{1}{2}}(\ell\mathcal{J} + \mathcal{L}D)^{-1}D^{-\frac{1}{2}}t} D^{\frac{1}{2}} I_0 \\ &= D^{-\frac{1}{2}} e^{-r(\ell\mathcal{J} + \mathcal{L}')^{-1}t} D^{\frac{1}{2}} I_0. \end{aligned}$$

Note that \mathcal{L}' is positive semi-definite and thus $\ell\mathcal{J} + \mathcal{L}'$ is invertible. Bearing in mind that 0 is an eigenvalue of the matrix \mathcal{L}' with the corresponding normalized eigenvector $\mathcal{U}_1 = (\mathbf{1}^\top D^{-1} \mathbf{1})^{-\frac{1}{2}} D^{-\frac{1}{2}} \mathbf{1}$, and by the spectral decomposition $\mathcal{L}' = \mathcal{U} \Lambda \mathcal{U}^\top$, we find that

$$\begin{aligned} I(t) &= D^{-\frac{1}{2}} e^{-r(\mathcal{U}(\ell\mathcal{J} + \Lambda)\mathcal{U}^\top)^{-1}t} D^{\frac{1}{2}} I_0 \\ &= D^{-\frac{1}{2}} \mathcal{U} e^{-r(\ell\mathcal{J} + \Lambda)^{-1}t} \mathcal{U}^\top D^{\frac{1}{2}} I_0 \\ &= D^{-\frac{1}{2}} \begin{bmatrix} \mathcal{U}_1 & \tilde{\mathcal{U}} \end{bmatrix} e^{-r \begin{bmatrix} \frac{1}{\ell} & 0 \\ 0_{(n-1) \times 1} & \tilde{\Lambda} \end{bmatrix} t} \begin{bmatrix} \mathcal{U}_1^\top \\ \tilde{\mathcal{U}}^\top \end{bmatrix} D^{\frac{1}{2}} I_0, \end{aligned}$$

where $\tilde{\Lambda} = \text{diag}\{\frac{1}{\lambda_2 + \ell}, \frac{1}{\lambda_3 + \ell}, \dots, \frac{1}{\lambda_n + \ell}\}$ and $0 < \lambda_2 < \lambda_3 < \dots < \lambda_n$ are nonzero eigenvalues of the matrix \mathcal{L}' . Let $\tilde{I}(t) = D^{\frac{1}{2}} I(t)$. Noting that by the Kirchhoff Law, $\mathbf{1}^\top I_0 = 0$, we have

$$\tilde{I}(t) = \tilde{\mathcal{U}} e^{-r\tilde{\Lambda}t} \tilde{\mathcal{U}}^\top \tilde{I}_0.$$

Since $\mathcal{U}_1^\top \tilde{I}_0 = 0$ we can write \tilde{I}_0 as the linear combination $\tilde{I}_0 = \tilde{\mathcal{U}} X$, $X \in \mathbb{R}^{(n-1) \times 1}$. Now we have

$$\tilde{I}(t) = \tilde{\mathcal{U}} e^{-r\tilde{\Lambda}t} X, \quad \|\tilde{I}(t)\|^2 = X^\top e^{-2r\tilde{\Lambda}t} X.$$

Hence

$$\begin{aligned} \|\tilde{I}(t)\|^2 &\geq e^{-\frac{2r}{\lambda_2 + \ell}t} \|\tilde{I}_0\|^2, \\ \tilde{I}^\top(t) D I(t) &\geq e^{-\frac{2r}{\lambda_2 + \ell}t} \tilde{I}_0^\top D I_0, \\ \|I(t)\| &\geq \mu e^{-\frac{r}{\lambda_2 + \ell}t} \|I_0\|, \end{aligned}$$

where

$$\mu := \sqrt{\frac{\min_i(\ell_{o_i})}{\max_i(\ell_{o_i})}}.$$

This yields $\Psi_{\text{NIR}} = \frac{\lambda_2 + \ell}{r}$. Note that the eigenvalues of \mathcal{L}' and $D\mathcal{L}$ are the same. This completes the proof. \blacksquare

Remark 3.3.7 [Output impedance with non-negligible resistances]

The results of Theorem 3.3.6 can be generalized to the case of non-uniform output impedances, each containing a nonzero resistor r_o and a nonzero inductor ℓ_o in series. In this case, the network can be modeled by

$$(r\mathcal{J} + \mathcal{L}D_r)I + (\ell\mathcal{J} + \mathcal{L}D_\ell)\dot{I} = \mathcal{L}V_o, \quad (3.17)$$

where $D_r := \text{diag}(r_{o_1}, r_{o_2}, \dots, r_{o_n})$ and $D_\ell := \text{diag}(\ell_{o_1}, \ell_{o_2}, \dots, \ell_{o_n})$. Analogously to the proof of Theorem 3.3.6, it can be shown that the network inductivity ratio is calculated as

$$\Psi_{\text{NIR}} = \min_{i \in \{2, 3, \dots, n\}} \frac{\lambda_{\ell_i} + \ell}{\lambda_{r_i} + r},$$

where λ_{ℓ_i} denotes the i th eigenvalue of the matrix $\mathcal{L}D_\ell$, and $\lambda_{\ell_1} = 0$. Similarly, λ_{r_i} denotes the i th eigenvalue of the matrix $\mathcal{L}D_r$, and $\lambda_{r_1} = 0$. \square

Exploiting the results of [85], bearing in mind that \mathcal{L} and D are both positive semi-definite matrices, we have

$$\lambda_2(\mathcal{L}) \min_i \ell_{o_i} \leq \lambda_2(D\mathcal{L}) \leq \lambda_2(\mathcal{L}) \max_i \ell_{o_i}. \quad (3.18)$$

These bounds can be used to ensure that the network inductivity ratio lies within certain values, without explicitly calculating the algebraic connectivity of the directed graph associated with the Laplacian $D\mathcal{L}$.

Optimizing the network inductivity ratio: The results proposed can be also exploited to maximize the diffusion of output impedances into the network. This can be achieved by an optimal distribution of the inductors among the sources such that the network inductivity ratio is maximized. Below is an example illustrating this point on a network with a star topology. Another example using Kron reduction and phasors will be provided in Section 3.4.

Example 3.3.8 [Maximizing the algebraic connectivity of a star graph]

Consider the graph \mathcal{G} with the Laplacian \mathcal{L} , consisting of four nodes in a star topology. The line lengths are 5 pu, 7 pu, and 9 pu, as depicted in Figure 3.5. Note that here again, the weights of the edges are the inverse of the distances. Attach the output impedances $D = \text{diag}\{\ell_{o_1}, \ell_{o_2}, \ell_{o_3}, \ell_{o_4}\}$ to each inverter, and assume that we have limited resources of inductors, namely ⁴

$$\sum_i \ell_{o_i} = c, \quad c \in \mathbb{R}^+. \quad (3.19)$$

⁴Note that the budget constraint (3.19) can also be used to reflect any disadvantage resulting from a large output impedance, e.g., the voltage drop.

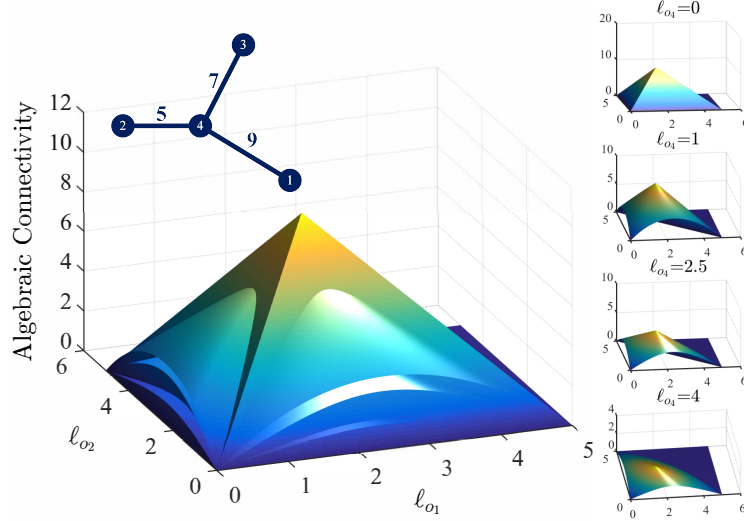


Figure 3.5: Algebraic connectivity of the directed graph associated with the Laplacian $D\mathcal{L}$, where \mathcal{L} is the Laplacian of the star graph shown in top left corner. The budget constraint is $\sum_i l_{o_i} = c = 5\text{mHz}$. On the right, the algebraic connectivity is plotted as a function of l_{o_1} and l_{o_2} for different values of l_{o_4} . Note that $l_{o_3} = c - l_{o_1} - l_{o_2} - l_{o_4}$. On the left, all the four subplots are merged. Clearly, the optimal algebraic connectivity is achieved where no output impedance is used for node 4 (the middle node), and $l_{o_1} = 2.20\text{mHz}$, $l_{o_2} = 1.23\text{mHz}$, $l_{o_3} = 1.57\text{mHz}$ are used for nodes 1, 2, and 3 respectively.

Figure 3.5 shows different values of the second smallest eigenvalue of the matrix $D\mathcal{L}$. We obtain that the maximal algebraic connectivity is achieved when no output impedance is used (wasted) for the node in the middle. Interestingly, the optimal value of output inductor for each node is proportional to its distance to the middle node.

Next we compare the performance of the droop controlled inverters in two different cases: i) the network with the optimized output impedances as above, and ii) the network with evenly distributed output impedances. To this end, suppose that a source is connected to the middle node (node 4 in Figure 3.5), and three constant power loads are connected to the outer nodes (nodes 1, 2, and 3 in Figure 3.5) via droop-controlled power converters with the parameters given by Table 7.1. Here, all the distribution lines are assumed to have the same reactance per length equal to $\omega\ell = 1.0 \frac{\Omega}{\text{km}}$ and resistance per length equal to $r = 0.1 \frac{\Omega}{\text{km}}$. At time $t = 0$, the loads are increased with 10% of their nominal value. The frequency of the inverters are shown in Figure 3.6. It is evident that the droop controllers perform better in the network with the optimized network inductivity ratio Ψ_{NIR} (top), compared to the case of

Table 3.1: Simulation Parameters

	Load ₁	Load ₂	Load ₃	Source
Measurement Delay (ms)	6	6	5	8
Droop Coefficient (pu)	0.07	0.14	0.14	0.28
Distance from the Source (m)	90	50	70	-
Voltage (pu)	1.05	1.10	0.95	0.96
Nominal Active Power (pu)	-0.9	-0.8	-1.2	1.5

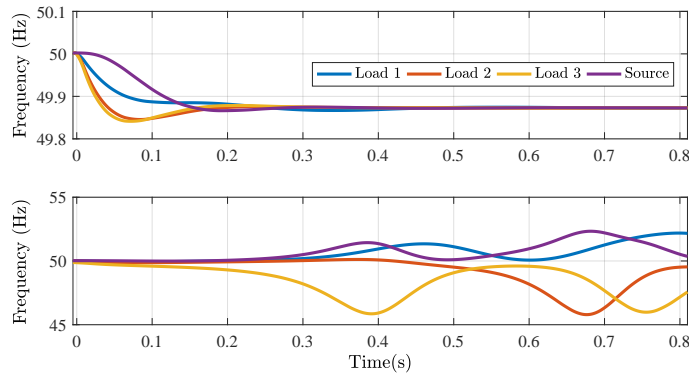


Figure 3.6: Comparison of droop controllers performance between the network with the optimized Ψ_{NIR} (top), and a network with evenly distributed output inductances (below).

evenly distributed output inductances (below), where the solutions fail to converge. \square

The results of this subsection for non-uniform output impedances allow for the analysis of the networks containing non-tunable output impedances, *e.g.*, constant impedance loads and synchronous generators/motors which can be modeled as a voltage source/sink behind a reactance. The optimization (and maximization of the algebraic connectivity) in this case involves only tuning the diagonal elements of the matrices D_r and D_l in (3.17) associated with the tunable output impedances.

3.4 Kron Reduction in Phasor Domain and the Network Inductivity Ratio

By leveraging Kron reduction, to eliminate the internal nodes (empty nodes in Figure 3.7), and using the phasor domain, it is sometimes possible to synthesize an RL circuit

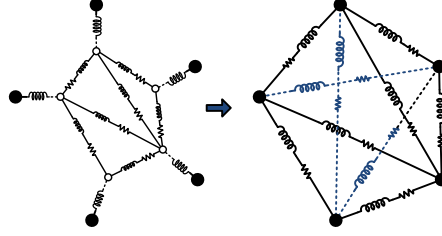


Figure 3.7: Kron reduction of an arbitrary graph with added output impedances.

for the augmented network model (3.4); see [149] for more details. As depicted in Figure 3.7, in the Kron reduced graph some of the edges coincide with the lines of the original network into which the output impedances were diffused, while others (dotted line) are created as a result of the Kron reduction. We refer to the former as *physical* and to the latter as *virtual* lines. To derive the Kron-reduced model, we first write the nodal currents as

$$\begin{bmatrix} I \\ 0 \end{bmatrix} = \begin{bmatrix} y_o \mathcal{J} & -y_o \mathcal{J} \\ -y_o \mathcal{J} & y_o \mathcal{J} + y_\ell \mathcal{L} \end{bmatrix} \begin{bmatrix} V_o \\ V \end{bmatrix},$$

where

$$y_o = \frac{1}{j\omega\ell_o}, \quad y_\ell = \frac{1}{r + j\omega\ell}.$$

The Kron-reduced model is then obtained as

$$\mathcal{Y}_{\text{red}} = y_o \left[\mathcal{J} - \left(\mathcal{J} + \frac{y_\ell}{y_o} \mathcal{L} \right)^{-1} \right]. \quad (3.20)$$

Since every path between the outer nodes of the graph passes only through internal nodes (see Figure 3.7), the resulting Kron-reduced network is a complete graph [40]. In the following example, we compare the line phase angles

$$\theta_{ij} := \arctan \frac{\text{Im}(1/\mathcal{Y}_{\text{red},ij})}{\text{Re}(1/\mathcal{Y}_{\text{red},ij})}$$

for the line $\{i, j\}$, to the phase angles suggested by Ψ_{NIR} , namely

$$\theta_{\text{NIR}} := \arctan(\omega\Psi_{\text{NIR}}). \quad (3.21)$$

Note that the term ω in the above is included to obtain reactance to resistance ratio from inductance to resistance ratio.

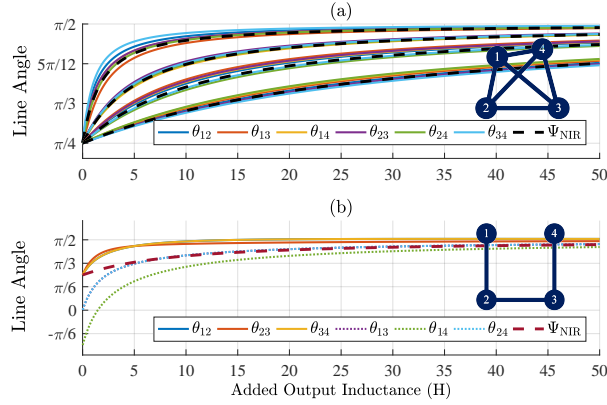


Figure 3.8: (a) Complete graph. The initial phase angle of the lines is $\frac{\pi}{4}$ and the line lengths are the following 4 cases (from top to bottom): $[\tau_{12}, \tau_{13}, \tau_{14}, \tau_{23}, \tau_{24}, \tau_{34}] = [5, 6, 9, 7, 4, 6]$; $[20, 19, 20, 21, 20, 22]$; $[40, 37, 35, 49, 46, 38]$; $[100, 105, 93, 87, 110, 89]$; (b) Path graph. Virtual lines are shown by dots. The initial phase angle of the lines is $\frac{\pi}{4}$ and the line lengths are equal to 5.

Example 3.4.1 [Line angles of a Kron-reduced Graph with uniform output impedances]

(a) Consider a 4-node complete graph with different distribution line lengths. As shown in Figure 3.8a, the proposed measure matches with the overall behavior of the line angles as the added output inductance increases. (b) Consider a 4-node uniform path graph. Figure 3.8b shows that the least inductivity behavior is observed for the virtual lines. Hence the less virtual lines the reduced graph contains, the more output impedance diffuses in the network, which is consistent with our results in Section 3.3. Also note that the inductance and resistance possess negative values at some edges for certain values of the output impedance. Therefore, it is difficult to extract a reasonable inductivity ratio for those edges from the Kron reduced phasor model. On the contrary, the proposed inductivity measure remains within the physically valid interval $\arctan(\omega\Psi_{\text{NIR}}) \in [0, \pi/2]$. \square

Example 3.4.1 shows that θ_{NIR} can be used as a measure that estimates the phase of the lines of the overall network. A desired amount of change in this measure can be optimized by appropriate choices of output impedances. The following example illustrates this case.

Example 3.4.2 [Output impedance optimization on the IEEE 13 node test feeder]

Figure 3.9 depicts the graph of the islanded IEEE 13 node test feeder. Here, all the distribution lines are assumed to have the same reactance per length equal to $\omega\ell = 1.2\frac{\Omega}{\text{mile}}$ and resistance per length equal to $r = 0.7\frac{\Omega}{\text{mile}}$, derived from the

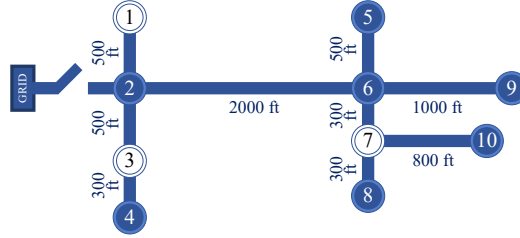


Figure 3.9: Schematic of the islanded IEEE 13 node test feeder graph. Power sources are connected to the (white) nodes 1, 3, and 7.

configuration 602 [39]. We consider the case where three inverters are connected to the nodes 1, 3, and 7, and the rest of the nodes are connected to constant current loads. After carrying out Kron reduction, the algebraic connectivity of the resulting Laplacian matrix is equal to 3.1. Before adding the output inductances, θ_{NIR} is equal to $\arctan \frac{\omega \ell}{r} = \frac{2\pi}{3}$. Based on the results of Theorem 3.3.1, for a 10% increase in θ_{NIR} , a uniform inductor of 3.21mH should be attached to the outputs of all the sources. However, in case non-uniform output inductors are to be used, by using the result of Theorem 3.3.6, the same increase in the network inductivity ratio can be achieved (optimally) with 0.95mH, 0.95mH, and 4.35mH inductors, for the nodes 1, 3, and 7 respectively. Both cases are feasible in practice since the typical values for inverter output filter inductance and implemented output virtual inductance range from 0.5mH to 50mH [18, 60, 62, 65, 71, 74, 84, 87]. However, note that the total inductance used in the (optimal) non-uniform case is considerably smaller than the one used in the uniform scheme. \square


3.5 Conclusion

In this chapter, the influence of the output impedance on the inductivity and resistivity of the distribution lines has been investigated. Two measures, network inductivity ratio and network resistivity ratio, were proposed and analyzed without relying on the ideal sinusoidal signals assumption (phasors). The analysis revealed the fact that the more connected the graph is, the more output impedance diffuses into the network, and the larger its effect will be. We have provided examples on how the impact of inductive output impedances on the network can be maximized in specific network topologies. We compared the proposed measure to the phase angles of the lines in a phasor-based Kron reduced network. Results confirm the validity and the effectiveness of the proposed metrics.

Chapter 4

Power Network Architecture: A communication-less master-slave microgrid

“The single biggest problem in communication is the illusion that it has taken place.”
– George Bernard Shaw

 NETWORK architecture plays an important role in stability and reliability of a power network. In this chapter, a design of a master-slave microgrid consisting of *grid-supporting* current source inverters and a synchronous generator is proposed. The inverters follow the frequency of the grid that is imposed by the synchronous generator. Hence, the proposed structure of the microgrid is steadily synchronized. We show that this method achieves power sharing without the need of any communication. Furthermore, no change in operation mode is needed during transitions of the microgrid, between islanded and grid-connected modes.

4.1 Introduction

As discussed in Chapter 1, a microgrid typically includes both synchronous generators and inverters. Inverters are divided into three categories. The first category, *grid-forming* inverters, act as voltage sources with fixed frequency and amplitude. In case the microgrid disconnects from the main grid and goes to the so-called *islanded mode*, these inverters can provide a reference for the voltage frequency. However, an islanded microgrid consisting of only grid-forming inverters suffers from poor power sharing and destructive interference (antiphases). In particular, one voltage source might bear a high percentage of the load, while the others provide a lower share of power. Furthermore, phase differences might lead to extreme voltage attenuation. *Grid-feeding* inverters form the second category, working as current sources following the frequency of the network. These sources are capable of injecting either a constant or a time-varying power regardless of the network load, *e.g.*, by the Maximum Power

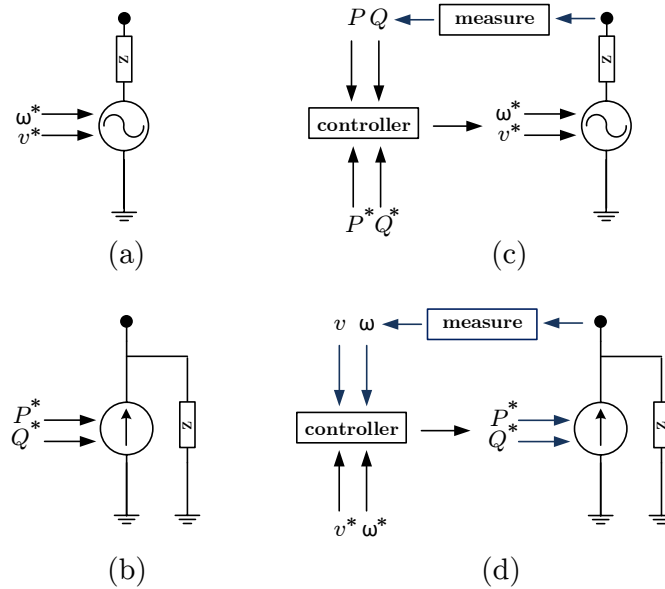


Figure 4.1: Inverter Categories; (a) Grid-Forming; (b) Grid-Feeding; (c) Grid-Supporting Voltage Source; (d) Grid-Supporting Current Source

Point Tracking (MPPT) method. Inverters of this type are extensively used in the wide area electrical power networks. The third category contains sources that are designed to contribute to the regulation and stability of the microgrid, which are called *grid-supporting*. This category includes both the Voltage Source Inverter (VSI) and the Current Source Inverter (CSI). Grid-supporting VSIs measure the active and reactive power they inject to the grid and determine the output voltage amplitude and frequency according to these measured values. Counter-wise, grid-supporting CSIs measure the voltage amplitude and frequency, in order to inject a desired amount of active and reactive power accordingly. Figure 1 depicts the inverter categories (for further discussion see [114]).

Controlling the grid-supporting inverters acting as VSI is mostly carried out by the design of a controller such that the sources artificially mimic the behavior and dynamics of a synchronous generator; *i.e.*, in case of a mismatch between the measured electrical output power and its nominal value, the frequency of the inverter deviates from the nominal value. In particular, droop controllers are well known to generate such a behavior. Similar to synchronous generators, these inverters are capable of *self-regulation* and therefore the network consisting of these inverters synchronize in frequency [124], [118], [91]. Furthermore, the power injection of such

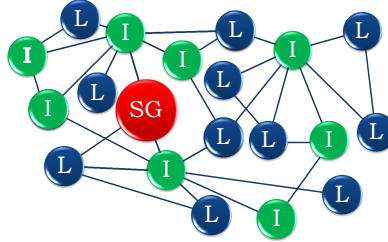


Figure 4.2: The proposed structure consists of a synchronous generator (SG) and a number of inverters (I) and power loads (L), with any arbitrary (connected) topology.

sources are shared proportional to the droop coefficients.

While a large number of articles have focused on VSI, few have investigated the deployment of the grid-supporting inverters acting as a CSI [114], [108], [113], which are the key components in our proposed microgrid design. These devices are capable of injecting, dynamically, the electrical power, while they are following the frequency of the grid. Current source inverters inject active and reactive currents according to the rotating frame of the grid voltage at their point of connection. Therefore they need a voltage source online in the grid to follow its frequency. Controlling a grid with such a scheme has been first suggested by [30] for operation of parallel uninterruptible power systems. However, the approach is not considered suitable for distributed generation (microgrid) mainly due to high communication requirements and the needs for supervisory control and extra cabling [64].

In this chapter, we propose a microgrid structure, consisting of one synchronous generator, or equivalently a droop-controlled VSI, as the main power source, and a number of grid-supporting CSIs; see Figure 4.2. During the islanded mode, inverters follow the frequency of the grid which is determined by the synchronous generator. Such a system design is close to a master-slave architecture yet without communication. Furthermore, using this architecture, no switching is needed to go through the transition from grid-connected to islanded mode and vice versa, and merely synchronizing the synchronous generator phase with the main grid suffices for going back to the grid-connected mode. In the case of the main generator failure, the so-called *tertiary control* can switch the master to another generator, similar to *high-crest current* method; see [56]. We show that our proposed system is stable and maintains power sharing, in an optimized manner. As a step towards practical applicability, an implementation of the proposed inverter is provided.

There are three main advantages of the proposed architecture over conventional droop-controlled VSIs. First, the voltage frequency of all sources are synchronized at all times, while droop-controlled VSIs located at different nodes, generate different

frequencies. Second, secondary control can be achieved without the need to any communication. In fact, we take advantage of the information embedded in frequency deviation as a result of the intrinsic droop characteristic of a synchronous generator avoiding further communication. Finally, there are physical advantages of using current source inverters over voltage source inverters such as smoother DC-side current, longer lifetime of energy storage, inherent voltage boosting capability, and lower costs [35].

This chapter is organized as follows: In Section 4.2, the structure and the control technique are elaborated. A model is suggested for the proposed microgrid and the system stability with the designed controller is investigated. Next, power sharing of the sources and cost optimization are discussed. In Section 4.3, an implementation of the proposed grid-supporting inverter is provided. Section 4.4 provides simulation results of the implemented model, and finally, Section 4.5 concludes this chapter.

4.2 Proposed Architecture and Control Technique

We propose an architecture for the microgrid, which contains a synchronous machine and multiple CSI inverters. This network is represented by a connected and undirected graph $\mathcal{G}(\mathcal{V}, \mathcal{E})$. The nodes $\mathcal{V} = \{1, \dots, n\}$ represent grid supporting inverters, a synchronous generator, and constant power loads, and the edges $\mathcal{E} \subset \mathcal{V} \times \mathcal{V}$ account for distribution lines. The nodes are partitioned as $\mathcal{V} = \mathcal{V}_G \cup \mathcal{V}_I \cup \mathcal{V}_L$, where \mathcal{V}_G , \mathcal{V}_I , and \mathcal{V}_L correspond to the synchronous generator, inverters, and loads respectively. We also denote the cardinality of \mathcal{V}_L and \mathcal{V}_I with n_I and n_L .

4.2.1 Model

We use the classical *swing equation* as the model of the synchronous generator [78]¹

$$M\dot{\omega} + D\omega = P_m - P_e, \quad (4.1)$$

where $M > 0$ is the moment of inertia,² $\omega \in \mathbb{R}$ is the frequency deviation from the nominal frequency, $D > 0$ is the damping coefficient, and P_m and P_e are the mechanical (input) and electrical (output) power respectively. The model (4.1) indicates that in case of a mismatch between mechanical power and electrical power, the synchronous generator rotor speed, as well as the voltage frequency, deviates from the nominal value.

¹Droop-controlled voltage source inverter can be modeled with similar dynamics; see [118].

²To be more precise, M is not the moment of inertia, but the *angular momentum at the nominal frequency*; see Section 5.2 later on.

Let $P_{I_i}, P_{L_i} > 0$ denote the injected power of the inverter and the power consumption of the load at node i . We propose the following model for the aforementioned microgrid structure:

$$\begin{aligned} M\dot{\omega} + D\omega &= P_G^* + u - P_e \\ P_{I_i} &= P_{I_i}^* + \Upsilon_i \\ P_{L_i} &= P_{L_i}^* + \delta_{L_i} \end{aligned} \quad (4.2)$$

together with the coupling equality

$$P_e + \sum_{i=1}^{n_I} P_{I_i} - \sum_{i=1}^{n_L} P_{L_i} = 0, \quad (4.3)$$

where $u \in \mathbb{R}$ is the control input of the synchronous generator, $\Upsilon_i \in \mathbb{R}$ is the control input of the inverter at node i , and $\delta_{L_i} \in \mathbb{R}$, is the (constant) deviation from the nominal power consumption. We assume that voltage magnitudes at each node in the network are constant and the reactive power injection at each node is identically zero. We also assume that all line reactances are assumed to be sufficiently low, that the network can be treated as a *supernode*. Note that the internal dynamics of P_e, P_I , and P_L are not crucial for our analysis and their coupling equality (4.3), represents the law of conservation of energy. Here, the distribution lines are assumed to be purely inductive implying that there is no active power dissipation in the distribution lines. We opt for nominal power values $P_G^*, P_{I_i}^*$, and $P_{L_i}^*$ that satisfy the power balance, *i.e.*,

$$P_G^* + \sum_{i=1}^{n_I} P_{I_i}^* - \sum_{i=1}^{n_L} P_{L_i}^* = 0. \quad (4.4)$$

The system (4.2) can be written in compact form as

$$M\dot{\omega} + D\omega = P_G^* + u - P_e \quad (4.5)$$

$$P_I = P_I^* + \Upsilon \quad (4.6)$$

$$P_L = P_L^* + \delta_L, \quad (4.7)$$

where $\Upsilon \in \mathbb{R}^{n_I}$ and $\delta_L \in \mathbb{R}^{n_L}$ are the inverter control input and load power, and represent the deviations from the nominal power values. We consider the power sharing vector $\xi \in \mathbb{R}^{n_I}$ to set the power injections of inverter controllers proportionally, *i.e.*, $\frac{\Upsilon_i}{\Upsilon_j} = \frac{\xi_i}{\xi_j}$. Without any loss of generality we assume that

$$\mathbf{1}^\top \xi = 1. \quad (4.8)$$

Hence, we rewrite Υ as

$$\Upsilon = v\xi, \quad (4.9)$$

where $v \in \mathbb{R}$ is the common control signal for all inverters and is to be designed later. Bearing in mind (4.6), (4.7), and (4.9), from (4.3) we have

$$P_e = \mathbf{1}^\top (P_L^* + \delta_L) - \mathbf{1}^\top (P_I^* + v\xi) .$$

By substituting this into (4.5), and using (4.8) we have

$$M\dot{\omega} + D\omega = P_G^* + u - \mathbf{1}^\top (P_L^* + \delta_L) + \mathbf{1}^\top P_I^* + v .$$

Finally, according to (4.4)

$$M\dot{\omega} + D\omega = u + v - \mathbf{1}^\top \delta_L . \quad (4.10)$$

This indicates that the controllers at the inverter nodes are aligned with the action of the synchronous generator controller. Note that the delays in the Phase Locked Loop (PLL) and Pulse Width Modulation (PWM) switchings are ignored and hence the frequency following feature of inverters is assumed to be instantaneous. Therefore, the frequency ω has the same value at all nodes.

4.2.2 Controller Design

Using an integral controller for the synchronous generator and proportional integral controllers for the inverters,³ we have:⁴

$$\dot{\chi} = \omega, \quad u = -\alpha\chi, \quad v = -\gamma\omega - \beta\chi . \quad (4.11)$$

Now, the system (4.10) can be described as

$$\begin{aligned} M\dot{\omega} + (D + \gamma)\omega &= \tilde{u} - \mathbf{1}^\top \delta_L \\ \dot{\chi} = \omega, \quad \tilde{u} &= -(\alpha + \beta)\chi . \end{aligned} \quad (4.12)$$

Proposition 4.2.1 [Stability]

For any $\alpha, \beta, \gamma > 0$, the equilibrium $(\omega, \chi) = (0, -(\alpha + \beta)^{-1}(\mathbf{1}^\top \delta_L))$ of system (4.12) is globally asymptotically stable (GAS).

Proof. Consider the (*shifted*) candidate Lyapunov function $W = \frac{1}{2}M\omega^2 + \frac{1}{2}(\alpha + \beta)(\chi - \bar{\chi})^2$. We have $\dot{W} = -(D + \gamma)\omega^2$. Observe that W is radially unbounded and has a strict minimum at $(0, -(\alpha + \beta)^{-1}(\mathbf{1}^\top \delta_L))$. By invoking LaSalle's invariance principle, the solutions converge to the largest invariant set for the system (4.12) *s.t.* $\omega = 0$. On

³A proportional controller for the synchronous generator can be included in D .

⁴Although the integral of the voltage frequency can be interpreted as the voltage phase, we avoid denoting it by θ , since here χ is a control variable and is not bounded to $[0, 2\pi)$.

this set, we have $\chi = -(\alpha + \beta)^{-1}(\mathbf{1}^\top \delta_L)$. This shows that all the solutions on the invariant set converge to the equilibrium $(0, -(\alpha + \beta)^{-1}(\mathbf{1}^\top \delta_L))$. This completes the proof. ■

Note that in the sense of architectural control, the goals of *primary* and *secondary* controls are achieved simultaneously. Contrary to the presented architecture, using integral controllers in the secondary control layer of a microgrid with conventional droop-controlled VSIs, fails to maintain load sharing [41] and is not considered a long time stable solution [56]. Here, the output power is regulated according to the frequency deviation of the grid, while in a droop-controlled voltage source inverter, the frequency is regulated according to the deviation from the nominal output power value. The advantage here is that the power network remains synchronized at all times. □

4.2.3 Power Sharing

Between Synchronous Generator and Inverters

Proposition 4.2.1 shows that, in the steady state, the deviations from the nominal power will be shared according to the ratio α/β ratio between the synchronous generator and the inverters:

$$\bar{u} = \left(\frac{\alpha}{\alpha + \beta}\right)\mathbf{1}^\top \delta_L, \quad \bar{v} = \left(\frac{\beta}{\alpha + \beta}\right)\mathbf{1}^\top \delta_L, \quad \frac{\bar{u}}{\bar{v}} = \frac{\alpha}{\beta}.$$

Hence, if the ratio α/β is set equal to the ratio of the nominal power of the synchronous generator to the sum of the inverter nominal power values, *i.e.*, $\frac{\alpha}{\beta} = \frac{P_G^*}{\sum_{i=1}^{n_I} P_{I,i}^*}$,

we have

$$\frac{P_G^* + \bar{u}}{\sum_{i=1}^{n_I} P_{I,i}^* + \bar{v}} = \frac{\alpha}{\beta},$$

which implies that the total power injections remain proportional in the steady state.

Between Inverters

The proposed inverters increase/decrease the power injection till the frequency of the microgrid is regulated and hence reach the steady state $\omega = 0$. The changes in power injections are shared according to the sharing vector ξ . Provided that some costs are assigned to the power injections of the inverters, optimization methods can be employed to minimize the energy cost. Here, we show that by a proper choice of

sharing vector ξ cost optimization can be achieved. We consider the quadratic cost function

$$C(\tilde{\Upsilon}) = \frac{1}{2} \tilde{\Upsilon}^\top \Lambda \tilde{\Upsilon},$$

where $\Lambda \in \mathbb{R}^{n_I}$ is a diagonal matrix of cost coefficients assigned to each node (inverter). By Proposition 4.2.1, at steady-state we have

$$\tilde{\Upsilon} = \frac{\beta}{\alpha + \beta} \mathbf{1}^\top \delta_L \xi.$$

Bearing in mind that $\mathbf{1}^\top \xi = 1$, we have $\mathbf{1}^\top \tilde{\Upsilon} = \frac{\beta}{\alpha + \beta} \mathbf{1}^\top \delta_L$. To minimize the Lagrangian function

$$L = \frac{1}{2} \tilde{\Upsilon}^\top \Lambda \tilde{\Upsilon} + \mu (\mathbf{1}^\top \tilde{\Upsilon} - \frac{\beta}{\alpha + \beta} \mathbf{1}^\top \delta_L),$$

we have

$$\mu = -\frac{\beta}{\alpha + \beta} \frac{\mathbf{1}^\top \delta_L}{\mathbf{1}^\top \Lambda^{-1} \mathbf{1}}.$$

Hence,

$$\tilde{\Upsilon} = \frac{\beta}{\alpha + \beta} \frac{\mathbf{1}^\top \delta_L}{\mathbf{1}^\top \Lambda^{-1} \mathbf{1}} \Lambda^{-1} \mathbf{1}.$$

In accordance with (4.9), the vector $\tilde{\Upsilon}$ can be rewritten as

$$\tilde{\Upsilon} = \left(\frac{\beta}{\alpha + \beta} \mathbf{1}^\top \delta_L \right) \xi_{\text{opt}} \quad (4.13)$$

where

$$\xi_{\text{opt}} = \frac{1}{\mathbf{1}^\top \Lambda^{-1} \mathbf{1}} \Lambda^{-1} \mathbf{1}. \quad (4.14)$$

Noting that (4.14) satisfies (4.8), any solution to system (4.12) is such that the corresponding inverter power injection $\Upsilon = v \xi_{\text{opt}}$ asymptotically converges to the optimal power injection (4.13). Note that various parameters can be interpreted as cost: Nominal power values (power ratings) [29], State of Charge (Soc) in storage systems [57], insolation level in photovoltaic (PV) systems, or wind power in wind turbines. Alike the established droop methods, these values can be transmitted to the nodes via a low-bandwidth communication (tertiary control).

Provided that the inverse of nominal power values are considered as cost coefficients, *i.e.*, $P_I^* = \Lambda^{-1} \mathbf{1}$, we have

$$\xi_{\text{opt}}^* = \frac{P_I^*}{\sum_{i=1}^{n_I} P_I^*}.$$

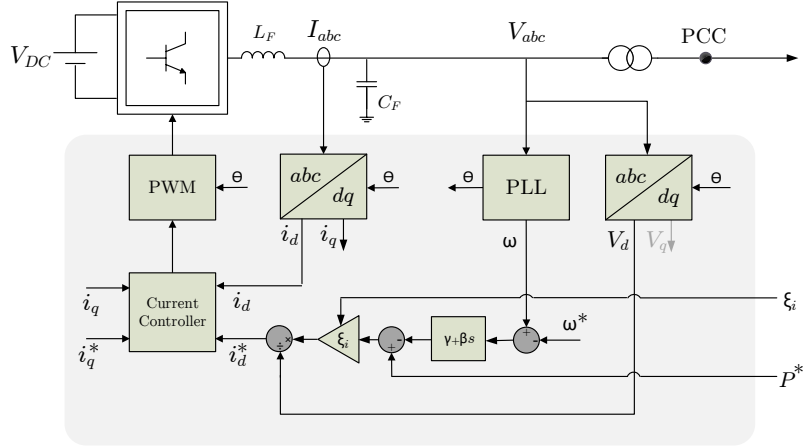


Figure 4.3: Implementation of the Proposed Grid-Supporting Inverter

Therefore

$$\frac{P_{I_i}}{P_{I_j}} = \frac{P_{I_i}^* + \Upsilon_i}{P_{I_j}^* + \Upsilon_j} = \frac{\xi_{\text{opt}_i}^*}{\xi_{\text{opt}_j}^*}.$$

This implies that in this case, the total power injections (nominal+deviation) of inverters remain proportional.

4.3 Implementation

Figure 2 depicts an implementation of the proposed grid-supporting current source inverter. The structure is similar to the CSI schematic provided in [114] with modifications in order to accommodate generating the desired current value (denoted by i^*).

The instantaneous power delivered by the inverter can be written as [1]

$$P = v_d i_d + v_q i_q, \quad (4.15)$$

where v_d, v_q and i_d, i_q are the direct and quadrature components of output current and voltage, in result of the $dq0$ transformation. Since the rotating frame is synchronized with the voltage by the phase locked loop (PLL), the quadrature component v_q is kept zero. Hence, (4.15) reads as

$$P = v_d i_d. \quad (4.16)$$

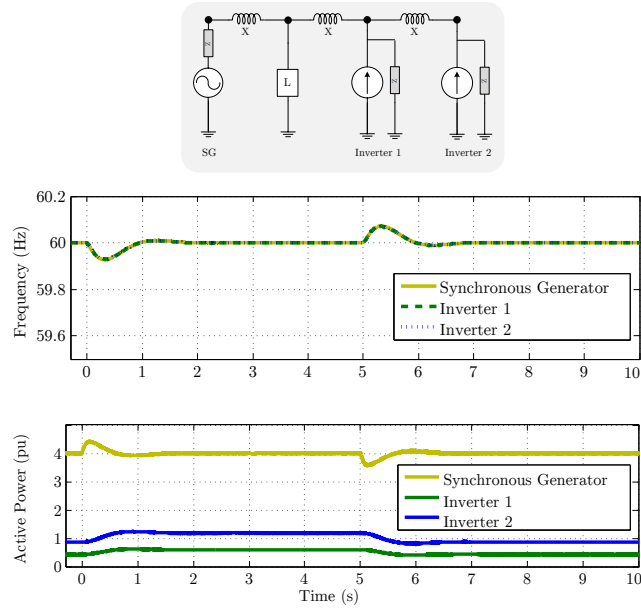


Figure 4.4: Simulation Schematic and Results

Bearing in mind that the output voltage v_d is assumed to be constant, the output power can be tuned by i_d :

The PLL measures the frequency, and the deviation from the nominal frequency is given as an input to the PI controller. The output is then added to the nominal power value P^* , assigned a gain proportional to the power sharing, and divided by v_d to generate the desired current $i_d^* = \frac{1}{v_d}(P_i^* + \Upsilon_i)$. PI controllers are used in the current controller block to set the output current i_d to i_d^* .

4.4 Simulation

The performance of the implementation model is simulated in SimPowerSystems. A synchronous generator is connected to two current source inverters in series via inductive lines. Here, the control input of the main generator is assumed to be constant ($\alpha = 0$). Figure 4.4 depicts output frequencies and output power of the sources. At $t = 0$ the load increases by 10% of its nominal value and again goes back to the nominal at $t = 5$. It can be observed that the inverters modify their output power proportional to the sharing vector xi , and the frequency is regulated to the

nominal value.

The parameters (per unit) used in this simulation are as follows: Synchronous Generator: $M = 0.1$, $D = 0.05$, $P_G^* = 1$, $u = 3$; Inverters: $\gamma = 0.15$, $\beta = 1.5$, $P_I^* = 1.5$, $\xi_1 = \frac{1}{3}$, $\xi_2 = \frac{2}{3}$; Load: $P_L^* = 5.5$, $\delta_L = 0.55$; Line Reactance: $X = 0.12$.

4.5 Conclusion

A microgrid with a master-slave architecture was proposed in which a synchronous generator acts as the master and grid-supporting current source inverters act as the slaves. A model is provided for this system and its stability is guaranteed by PI controllers. Furthermore, an implementation for the proposed inverter is provided. Results show that the proposed architecture achieve (optimized) power sharing and frequency regulation without the need to any communication.

Chapter 5

Power Sources I: Modeling Synchronous Generators with Improved Swing Equation

“Life swings like a pendulum backward and forward, between pain and boredom.”

– Arthur Schopenhauer



IN this chapter, we investigate the properties of an improved swing equation model for synchronous generators. This model is derived by omitting the main simplifying assumption of the conventional swing equation. We carry out a nonlinear analysis for the stability and frequency regulation, and provide region of attraction estimates for two scenarios. First we study the case where a synchronous generator is connected to a constant power load. Second, we inspect the case of a single machine connected to an infinite bus. Finally, the different behaviors of the conventional and improved swing equations are depicted by numerical simulations.

5.1 Introduction

As mentioned in Chapter 1, a major challenge for control of microgrids is the unpredictable sudden variations in power demand and supply. Hence designing controllers for the electrical sources that bear such perturbations, calls for rethinking of the accuracy of the models that were (mostly) valid for the classical electrical systems.

Despite the extensive advances in extracting energy from renewable sources, synchronous generators are still the main supplier of the implemented microgrids; see, *e.g.*, [120, 131, 151]. Therefore, to assure stability and frequency regulation of the power grid, it appears crucial to investigate the accuracy of the electrical and dynamical models of these machines. While a large number of articles have exploited the classical *swing equation* as the model for the synchronous generator, a few have recently brought up doubts about its accuracy and validity, and proposed models of

higher accuracy [24, 25, 50, 101, 102, 143, 160]. Although some promising models are provided [50], [101], the use of such models in power networks is rather complicated.

In this chapter, we provide a nonlinear analysis for an improved yet easy-to-use swing equation to fulfill higher accuracy in analysis and modeling of the synchronous generator that can also be exploited in small-scale networks. We first explicate the contradicting assumptions in obtaining the conventional swing equation, and elaborate deriving the improved model. In Section III, as the first scenario, we look into the properties of the model when the generator is connected to a Constant Power Load (CPL), and provide an estimate of the region of attraction through nonlinear analysis. Further in Section IV, the second scenario, which is mainly referred to as *Single Machine Infinite Bus* (SMIB), is investigated. We provide analytical estimates of the region of attraction for both conventional and improved swing models in this case. Finally, simulations are provided to compare the models.

5.2 Conventional and Improved Swing Equations

The mechanical dynamics of the synchronous generator reads as [78]

$$J\dot{\omega} + D_d(\omega - \omega^*) = \tau_m - \tau_e, \quad (5.1)$$

where $\omega \in \mathbb{R}_{>0}$ is the rotor shaft velocity (mechanical rad/s), $J > 0$ is the total moment of inertia of the turbine and generator rotor ($kg\ m^2$), $\omega^* > 0$ is the angular velocity associated with the nominal frequency (50or60Hz),¹ $\tau_m \in \mathbb{R}_{>0}$ is the net mechanical shaft torque ($N\ m$), $\tau_e \in \mathbb{R}_{>0}$ is the counteracting electromagnetic torque ($N\ m$), and $D_d > 0$ is the damping-torque coefficient ($N\ m\ s$). The mechanical rotational loss due to friction is ignored. Bearing in mind that $\tau_m = \frac{P_m}{\omega}$ and $\tau_e = \frac{P_e}{\omega}$ we can model the synchronous generator as

$$J\omega\dot{\omega} + D_d\omega(\omega - \omega^*) = P_m - P_e, \quad (5.2)$$

where P_m and P_e are the mechanical (physical input) and electrical (physical output) power respectively.

In the conventional swing equation, $J\omega$ and $D_d\omega$ are approximated by constants $M = J\omega^*$ and $A = D_d\omega^*$.

$$M\dot{\omega} + A(\omega - \omega^*) = P_m - P_e, \quad (5.3)$$

where $M > 0$ is the angular momentum associated with the nominal frequency, and $A > 0$ is the (new) damping coefficient. In other words, the swing equation is derived

¹The assumption here is that ω^* is fixed by the network.

supposing that $\omega = \omega^*$. Such an assumption is in contradiction with the proof of stability and frequency regulation of the synchronous generator. Therefore we adhere to the equation (5.2) and try to investigate the stability and frequency regulation through a nonlinear approach. This model has been first suggested by [160], where however, the stability of the synchronous generator (connected to an infinite bus) was analyzed with the small-signal (linearization) techniques. Consistently with [160], we refer to (5.2) as the *improved swing equation*.

5.3 Synchronous Generator Connected to a Constant Power Load (CPL)

In this scenario, we assume that both the injected and extracted power (P_m and P_e) are constant.

5.3.1 Stability

Let $\bar{\omega} \in \mathbb{R}$ be an equilibrium of (5.2). Then, clearly

$$D_d \bar{\omega} (\bar{\omega} - \omega^*) = P_m - P_e . \quad (5.4)$$

The equation above admits two (distinct) real solutions if and only if

$$P_m - P_e > -\frac{1}{4} D_d \omega^{*2} , \quad (5.5)$$

which will be a standing assumption in this section. Under this assumption, we obtain the following two equilibria for system (5.2):

$$\bar{\omega}_s = \frac{\omega^* + \sqrt{\Delta}}{2} , \quad \bar{\omega}_u = \frac{\omega^* - \sqrt{\Delta}}{2} , \quad (5.6)$$

where

$$\Delta := \omega^{*2} + 4 \frac{P_m - P_e}{D_d} . \quad (5.7)$$

Note that $\Delta > 0$ by (5.5). Observe that

$$\bar{\omega}_s > \bar{\omega}_u , \quad (5.8)$$

$$\bar{\omega}_u = \omega^* - \bar{\omega}_s . \quad (5.9)$$

First, we show that $\bar{\omega}_s$ is locally stable and $\bar{\omega}_u$ is locally unstable. For the moment, we assume that the set $\mathbb{R}_{>0}$ is positive invariant for the system (5.2), and $\omega(0) > 0$.

We will relax this assumption later, once a Lyapunov argument is provided. Now, let dynamics (5.2) be rewritten as $\dot{\omega} = f(\omega)$, where

$$f(\omega) = \frac{1}{J} \left(-D_d(\omega - \omega^*) + \frac{P_m - P_e}{\omega} \right).$$

We have

$$\frac{\partial f}{\partial \omega} = \frac{1}{J} \left(-D_d - \frac{P_m - P_e}{\omega^2} \right).$$

By using (5.4) and (5.9), we find that

$$\frac{\partial f}{\partial \omega} = \frac{D_d}{J} \left(\frac{\bar{\omega}_s \bar{\omega}_u}{\omega^2} - 1 \right). \quad (5.10)$$

Bearing in mind inequality (5.8), it is easy to check that $\frac{\partial f}{\partial \omega} > 0$ around $\omega = \bar{\omega}_u$, and $\frac{\partial f}{\partial \omega} < 0$ around $\omega = \bar{\omega}_s$. Hence $\omega = \bar{\omega}_u$ is repulsive. Now, the following theorem addresses the stability of the equilibrium $\bar{\omega}_s$ in (5.6).

Theorem 5.3.1 [Stability of an SG connected to a CPL]

Let Δ be given by (5.7) and assume that (5.5) holds. Then the set $\Omega_s = \{\omega \in \mathbb{R}_{>0} : \omega > \omega_u\}$ is the region of attraction of the asymptotically stable equilibrium $\omega = \bar{\omega}_s$, where $\bar{\omega}_u$ and $\bar{\omega}_s$ are given by (5.6).

Proof. Consider the (*shifted*) candidate Lyapunov function

$$V(\omega) = \frac{1}{2} J (\omega - \bar{\omega}_s)^2.$$

We have

$$\dot{V} = \omega^{-1} (\omega - \bar{\omega}_s) \left(P_m - P_e - D_d \omega (\omega - \omega^*) \right).$$

The fact that ω stays away from zero will be made clear later. According to (5.4) this leads to

$$\begin{aligned} \dot{V} &= \omega^{-1} (\omega - \bar{\omega}_s) \left(D_d \bar{\omega}_s (\bar{\omega}_s - \omega^*) - D_d \omega (\omega - \omega^*) \right) \\ &= -\omega^{-1} D_d (\omega - \bar{\omega}_s) \left(\omega^2 - \omega \omega^* + \bar{\omega}_s \omega^* - \bar{\omega}_s^2 \right) \\ &= -D_d \omega^{-1} (\omega - \bar{\omega}_s) \left((\omega - \bar{\omega}_s) (\omega + \bar{\omega}_s - \omega^*) \right) \\ &= -D_d (\omega - \bar{\omega}_s)^2 \left(1 - \frac{\bar{\omega}_u}{\omega} \right), \end{aligned}$$

where we have used $\bar{\omega}_u = \omega^* - \bar{\omega}_s$. Hence \dot{V} is negative definite on the set Ω_s . Note that since the term $(\omega - \bar{\omega}_s)^2 = 2JV(\omega)$ is strictly decreasing in Ω_s , ω stays away

from $\omega = \max\{0, \omega_u\}$ as time goes by. This proves that $\omega(t) > \max\{0, \omega_u\}$, $\forall t > 0$, and hence Ω_s is positively invariant. Furthermore as $(\omega - \bar{\omega}_s)^2 = 2JV(\omega)$ is strictly increasing for all $\omega < \omega_u$, all other trajectories starting from any initial condition outside the set Ω_s , stay away from the equilibrium ω_s . Note that if the initial condition is $\omega(0) = \omega_u$, then $\dot{V} = 0$, and hence $\omega = \omega_u$ for all $t > 0$. This completes the proof. ■

Note that the Lyapunov function $V(\omega) = \frac{1}{2}J(\omega - \bar{\omega}_s)^2$ is a shifted version of the actual kinetic energy of the physical system, whereas the commonly used Lyapunov function for the swing equation, $\frac{1}{2}M(\omega - \bar{\omega}_s)^2 = \frac{1}{2}J\omega^*(\omega - \bar{\omega}_s)^2$, does not have a physical interpretation.

Remark 5.3.2 [Taking mechanical losses into account]

We can add the viscous damping coefficient D_m accounting for the mechanical losses ($N\ m\ s$), modifying the dynamics (5.1) as

$$J\dot{\omega} + D_m\omega + D_d(\omega - \omega^*) = \tau_m - \tau_e ,$$

which can be rewritten as

$$J\omega\dot{\omega} + (D_m + D_d)\omega(\omega - \frac{D_d}{D_m + D_d}\omega^*) = P_m - P_e .$$

Defining $D := D_m + D_d$ and $\tilde{\omega}^* := \frac{D_d}{D_m + D_d}\omega^*$ we obtain

$$J\omega\dot{\omega} + D\omega(\omega - \tilde{\omega}^*) = P_m - P_e ,$$

which is analogous to the improved swing equation (5.2). Therefore the stability results extend to the case with mechanical losses. □

5.3.2 Shifted Passivity Property

To facilitate the control design, in this section we investigate the shifted passivity of the system (5.2), with the control input u (controllable mechanical power) and the output y written as

$$\begin{aligned} J\omega\dot{\omega} + D_d\omega(\omega - \omega^*) &= u + P_m - P_e \\ y &= \frac{\omega - \omega^*}{\omega} . \end{aligned} \tag{5.11}$$

Note that here the output y is dimensionless. Therefore, yu has the dimension of physical power, which is consistent with the energy dissipation inequality (see (5.16))

later on). This does not hold for the conventional swing equation where ω is taken as the output and thus y_u does not have a meaningful physical dimension.

Now, let the triple $(\bar{u}, \bar{\omega}, \bar{y})$ be an input-state-output solution of (5.11) with

$$\begin{aligned} D_d \bar{\omega} (\bar{\omega} - \omega^*) &= \bar{u} + P_m - P_e \\ \bar{y} &= \frac{\bar{\omega} - \omega^*}{\bar{\omega}}. \end{aligned} \quad (5.12)$$

Assume that

$$\bar{u} + P_m - P_e > -\frac{1}{4} D_d \omega^{*2}. \quad (5.13)$$

Then the dynamics (5.11) possesses the equilibria

$$\bar{\omega}_s = \frac{\omega^* + \sqrt{\Delta}}{2}, \quad \bar{\omega}_u = \frac{\omega^* - \sqrt{\Delta}}{2} \quad (5.14)$$

where with a little abuse of the notation

$$\Delta := \omega^{*2} + 4 \frac{\bar{u} + P_m - P_e}{D_d}. \quad (5.15)$$

Now, we have the following proposition:

Proposition 5.3.3 [Shifted Passivity]

Consider the (*shifted*) candidate Lyapunov function

$$W(\omega) = \frac{1}{2} J (\omega - \bar{\omega}_s)^2 \frac{\omega^*}{\bar{\omega}_s}$$

and assume that (5.13) holds. Then, $W(\omega)$ computed along any solution to (5.11) satisfies

$$\dot{W} < (y - \bar{y})(u - \bar{u}), \quad (5.16)$$

as long as the solution stays within the set $\Omega_k = \{\omega \in \mathbb{R}_{>0} : W(\omega) \leq \frac{1}{2} J \Delta \frac{\omega^*}{\bar{\omega}_s}\}$. This amounts to an shifted passivity property with respect to $(\bar{u}, \bar{\omega}, \bar{y})$.

Proof. We have

$$\begin{aligned}
\dot{W} &= \left(\frac{1}{\omega}\right) \left(\frac{\omega^*}{\bar{\omega}_s}\right) (\omega - \bar{\omega}_s) \left(u + P_m - P_e - D_d \omega (\omega - \omega^*) \right. \\
&\quad \left. - \bar{u} - P_m + P_e + D_d \bar{\omega}_s (\bar{\omega}_s - \omega^*) \right) \\
&= \left(\frac{\omega - \omega^*}{\omega} - \frac{\bar{\omega}_s - \omega^*}{\bar{\omega}_s} \right) (u - \bar{u}) \\
&\quad - D_d \left(\frac{\omega^* (\omega - \bar{\omega}_s)}{\omega \bar{\omega}_s} \right) \left((\omega - \bar{\omega}_s) (\omega + \bar{\omega}_s - \omega^*) \right) \\
&= (y - \bar{y}) (u - \bar{u}) \\
&\quad - D_d (\omega - \bar{\omega}_s)^2 \left(1 - \frac{\bar{\omega}_u}{\omega} \right) \left(\frac{\omega^*}{\bar{\omega}_s} \right). \tag{5.17}
\end{aligned}$$

Hence the inequality (5.16) holds as long as the solutions evolve in the set $\Omega'_k = \{\omega \in \mathbb{R}_{>0} : \omega \geq \bar{\omega}_u\}$. The fact that $\Omega_k \subseteq \Omega'_k$ follows analogously to the proof of Theorem 5.3.1. \blacksquare

5.3.3 Frequency Regulation

In this section, we investigate the frequency regulation of the system by an integral controller. Motivated by Proposition 5.3.3, we propose the controller for system (5.11) as

$$\begin{aligned}
\dot{\xi} &= y = \frac{\omega - \omega^*}{\omega} \\
u &= -\xi. \tag{5.18}
\end{aligned}$$

Note that for the purpose of frequency regulation, the solution (equilibrium) of interest for the system (5.11), (5.18), is given by

$$\bar{u} = -\bar{\xi} = -(P_m - P_e), \quad \bar{\omega} = \omega^*, \quad \bar{y} = 0, \tag{5.19}$$

which trivially satisfies the inequality (5.13). In addition, for the solution above, the quantities in (5.14) and (5.15) are computed as $\bar{\omega}_s = \omega^*$, $\bar{\omega}_u = 0$, $\Delta = \omega^{*2}$. Therefore, the dissipation equality (5.17) in this case reduces to

$$\dot{W} = (y - \bar{y}) (u - \bar{u}) - D_d (\omega - \bar{\omega}_s)^2. \tag{5.20}$$

The following theorem establishes the convergence of the solutions to the desired equilibrium associated with the nominal frequency regulation.

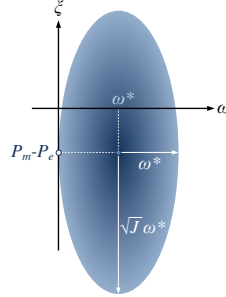


Figure 5.1: Region of attraction for the system (5.11), (5.18) is estimated with the oval characterized by (7.46).

Theorem 5.3.4 [Frequency regulation]

Consider the candidate Lyapunov function

$$U(\xi, \omega) = W_c(\xi) + W(\omega)$$

where $W_c = \frac{1}{2}(\xi - \bar{\xi})^2$ and $W = \frac{1}{2}J(\omega - \omega^*)^2$. Then the solutions of the closed loop system (5.11), (5.18), starting from any initial condition in the set $\mathcal{O} = \{(\xi, \omega) \in \mathbb{R}^2 : U < \frac{1}{2}J\omega^{*2}\}$ converge asymptotically to the equilibrium $(P_m - P_e, \omega^*)$.

Proof. First note that for all $x \in \mathcal{O}$, we have $W < \frac{1}{2}J\omega^{*2}$, and hence $\omega > 0$. Hence the system is well-defined in the set \mathcal{O} . Now observe that $\dot{W}_c = \omega^{-1}(\omega - \omega^*)(\xi - \bar{\xi})$. Hence, by (5.20) we find that

$$\dot{U} = -D_d(\omega - \omega^*)^2. \quad (5.21)$$

As the right hand side of the above equality is nonpositive, we conclude that the set \mathcal{O} is forward invariant along the solution (ξ, ω) , and thus (5.21) is valid for all time. Now, observe that U is radially unbounded and has a strict minimum at $(\xi, \omega) = (P_m - P_e, \omega^*)$. Then by invoking LaSalle's invariance principle, the solutions converge to the largest invariant subset of \mathcal{O} , in which $\omega = \omega^*$ and $\dot{u} = P_e - P_m$. The latter shows that all the solutions on the invariant set \mathcal{O} converge asymptotically to the equilibrium $(\xi, \omega) = (P_m - P_e, \omega^*)$. We can rewrite the set \mathcal{O} as

$$\left(\frac{\omega - \omega^*}{\omega^*}\right)^2 + \left(\frac{\xi - \bar{\xi}}{\sqrt{J}\omega^*}\right)^2 < 1. \quad (5.22)$$

This set guarantees ω to remain in the positive half-line $\mathbb{R}_{>0}$ for ω (see Figure 5.1). ■

5.4 Synchronous Generator Connected to an Infinite Bus

In this scenario we consider the case of SMIB, where the synchronous generator is connected to an *infinite bus* through an inductive line. An infinite bus is a node with fixed voltage and frequency (50 or 60Hz).

5.4.1 Stability of the Improved Swing Model

It can be shown that the power delivered by the synchronous generator to the bus is $\gamma \sin(\delta)$ where δ is the voltage angle relative to the infinite bus, and $\gamma := \frac{V_g V_b}{X}$. Here, the voltages (V_g, V_b) and the reactance of the line (X) are assumed to be constant. The dynamics of an SMIB system modeled with the improved swing equation (5.2) is

$$\begin{aligned} \dot{\delta} &= \omega - \omega^* \\ J\omega\dot{\omega} + D_d\omega(\omega - \omega^*) &= P_m - \gamma \sin(\delta) , \end{aligned} \quad (5.23)$$

where the mechanical input $P_m > 0$ is considered constant. It is easy to check that $(\delta, \omega) = (\arcsin \frac{P_m}{\gamma}, \omega^*)$ is the equilibrium of the system (5.23).

Theorem 5.4.1 [Stability of an SMIB with the improved swing model]
Consider the (*shifted*) candidate Lyapunov function

$$V(\delta, \omega) = V_k(\omega) + V_p(\delta) ,$$

where

$$V_k(\omega) = \frac{1}{2}J(\omega - \omega^*)^2 , \quad V_p(\delta) = \frac{\gamma}{\omega^*}[-\cos \delta + \cos \bar{\delta} - (\delta - \bar{\delta}) \sin \bar{\delta}]$$

are associated with the kinetic and potential energy,² and $\bar{\delta} = \arcsin \frac{P_m}{\gamma}$. Assume that

$$\omega^* > \sqrt{\frac{\gamma}{D_d}} \quad (5.24)$$

and

$$\frac{P_m}{\gamma} < \frac{2}{\pi} . \quad (5.25)$$

Let $c := \min(c_k, c_p)$, where

$$c_k := \frac{1}{2}J(\omega^* - \frac{\gamma}{D_d\omega^*})^2 , \quad c_p := V_p(\frac{\pi}{2}) .$$

²The shifted functions are constructed using Bregman distance; see Remark 2.3.4.

Then the solutions of the system (5.23) starting from any initial condition in the set $\Omega = \{(\delta, \omega) \in [-\pi, \pi] \times \mathbb{R} : V(\delta, \omega) \leq c\}$ converge asymptotically to the equilibrium $(\delta, \omega) = (\arcsin \frac{P_m}{\gamma}, \omega^*)$.

Proof. Observe that $V_p(\delta)$ has a minimum at $\bar{\delta}$ and is convex within the set $\Omega_p = \{\delta \in [-\frac{\pi}{2}, \frac{\pi}{2}]\}$. We here show that $\Omega \subset \Omega_p$. Having $V_k(\omega) > 0$, the inequality $V(\delta, \omega) < c$ results in $V_p(\delta) < c_p$ and reads as

$$\cos \delta > \left(\frac{\pi}{2} - \delta\right) \sin \bar{\delta}. \quad (5.26)$$

The inequality (5.26) contains a unique subset of Ω_p . More precisely, under the criterion $0 < \bar{\delta} < \arcsin \frac{2}{\pi}$ as a result of (5.25), there exists $\delta^- \in (-\frac{\pi}{2}, \frac{\pi}{2})$ such that (5.26) holds for all $\delta \in [\delta^-, \frac{\pi}{2}]$. Figure 6.3 shows an example interval for δ that satisfies (5.26) and consequently the energy function V_p remains convex ($\Omega \subset \Omega_p$).

Now, it remains to prove that $\dot{V} < 0$. We have

$$\begin{aligned} \dot{V} &= -D_d(\omega - \omega^*)^2 - \frac{\gamma}{\omega}[(\omega - \omega^*)(\sin \delta - \sin \bar{\delta})] \\ &\quad + \frac{\gamma}{\omega^*}[(\omega - \omega^*)(\sin \delta - \sin \bar{\delta})] \\ &= -(\omega - \omega^*)^2 \left(D_d - \frac{\gamma}{\omega \omega^*}(\sin \delta - \sin \bar{\delta})\right). \end{aligned}$$

Note that $\sin \delta - \sin \bar{\delta} < 1$. Hence $\dot{V} < 0$ on the set $\Omega_k = \{\omega \in \mathbb{R} : \omega > \frac{\gamma}{D_d \omega^*}\}$. Here we show that $\Omega \subset \Omega_k$. In the set Ω we have $V(\delta, \omega) < c$ which leads to $V_k(\omega) < c_k$. Therefore

$$(\omega - \omega^*)^2 < \left(\omega^* - \frac{\gamma}{D_d \omega^*}\right)^2,$$

and using (5.24),

$$\frac{\gamma}{D_d \omega^*} < \omega < 2\omega^* - \frac{\gamma}{D_d \omega^*}. \quad (5.27)$$

The left hand side of the inequality (5.27) shows that $\Omega \subset \Omega_k$.

Observe that U has a strict minimum at $\omega = \omega^*$ and $\delta = \bar{\delta}$, and the solutions are bounded to $\frac{\gamma}{D_d \omega^*} < \omega < 2\omega^* - \frac{\gamma}{D_d \omega^*}$ and $\delta^- < \delta < \frac{\pi}{2}$. By invoking LaSalle's invariance principle, the solutions converge to the largest invariant subset of Ω for (5.23) s.t. $\omega = \omega^*$. On this set, the solution to (5.23) satisfy $\delta = \arcsin \frac{P_m}{\gamma}$. This shows that all the solutions on the invariant set converge asymptotically to the equilibrium $(\arcsin \frac{P_m}{\gamma}, \omega^*)$. ■

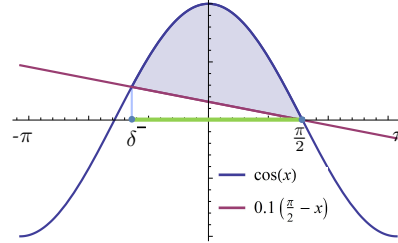


Figure 5.2: The estimate of the system (5.23) region of attraction ($V_p(\delta) < c_p$) for $\bar{\delta} = \arcsin 0.1$ confines δ in $[-0.4\pi + 0.5\pi]$ (green). On such an interval, $V_p(\delta)$ remains positive and convex.

Remark 5.4.2 [Is the assumption (5.25) restrictive?]

The assumption $\frac{P_m}{\gamma} < \frac{2}{\pi}$ results in $\bar{\delta} < \arcsin \frac{2}{\pi}$, which means that, at the steady state, the angle between the synchronous generator and the infinite bus should be less than about 40° . In practice, the steady state angle is much lower (see, e.g., [156]). Note that this assumption is made merely for characterizing the region of attraction, otherwise, it is not necessary for the proof of local stability, since V is convex around the equilibrium ($\frac{\partial^2 V}{\partial \delta^2} \big|_{\delta=\bar{\delta}} = \cos \bar{\delta} > 0$). \square

5.4.2 Comparison with the Swing Equation

In this subsection, we compare the results of the improved model with the swing equation. The dynamics of a synchronous generator modeled by the swing equation and connected to an infinite bus is

$$\begin{aligned} \dot{\delta} &= \omega - \omega^* \\ M\dot{\omega} + A(\omega - \omega^*) &= P_m - \gamma \sin(\delta), \end{aligned} \quad (5.28)$$

where the mechanical input $P_m > 0$ is considered constant. It is straightforward to see that the equilibrium of the system (5.28) is $(\delta, \omega) = (\arcsin \frac{P_m}{\gamma}, \omega^*)$.

Corollary 5.4.3 [Stability of an SMIB with the swing model]

Consider the candidate Lyapunov function $V(\delta, \omega) = V_k(\omega) + V_p(\delta)$, where

$$V_k(\omega) = \frac{1}{2}M(\omega - \omega^*)^2$$

and

$$V_p(\delta) = \gamma[-\cos \delta + \cos \bar{\delta} - (\delta - \bar{\delta}) \sin \bar{\delta}].$$

Assume that $\frac{P_m}{\gamma} < \frac{2}{\pi}$ and let $c := V_p(\frac{\pi}{2})$. Then the solutions of the SMIB system described by the swing equation (5.28) starting from any initial condition in the set

$\Omega = \{(\delta, \omega) \in [-\pi, \pi] \times \mathbb{R} : V(\delta, \omega) < c\}$ converge asymptotically to the equilibrium $(\delta, \omega) = (\arcsin \frac{P_m}{\gamma}, \omega^*)$.

Proof. The proof is similar to the proof of the Theorem 5.4.1 and therefore omitted. Note that here, $\dot{V} = -A(\omega - \omega^*)^2$, and hence to prove stability, the condition $V < V_p(\frac{\pi}{2})$ suffices. ■

Corollary 5.4.3 and Theorem 5.4.1 characterize similar estimates for region of attraction of both models (improved swing and the conventional one) if $c_k \geq c_p$ (and as a result $c = c_p$).

5.5 Numerical Simulation

Here we provide examples depicting the mismatch between the behavior of the two models, swing and improved swing equations. In all simulations, the parameters are set as follows: $M = 0.2$, $A = 0.04$, $\omega^* = (2\pi)60$, and $\gamma = 2$. Note that $J = \frac{M}{\omega^*}$ and $D_d = \frac{A}{\omega^*}$.

5.5.1 CPL: Example 1

As described in Subsection 5.3.1, the steady state value of the frequency differs for the swing equation and the improved swing model under similar CPLs. Figure 5.3(a) illustrates this issue. In this example, we set $P_m = 1\text{pu}$ and $P_e = 2\text{pu}$, and start from the initial condition $f(0) = 60\text{Hz}$. The steady state value of the frequency is 56.02Hz for the swing equation, and 55.72Hz for the improved swing model.

5.5.2 CPL: Example 2

The region of attraction for the improved swing equation, when connected to a CPL, was provided in Subsection 5.3.1 (Ω_s in Theorem 5.3.1). Figure 5.3(b) illustrates a solution that initiates outside this domain, and becomes unstable. However, the conventional swing equation is falsely depicting that the system remains stable. Here, we set $P_m = 1\text{pu}$ and $P_e = 4.65\text{pu}$, and start from $f(0) = 24\text{Hz}$. According to Theorem 5.3.1, the region of attraction allows for $f > 25\text{Hz}$.

5.5.3 CPL: Example 3

According to Subsection 5.3.1, real equilibria exist, only if the condition (5.5) is satisfied. Figure 5.3(c) shows that the system becomes unstable if the inequality (5.5) is violated. Note that the stability of the swing equation, connected to a CPL, does

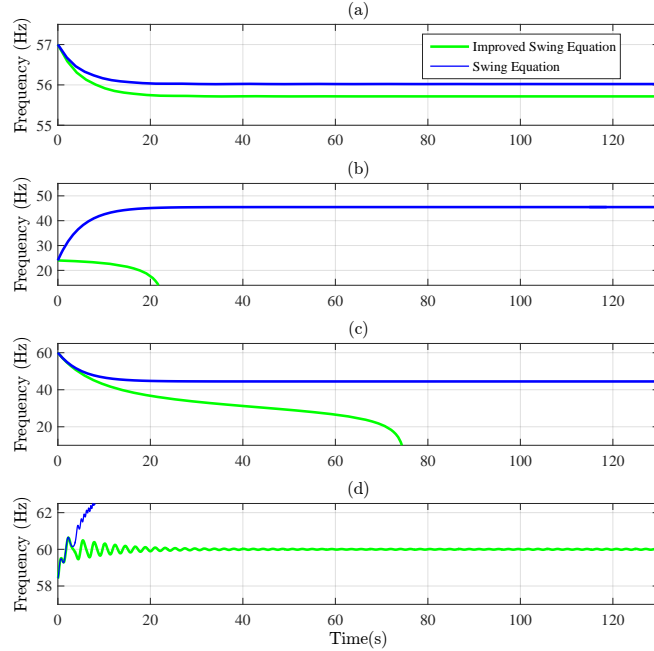


Figure 5.3: Simulation results for the examples of Section 5.5.

not require any condition. In this example, we set $P_m = 1\text{pu}$ and $P_e = 4.90\text{pu}$. With these values, the discriminant Δ , as defined in (5.7), possesses a negative value.

5.5.4 SMIB: Different Behavior

The behaviors of both systems, conventional and improved, are similar when connected to an infinite bus. However still with some specific initial conditions, the systems act quite differently. Figure 5.3(d) illustrates an example of this different behavior. Note that here, the initial condition is outside the estimate of the region of attraction in both models.

5.5.5 SMIB: Region of Attraction

Figure 5.4 illustrates the phase portrait of the system (5.23) and the Lyapunov function $V(\delta, \omega)$ level sets. It is verified that our estimate of the domain of attraction is not very conservative. All solutions (dotted green) within the Lyapunov level set $V(\delta, \omega) = c$ (dark blue) converge to the equilibrium $(\delta, \omega) = (\frac{\pi}{6}, 2\pi \times 60)$. Here, $c_p < c_k$, and

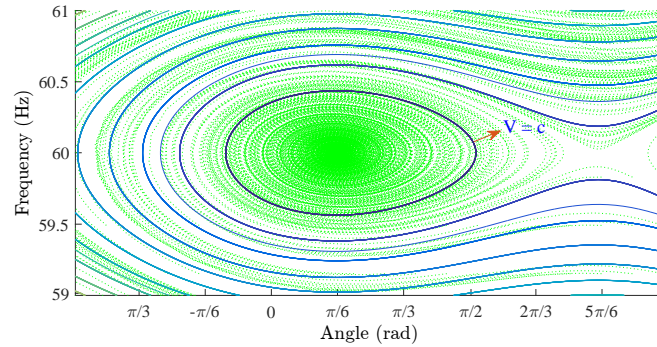


Figure 5.4: The estimate of the domain of attraction for system (5.23) (SMIB).

hence $c = c_p = V_p(\frac{\pi}{2})$. Note that there are solutions outside the estimate of region of attraction that still converge, however the solutions further away from the estimate of domain of attraction diverge from the equilibrium.

5.6 Conclusion

We have investigated the properties of an improved swing equation, as a model for synchronous generators. Two scenarios are analyzed in this chapter. First, the stability of a single generator connected to a CPL is shown, and frequency regulation is achieved through the proposed integral controller. In the second scenario, the synchronous machine is connected to an infinite bus. As a contribution with respect to [160], where similar dynamics are investigated through linearization, here, a nonlinear Lyapunov analysis is provided to prove stability and frequency regulation. Finally, simulations are carried out to show that the swing equation model gives rise to a behavior that does not match with the one suggested by the improved swing equation. Moreover in [148], it was shown that the behavior of the improved swing equation is closer to the FP model. As it will be shown in the next chapter, and under more restrictive conditions, stability of a network of sources modeled by the improved swing equation is guaranteed.

Chapter 6

Power Sources II: Power Converters with Capacitive Inertia

“It is not inertia alone that is responsible for human relationships repeating themselves from case to case, indescribably monotonous and unrenewed: it is shyness before any sort of new, unforeseeable experience with which one does not think oneself able to cope.”

– Rainer Maria Rilke, *Letters to a Young Poet*



ACK of inertia is an emerging concern for design and development of inverter dominated networks. This chapter addresses the problem of stability and frequency regulation of a recently proposed inverter, where the DC-side capacitor emulates the inertia of a synchronous generator. First, we remodel the dynamics from the electrical power perspective. Second, using this model, we show that the system, connected to a constant power load, is stable, and the frequency can be regulated by a suitable choice of the controller. Next, and as the main focus of this chapter, we analyze the stability of a network of these inverters, and show that frequency regulation can be achieved by an appropriate controller design. Finally, a numerical example is provided which illustrates the effectiveness of the method.

6.1 Introduction

Along with the emergence of the renewable energy sources in power networks, and consequently the increasing usage of power converters, new issues and concerns regarding stability of the grid have arisen. Recently, the problem of low inertia of inverter dominated systems has been extensively investigated. In classical electrical grids, synchronous generators dominated the power source types in the network. These machines possess a massive rotational part, rotating at the same frequency

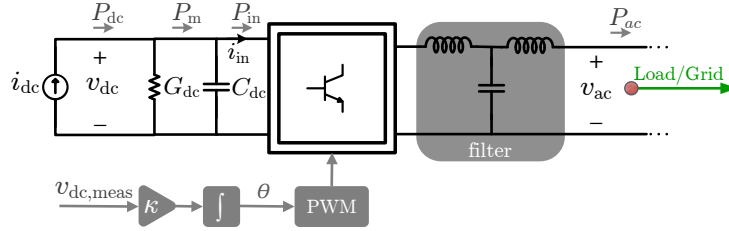


Figure 6.1: Schematic of an inverter with capacitive inertia (ICI)

as that of the generated electrical sinusoidal voltage. The kinetic energy of such rotation takes the role of an energy reservoir. When an abrupt increase or decrease occurs in the load, the kinetic energy of the synchronous machine is injected into, or absorbed from the network, respectively. In conventional power converters, the absence of this reservoir jeopardizes the stability of the network, and leads to new frequency instability issues in power systems [15, 133, 136]. Inverters possess fast frequency dynamics and the traditional control strategies are too slow to prevent large frequency deviations and their consequences [136]. In particular, in networks with low inertia, the rate of change of frequency (ROCOF) may be large enough to activate the load-shedding switches of a power network, even with a small power imbalance [43]. As a remedy to this problem, the concept of *Virtual Inertia* has been introduced and various methods have been proposed, so that the inverters emulate the behavior of synchronous generators [2, 11, 46, 97, 122, 128, 137, 144, 159].

Although a better performance of the inverters results with this emulation, the virtual inertia cannot react instantaneously. This is due to the fact that the AC measurements play a major role in mimicking the inertia [43], and hence the inevitable delay in these measurements slows down the emulating behavior. Therefore, as an alternative, methods to provide an instantaneous physical inertia have been proposed. More specifically in [5, 146, 147], the energy stored in the DC-side capacitor of the inverter is employed as a replacement of the kinetic energy stored in the rotor of a synchronous generator. The DC-side capacitor is an inherent element in most inverters. We refer to these devices as *Inverters with Capacitive Inertia (ICI)* throughout the chapter. Recently, a promising and detailed nonlinear model of such devices is provided in [34, 69], where the generated frequency is proportional to the measured voltage of the DC-side capacitor (see Figure 6.1). However in [34, 69], the stability of the inverter, connected to a single load or a network, was not investigated. Note that, as previously mentioned, the motivation for emulating inertia is to alleviate the stability problems of low-inertia networks, that are dominated by inverters.

In this chapter, we remodel the ICI dynamics in [69] from a power perspective, in order to ease the stability analysis of these devices in several scenarios. In Section 6.2,

the case of a single inverter connected to a constant power load will be investigated. A primary controller is provided, which guarantees stability of the system. Next, it is shown that the frequency can be regulated to its nominal value by a secondary controller. In Section 6.3, stability of a network of ICIs is investigated, and a distributed controller is proposed to regulate the frequencies to the desired value. Finally, a numerical example illustrates the effectiveness of the method.

6.2 Single Inverter with Capacitive Inertia

In this section, we first explain briefly how a single inverter is modeled in [69], and next we reconfigure the model from the electrical power perspective. Finally the control method is elaborated.

6.2.1 ICI Model in [69]

Figure 6.1 depicts the schematic of an ICI, which is based on the averaged model of a three-phase converter. For the sake of clarity, the electrical circuit of one phase is shown. The electrical part, shown in black, consists of a controllable current source i_{dc} , a resistor with the conductance G_{dc} , and a capacitor C_{dc} in the DC-side. The switching block in the middle converts the DC current to an alternating current. This conversion is carried out via a pulse width modulation (PWM) unit which provides on/off signals to the switching block, according to a given phase angle input θ . A low-pass *LCL* filter in the AC-side eliminates the high frequency harmonics of the output signal. This process generates a sinusoidal voltage v_{AC} with the phase angle θ .

In a synchronous generator, when the power demand is more than the mechanical input power, the lacking amount of energy is extracted from the kinetic energy of the rotor $\frac{1}{2}J\omega^2$, and hence the angular velocity of the rotor decreases, and the frequency of the output voltage drops. Similarly, in power converters with a DC-side capacitor, the extra power demand is released from the energy stored in the capacitor ($\frac{1}{2}C_{dc}v_{dc}^2$). However, contrary to the inertia of a synchronous generator, if the voltage of the DC-side drops, this will not be visible in the output frequency at the AC-side. As a remedy, in [34, 69], the frequency $\omega = \dot{\theta}$ of the output voltage v_{AC} is tuned to be proportional to v_{dc} . This mechanism is fulfilled via an integral action over the measured voltage v_{dc} , with an integral coefficient κ . The generated signal is then fed as the PWM signal to the switching block, i.e. $\dot{\theta} = \kappa v_{dc}$ (see Figure 6.1). Hence we have

$$\omega = \kappa v_{dc} , \tag{6.1}$$

where a reasonable choice for the integral coefficient is $\kappa = \frac{\omega^*}{v_{dc}^*}$, with $\omega^* > 0$ denoting the desired frequency (angular velocity corresponding to 50 Hz or 60 Hz). Furthermore, using Kirchhoff's current law in the DC side, we have

$$C_{dc}\dot{v}_{dc} = -G_{dc}v_{dc} - i_{in} + i_{dc} . \quad (6.2)$$

Combining (6.1) and (6.2) we obtain the model [69]

$$J\dot{\omega} = -D\omega - \frac{i_{in}}{\kappa} + \frac{i_{dc}}{\kappa} , \quad (6.3)$$

where $J = \frac{C_{dc}}{\kappa^2}$ and $D = \frac{G_{dc}}{\kappa^2}$.

6.2.2 ICI Model from the Electrical Power Perspective

We can rewrite the system (6.3) as

$$J\dot{\omega} = -D\omega - \frac{P_{in}}{\kappa v_{dc}} + \frac{i_{dc}}{\kappa} ,$$

where $P_{in} = v_{dc}i_{in}$ is the electrical power that is injected into the switching block. Assuming that no power is dissipated in the switching block and the *LCL* filter (see Figure 6.1), i.e. $P_{in} \simeq P_{AC}$, we obtain

$$J\dot{\omega} = -D\omega - \frac{P_{AC}}{\omega} + u , \quad (6.4)$$

where $u = \kappa^{-1}i_{dc}$ is treated as the control input.

6.2.3 Primary Control

Consider an ICI modeled by (6.4) connected to a constant power load $P_{AC} = P_\ell$. To provide a primary control, we propose the control input

$$u = D\omega^* + \omega^{-1}P_m , \quad (6.5)$$

where $P_m \in \mathbb{R}_{>0}$ will be designed later. This design is inspired by the following remark.

Remark 6.2.1 [Interpretation of P_m]

Around the nominal frequency $\omega = \omega^*$, the term P_m in (6.5) represents the power injection behind the capacitor C_{dc} (see Figure 6.1). To see this, notice that we can rewrite (6.5) as

$$\frac{v_{dc}^*}{\omega^*} i_{dc} = G_{dc} \frac{v_{dc}^{*2}}{\omega^*} + \frac{P_m}{\omega^*} ,$$

where we used $u = \kappa^{-1}i_{dc}$, $D = \kappa^{-2}G_{dc}$, and $\kappa = \frac{\omega^*}{v_{dc}^*}$. Hence we have

$$P_m = P_{dc}^* - G_{dc}v_{dc}^{*2}.$$

Note that the first term is the nominal DC power, and the second term is the power dissipated in the DC-side resistor in the nominal frequency. \square

Since $\omega = \kappa v_{dc}$, where v_{dc} is a DC value measured for generating the PWM signal, no additional measurement is required to implement this controller. In this section, we assume a constant $P_m = P_\ell^*$, where $P_\ell^* > 0$ is an estimate of the nominal load. Now, the model (6.4) can be rewritten as

$$J\dot{\omega} = -D(\omega - \omega^*) + \frac{P_\ell^* - P_\ell}{\omega}. \quad (6.6)$$

The model (6.6) indicates a droop-like behavior. That is, the frequency will drop if the power extracted by the load is larger than the nominal power, and will increase otherwise. In fact, the dynamics (6.6) resembles that of a synchronous generator modeled with the *improved swing equation* (5.2), with inertia $J = \frac{C_{dc}}{\kappa^2}$, damping coefficient $D = \frac{G_{dc}}{\kappa^2}$, and mechanical input power P_ℓ^* .

Assume that the maximum power mismatch (lack of power) $P_\ell - P_\ell^*$ is such that

$$\Delta := \omega^{*2} - 4\frac{P_\ell - P_\ell^*}{D} > 0. \quad (6.7)$$

Then the dynamics (6.6) has the following two equilibria

$$\omega_s = \frac{1}{2}(\omega^* + \sqrt{\Delta}), \quad \omega_u = \frac{1}{2}(\omega^* - \sqrt{\Delta}). \quad (6.8)$$

According to Theorem 5.3.1, the equilibrium point $\omega = \omega_s$ is asymptotically stable. A secondary controller is needed to eliminate the static deviation of ω_s from the nominal frequency ω^* .

Remark 6.2.2 [Additional damping]

According to (6.7), a larger damping coefficient (D), allows for larger power deviations. However, this requires a larger G_{dc} , and consequently more power loss ($v_{dc}^2 G_{dc}$) in the DC-side resistor. Therefore, a proportional controller term can be added to the control input. In particular, let $u = D\omega^* + \omega^{-1}P_m + u_p$, where $u_p = \tilde{D}(\omega - \omega^*)$ for some $\tilde{D} > 0$. In this case, the damping term in (6.6) modifies to $(D + \tilde{D})(\omega - \omega^*)$. \square

6.2.4 Secondary Control

Aiming at the frequency regulation of the system (6.4), we propose the controller as

$$\begin{aligned} \dot{\chi} &= -\omega^{-1}(\omega - \omega^*) \\ u &= D\omega^* + \omega^{-1}\chi. \end{aligned} \quad (6.9)$$

Note that here, compared to the primary controller, the term P_m in (6.5) is not a constant, but a state variable integrating the frequency deviation. This controller regulates the frequency to the nominal ω^* in the steady state of the system (6.4) (see Remark 6.3.7 later on).

6.3 Network of Inverters with Capacitive Inertia

In this section, we investigate the stability and the frequency regulation in a network of ICIs.

6.3.1 Network Model

Consider an inverter-based network, where each bus is connected to an inverter and a local constant power load P_ℓ . The topology of the grid is represented by a connected undirected graph $\mathcal{G}(\mathcal{V}, \mathcal{E})$, with node set \mathcal{V} , and edge set \mathcal{E} , given by a set of unordered pairs $\{i, j\}$ of distinct vertices i and j . Let $n = |\mathcal{V}|$ and $m = |\mathcal{E}|$. As it was shown in Chapter 3, the lines can be assumed to be dominantly inductive due to the inductive output impedance of the inverters, *i.e.*, two nodes $\{i, j\} \in \mathcal{E}$ are connected by a nonzero inductance. The set of neighbors of the i th node is denoted by $\mathcal{N}_i = \{j \in \mathcal{V} \mid \{i, j\} \in \mathcal{E}\}$.

Calculation of the active power transferred via a power line is in general cumbersome, and complicates the network stability analysis. To remove this obstacle, we take advantage of phasor approximations. The relative phase angles are denoted in short by $\theta_{ij} := \theta_i - \theta_j$, $\{i, j\} \in \mathcal{E}$. Now let $\gamma_k := \frac{|V_i||V_j|}{X_{ij}}$, $k \sim \{i, j\}$, where X_{ij} represents the reactance of the line connecting nodes i and j , and $|V_i|$ denotes the magnitude of the voltage at node i , which is assumed to be constant. Then the active power transferred via the inductor between nodes i and j is calculated as

$$P_{ij} = \gamma_k \sin \theta_{ij}, \quad k \sim \{i, j\}.$$

Hence, the injected active power by the inverter at each node P_{AC_i} is given by

$$P_{AC_i} = P_{\ell_i} + \sum_{\substack{j \in \mathcal{N}_i \\ k \sim \{i, j\}}} \gamma_k \sin \theta_{ij}, \quad (6.10)$$

where P_{ℓ_i} denotes the local load connected to node i . Note that the phasor approximation is only exploited to write the expression of the active power above.

For every node i we have

$$\begin{aligned} \dot{\theta}_i &= \omega_i \\ J_i \dot{\omega}_i &= u_i - \omega_i^{-1} P_{AC_i} - D_i \omega_i. \end{aligned}$$

With a little abuse of notation, using (6.10), the network can be written in vector form as

$$\begin{aligned} \dot{\theta} &= \omega \\ J\dot{\omega} &= u - \langle \omega \rangle^{-1} (P_\ell + B\Gamma \sin(B^\top \theta)) - D\omega, \end{aligned} \quad (6.11)$$

where $\theta = \text{col}(\theta_i)$, $\omega = \text{col}(\omega_i)$, $J = \text{diag}\{J_1, \dots, J_n\}$, $u = \text{col}(u_i)$, $P_\ell = \text{col}(P_{\ell_i})$, $D = \text{diag}\{D_1, \dots, D_n\}$, B is the incidence matrix, and $\Gamma = \text{diag}\{\gamma_1, \dots, \gamma_m\}$, with indices indicating the node/edge numbers.

Note that if (θ, ω) is a solution to (6.11) for given u and P_ℓ , then $(\theta + \mathbf{1}\alpha, \omega)$ is also a solution to (6.11) for any constant $\alpha \in \mathbb{R}$. To exclude this rotational invariance, it is convenient to introduce a different set of coordinates, representing the phase angle differences, given by $\eta := B^\top \theta$. Then the model (6.11) modifies to

$$\begin{aligned} \dot{\eta} &= B^\top \omega \\ J\dot{\omega} &= u - \langle \omega \rangle^{-1} (P_\ell + B\Gamma \sin \eta) - D\omega. \end{aligned} \quad (6.12)$$

6.3.2 Primary Control

The goal of primary control is to design a proportional controller $u = k(\omega)$, such that all frequencies converge to the same value, corresponding to a stable equilibrium of the system. To this end, analogous to the case of a single ICI, and with a little abuse of notation, we propose the control input

$$u = D\mathbf{1}\omega^* + \langle \omega \rangle^{-1} P_m. \quad (6.13)$$

For a constant setpoint $P_m = P_\ell^* = \text{col}(P_{\ell_i}^*)$, the dynamics (6.12) reads as

$$\begin{aligned} \dot{\eta} &= B^\top \omega \\ J\dot{\omega} &= \langle \omega \rangle^{-1} (P_\ell^* - P_\ell - B\Gamma \sin \eta) - D(\omega - \mathbf{1}\omega^*). \end{aligned} \quad (6.14)$$

Note that $\eta(0) = B^\top \theta(0)$, and hence $\eta(t) \in \text{im } B^\top$ for all $t \geq 0$. Therefore, we can restrict the domain of solutions to $(\eta, \omega) \in \mathcal{X} := \text{im } B^\top \times \mathbb{R}^n$, which is clearly forward invariant.

Note that the choice of the setpoint P_ℓ^* is decided based on an estimate of the load P_ℓ . We assume that the maximum mismatch (lack of power) $P_\ell - P_\ell^*$ is such that

$$\Delta_N := \omega^{*2} - 4 \frac{\mathbf{1}^\top (P_\ell - P_\ell^*)}{\mathbf{1}^\top D \mathbf{1}} > 0. \quad (6.15)$$

It is easy to see that the condition (6.15) guarantees the existence of an equilibrium for system (6.14). Next, we characterize the equilibria of (6.14).

Lemma 6.3.1 Assume that (6.15) holds. Then the points $(\eta_s, \mathbb{1}\omega_s)$ and $(\eta_u, \mathbb{1}\omega_u)$ are two equilibria of system (6.14) if and only if

$$\begin{aligned} P_\ell^* - P_\ell &= B\Gamma \sin \eta_s + D\mathbb{1}\omega_s(\omega_s - \omega^*), \\ P_\ell^* - P_\ell &= B\Gamma \sin \eta_u + D\mathbb{1}\omega_u(\omega_u - \omega^*), \end{aligned} \quad (6.16)$$

where

$$\omega_s = \frac{1}{2}(\omega^* + \sqrt{\Delta_N}), \quad \omega_u = \frac{1}{2}(\omega^* - \sqrt{\Delta_N}), \quad (6.17)$$

Proof. By the first equality in (6.14) it follows that $\omega = \mathbb{1}\tilde{\omega}$ for some $\tilde{\omega}$. By premultiplying the second equality in (6.14) by $\mathbb{1}^\top$, we obtain $\mathbb{1}^\top(P_\ell^* - P_\ell) = \mathbb{1}^\top D\mathbb{1}\tilde{\omega}(\tilde{\omega} - \omega^*)$, which is a quadratic equation with the roots given by (6.17). ■

The equilibrium of interest here is $(\eta_s, \mathbb{1}\omega_s)$. In fact, the other equilibrium can be shown to be unstable. Lemma 6.3.1 imposes the following assumption:

Assumption 6.3.2 For given P_ℓ and P_ℓ^* satisfying (6.15), there exists $\eta_s \in \text{im } B^\top \cap (-\frac{\pi}{2}, \frac{\pi}{2})^m$ such that (6.16) is satisfied.

The additional constraint $\eta_s \in (-\frac{\pi}{2}, \frac{\pi}{2})^m$ is needed for stability of the equilibrium and is ubiquitous in the literature, often referred to as the *security constraint* [42]. To prove stability of the equilibrium $(\eta_s, \mathbb{1}\omega_s)$, we consider first the energy function

$$V(x) = \frac{1}{2}\omega^\top J\omega - \omega_s^{-1}\mathbb{1}^\top \Gamma \cos \eta, \quad (6.18)$$

with $x = \text{col}(\eta, \omega)$. We shift this energy function to

$$V_s(x) = V(x) - (x - \bar{x})^\top \nabla \bar{V} - \bar{V}, \quad (6.19)$$

where $\bar{x} = (\eta_s, \mathbb{1}\omega_s)$. As mentioned in Chapter 2, V_s is positive definite locally if the function V is strictly convex around \bar{x} [20]. By calculating the first and second partial derivatives of V_s , it is easy to observe that V_s is strictly convex and takes its minimum at $x = \bar{x}$, provided that $\eta_s \in (-\frac{\pi}{2}, \frac{\pi}{2})^m$. Now, we are ready to state the main result of this subsection:

Theorem 6.3.3 Suppose that Assumption 6.3.2 holds. Then there exists a neighborhood Ω of $(\eta_s, \mathbb{1}\omega_s)$ such that any solution (η, ω) to (6.14) that starts in Ω , asymptotically converges to the equilibrium point $(\eta_s, \mathbb{1}\omega_s)$.

Proof. First, observe that by substituting $P_\ell^* - P_\ell$ from (6.16) the system (6.14) can be written as

$$\begin{aligned} \dot{\eta} &= B^\top (\omega - \mathbb{1}\omega_s) \\ J\dot{\omega} &= - \langle \omega \rangle^{-1} \left(B\Gamma(\sin \eta - \sin \eta_s) \right. \\ &\quad \left. + D(\langle \omega \rangle(\omega - \mathbb{1}\omega^*) - \mathbb{1}\omega_s(\omega_s - \omega^*)) \right). \end{aligned} \quad (6.20)$$

Consider the Lyapunov function V_s given by (6.18)-(6.19). Computing the time derivative of V_s along the solutions of (6.20) yields

$$\begin{aligned} \dot{V}_s &= - (\omega - \mathbb{1}\omega_s)^\top \langle \omega \rangle^{-1} \left(B\Gamma(\sin \eta - \sin \eta_s) \right. \\ &\quad \left. + D(\langle \omega \rangle(\omega - \mathbb{1}\omega^*) - \mathbb{1}\omega_s(\omega_s - \omega^*)) \right) \\ &\quad + \omega_s^{-1} (\Gamma(\sin \eta - \sin \eta_s))^\top B^\top (\omega - \mathbb{1}\omega_s) \\ &= - (\omega - \mathbb{1}\omega_s)^\top \left(\langle \omega \rangle^{-1} B\Gamma(\sin \eta - \sin \eta_s) \right. \\ &\quad \left. - \omega_s^{-1} B\Gamma(\sin \eta - \sin \eta_s) \right) \\ &\quad - (\omega - \mathbb{1}\omega_s)^\top \langle \omega \rangle^{-1} D[\omega + \mathbb{1}\omega_s - \mathbb{1}\omega^*](\omega - \mathbb{1}\omega_s). \end{aligned}$$

Bearing in mind that $\omega^* - \omega_s = \omega_u$, where ω_u is given by (6.17), we have

$$\begin{aligned} \dot{V}_s &= (\omega - \mathbb{1}\omega_s)^\top \left(\langle \omega \rangle - \omega_s J_n \right) \langle \omega \rangle^{-1} \omega^{*-1} B\Gamma(\sin \eta - \sin \eta_s) \\ &\quad - (\omega - \mathbb{1}\omega_s)^\top D \langle \omega \rangle^{-1} \langle \omega - \mathbb{1}\omega_u \rangle (\omega - \mathbb{1}\omega_s). \end{aligned}$$

Hence, we obtain

$$\begin{aligned} \dot{V}_s &= - (\omega - \mathbb{1}\omega_s)^\top \langle \omega \rangle^{-1} \\ &\quad \left(D \langle \omega - \mathbb{1}\omega_u \rangle - \omega_s^{-1} \langle z(\eta) \rangle \right) (\omega - \mathbb{1}\omega_s) \end{aligned}$$

with

$$z(\eta) := B\Gamma(\sin \eta - \sin \eta_s).$$

Since $D > 0$, $\omega_s > 0$, $\langle \mathbb{1}\omega_s - \mathbb{1}\omega_u \rangle = \sqrt{\Delta_N} J_n > 0$, and $z(\eta_s) = 0$, there exists a neighborhood Ω^+ around $(\eta_s, \mathbb{1}\omega_s)$ such that

$$\langle \omega - \mathbb{1}\omega_u \rangle > 0, \quad D \langle \omega - \mathbb{1}\omega_u \rangle - \omega_s^{-1} \langle z(\eta) \rangle > 0$$

for all $(\eta, \omega) \in \Omega^+$. Take a (nontrivial) compact level set Ω of V_s contained in this set, i.e., $\Omega \subset \Omega^+$. Note that such Ω always exists for sufficiently small $r > 0$, $\Omega = \{x \mid x \in \Omega^+ \text{ and } V_s(x) \leq r\}$. The compactness follows from convexity of V_s . The set Ω is clearly forward invariant as \dot{V}_s is nonpositive at any point within this set. Now, by

LaSalle's invariance principle, solutions of the system initialized in Ω converge to the largest invariant set \mathcal{M} in Ω , where $\dot{V}_s = 0$. On this invariant set we have $\omega = \mathbb{1}\omega_s$. By using the second equality in (6.20), we obtain that

$$0 = B\Gamma(\sin(\eta) - \sin(\eta_s)) \quad (6.21)$$

on the invariant set. Recall that $\eta, \eta_s \in \text{im } B^\top$, namely $\eta = B^\top\theta$ and $\eta_s = B^\top\theta_s$, for some vectors θ and θ_s . By multiplying (6.21) from the left with $(\theta - \theta_s)^\top$, we find that

$$0 = (\eta - \eta_s)^\top \Gamma(\sin(\eta) - \sin(\eta_s)).$$

This results in $\eta = \eta_s$, as the compact level sets are constructed in a neighborhood of $\eta_s \in (-\frac{\pi}{2}, \frac{\pi}{2})^m$, where $\sin(\eta_k)$ is strictly monotone for each $k = 1, 2, \dots, m$. This completes the proof. ■

6.3.3 Secondary Control

The primary controller stabilizes the system at the frequency ω_s , which in general is not equal to the nominal frequency ω^* . In this section, we aim at (optimally) regulating the frequency of the system (6.12) via the controller (6.13), such that a unique equilibrium with $\omega_s = \omega^*$ is achieved. Note that $\omega_s = \omega^*$ if and only if

$$\mathbb{1}^\top P_m = \mathbb{1}^\top P_\ell. \quad (6.22)$$

We associate a diagonal matrix $Q = \text{diag}\{q_1, \dots, q_n\}$ with the power generation costs, where $q_i > 0$ is the cost coefficient of the power generation of the i th inverter. Here we seek for an optimal resource allocation such that the control signal $P_m = \text{col}(P_{m_i})$ minimizes the quadratic cost function

$$C(P_m) = \frac{1}{2} P_m^\top Q P_m, \quad (6.23)$$

subject to the power balance constraint given by (6.22). Following the standard Lagrange multipliers method, the optimal control P_m^* that minimizes (6.23) is computed as

$$P_m^* = \frac{Q^{-1} \mathbb{1} \mathbb{1}^\top P_\ell}{\mathbb{1}^\top Q^{-1} \mathbb{1}}. \quad (6.24)$$

An immediate consequence of the above is that the load is proportionally shared among the inverters, i.e.,

$$(P_m^*)_i Q_i = (P_m^*)_j Q_j, \quad (6.25)$$

for all $i, j \in \mathcal{V}$. To achieve the optimal cost, and inspired by [4, 42, 124, 134], we propose the controller given by

$$\begin{aligned}\dot{\xi} &= -\mathcal{L}\xi - Q^{-1}\langle\omega\rangle^{-1}(\omega - \mathbf{1}\omega^*) \\ P_m &= Q^{-1}\xi,\end{aligned}\tag{6.26}$$

where \mathcal{L} is the Laplacian matrix of an undirected connected communication graph. The term $-Q^{-1}\langle\omega\rangle^{-1}(\omega - \mathbf{1}\omega^*)$ regulates the frequency to the nominal frequency, while the consensus based algorithm $-\mathcal{L}\xi$ aims at steering the input to the optimal one given by (6.24). Having (6.12)-(6.13), and (6.26), the overall system reads as

$$\begin{aligned}\dot{\eta} &= B^\top\omega \\ J\dot{\omega} &= \langle\omega\rangle^{-1}(Q^{-1}\xi - P_\ell - B\Gamma \sin \eta) - D(\omega - \mathbf{1}\omega^*) \\ \dot{\xi} &= -\mathcal{L}\xi - Q^{-1}\langle\omega\rangle^{-1}(\omega - \mathbf{1}\omega^*).\end{aligned}\tag{6.27}$$

Note that $\eta(0) = B^\top\theta(0)$, and hence $\eta(t) \in \text{im } B^\top$ for all $t \geq 0$. Consequently, we can restrict the domain of solutions of (6.27) to $(\eta, \omega, \xi) \in \mathcal{X} := \text{im } B^\top \times \mathbb{R}^n \times \mathbb{R}^n$ which is clearly forward invariant. Next, we characterize the equilibrium of the above system.

Lemma 6.3.4 The point $(\bar{\eta}, \bar{\omega}, \bar{\xi}) \in \mathcal{X}$ is an equilibrium of (6.27) if and only if it satisfies

$$\begin{aligned}Q^{-1}\bar{\xi} - P_\ell - B\Gamma \sin \bar{\eta} &= 0 \\ \bar{\omega} = \mathbf{1}\omega^*, \quad \bar{\xi} &= \frac{\mathbf{1}\mathbf{1}^\top P_\ell}{\mathbf{1}^\top Q^{-1}\mathbf{1}}.\end{aligned}\tag{6.28}$$

Proof. By the first equality in (6.27) it follows that $\omega = \mathbf{1}\bar{\omega}$ for some $\bar{\omega}$. By premultiplying the third equality in (6.27) by $\mathbf{1}^\top$, we obtain that $\mathbf{1}^\top Q^{-1}\langle\omega\rangle^{-1}(\bar{\omega} - \omega^*) = 0$, which implies that $\bar{\omega} = \omega^*$. In addition, $\bar{\xi} = \mathbf{1}\tilde{\xi}$ for some $\tilde{\xi} \in \mathbb{R}$. Again, by premultiplying the second equation by $\mathbf{1}^\top$, we have $\mathbf{1}^\top Q^{-1}\mathbf{1}\tilde{\xi} - \mathbf{1}^\top P_\ell = 0$, implying $\bar{\xi} = \frac{\mathbf{1}\mathbf{1}^\top P_\ell}{\mathbf{1}^\top Q^{-1}\mathbf{1}}$. ■

Lemma 6.3.4 imposes the following assumption:

Assumption 6.3.5 For given P_ℓ , there exists $\bar{\eta} \in \text{im } B^\top \cap (-\frac{\pi}{2}, \frac{\pi}{2})^m$ such that

$$\left(\frac{Q^{-1}\mathbf{1}\mathbf{1}^\top}{\mathbf{1}^\top Q^{-1}\mathbf{1}} - J_n \right) P_\ell - B\Gamma \sin \bar{\eta} = 0.$$

To prove frequency regulation, we exploit the energy function

$$W(x) = \frac{1}{2}\omega^\top J\omega - \omega^{*-1}\mathbf{1}^\top \Gamma \cos \eta + \frac{1}{2}\xi^\top \xi,\tag{6.29}$$

with $x = \text{col}(\eta, \omega, \xi)$. Note that the only difference with (6.18) is the addition of the quadratic term associated with the states of the controller. For the analysis, as before, we use the shifted version

$$W_s(x) = W(x) - (x - \bar{x})^\top \nabla \bar{W} - \bar{W}. \quad (6.30)$$

where $\bar{x} = (\bar{\eta}, \bar{\omega}, \bar{\xi})$. Noting that $\bar{\eta} \in (-\frac{\pi}{2}, \frac{\pi}{2})^m$, it is easily verified that W_s is positive definite around its local minimum $x = \bar{x}$. Again it is easy to verify that W_s takes its minimum at $x = \bar{x}$, provided that $\bar{\eta} \in (-\frac{\pi}{2}, \frac{\pi}{2})^m$. Now, we have the following result.

Theorem 6.3.6 Suppose that Assumption 6.3.5 holds. Then there exists a neighborhood Ω of $(\bar{\eta}, \bar{\omega}, \bar{\xi})$ such that any solution (η, ω, ξ) to (6.27) that starts in Ω , asymptotically converges to the equilibrium point $(\bar{\eta}, \bar{\omega}, \bar{\xi})$. Moreover, the vector P_m converges to the optimal power injection P_m^* given by (6.24).

Proof. First, observe that by substituting P_ℓ from (6.28) the system (6.27) can be written as

$$\begin{aligned} \dot{\eta} &= B^\top (\omega - \mathbb{1}\omega^*) \\ J\dot{\omega} &= \langle \omega \rangle^{-1} (Q^{-1}(\xi - \bar{\xi}) \\ &\quad - B\Gamma(\sin \eta - \sin \bar{\eta})) - D(\omega - \mathbb{1}\omega^*) \\ \dot{\xi} &= -\mathcal{L}(\xi - \bar{\xi}) - Q^{-1}\langle \omega \rangle^{-1}(\omega - \mathbb{1}\omega^*) \end{aligned} \quad (6.31)$$

Analogous to the proof of Theorem 6.3.3, the time derivative of W_s given by (6.29)-(6.30) along the solutions of (6.31) is computed as

$$\begin{aligned} \dot{W}_s &= -(\xi - \bar{\xi})^\top \mathcal{L}(\xi - \bar{\xi}) \\ &\quad - (\omega - \mathbb{1}\omega^*)^\top \left(D - \omega^{*-1}\langle \omega \rangle^{-1}\langle z(\eta) \rangle \right) (\omega - \mathbb{1}\omega^*) \end{aligned}$$

with

$$z(\eta) = B\Gamma(\sin \eta - \sin \bar{\eta}).$$

Since $D > 0$, $\omega^* > 0$, and $z(\bar{\eta}) = 0$, there exists a neighborhood Ω^+ around $(\bar{\eta}, \bar{\omega}, \bar{\xi})$ such that

$$D - \omega^{*-1}\langle \omega \rangle^{-1}\langle z(\eta) \rangle > 0$$

for all $(\eta, \omega, \xi) \in \Omega^+$. Take a (nontrivial) compact level set Ω of W_s contained in this set, i.e., $\Omega \subset \Omega^+$. Again note that such Ω always exists for sufficiently small r , $\Omega = \{x \mid x \in \Omega^+ \text{ and } W_s(x) \leq r\}$. Noting that Ω is forward invariant, by LaSalle's invariance principle, solutions of the system initialized in Ω converge to the largest invariant set \mathcal{M} in Ω with $\dot{W}_s = 0$. On this invariant set we have $\omega = \mathbb{1}\omega^*$, and $\mathcal{L}\xi = 0$

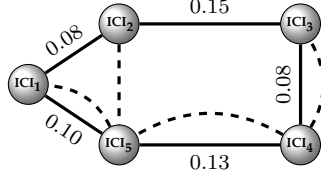


Figure 6.2: The solid lines denote the power lines in \mathcal{G} , and the dashed lines depict the communication links with the Laplacian \mathcal{L} . The values over the edges are the reactance of the lines.

implying that $\xi = \bar{\xi} + \alpha \mathbf{1}$ for some $\alpha \in \mathbb{R}$. By premultiplying the second equality in (6.31) with $\mathbf{1}^\top$, on the invariant set we have $0 = \mathbf{1}^\top Q^{-1}(\bar{\xi} + \alpha \mathbf{1} - \bar{\xi})$, which yields $\alpha = 0$ and thus $\xi = \bar{\xi}$. This means that $P_m = Q^{-1}\bar{\xi}$ on the invariant set, which coincides with the expression of optimal power injection P_m^* given by (6.24), noting the last equality in (6.28). Finally, by using an analogous argument to the proof of Theorem 6.3.3, we conclude that $\eta = \bar{\eta}$ on the invariant set, which completes the proof. ■

Remark 6.3.7 [An ICI connected to a constant load]

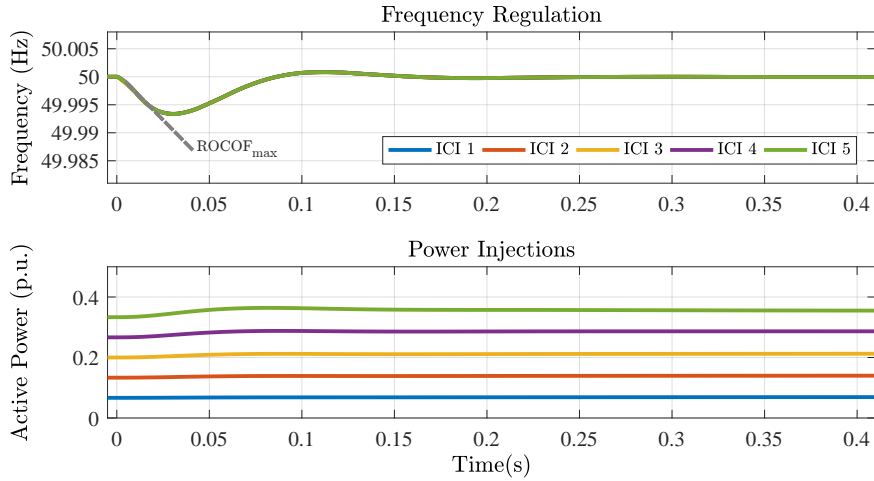
We can treat a single ICI modeled by (6.4)-(6.9) as the special case of the network modeled by (6.27) with $\mathcal{L} = 0$, $n = 1$, $Q = 1$, and $\Gamma = 0$. Hence the controller regulates the frequency to its nominal value also in the case of a single ICI connected to a constant load. □

6.4 Numerical Example

We illustrate the results by a numerical example of a power network consisting of five ICIs. The interconnection topology (solid lines) and the communication graph (dashed lines) are shown in Figure 6.2. The reactance of the lines are depicted along the edges. The inverter setpoints and other network parameters are chosen as shown in Table 6.1. The system is initially at steady-state with the constant power loads P_{ℓ_i} . At time $t = 0$, loads P_{ℓ_1} , P_{ℓ_3} , and P_{ℓ_5} are increased by 10 percent of their original values. The frequency evolution and the active power injections are depicted in Figure 6.3. It is observed that the system regulates the frequency to its nominal value 50 Hz. Note that the frequencies at the various nodes are so similar to each other, that no difference can be noticed in the plot. The system shows a safe maximum rate of change of frequency $\text{ROCOF}_{\max} = 0.3 \text{ Hz/s}$ (ENTSOE standard threshold for the maximum ROCOF is 1 Hz/s [48]), which can be diminished further using larger

Table 6.1: Simulation Parameters

	ICI ₁	ICI ₂	ICI ₃	ICI ₄	ICI ₅
C_{dc_i} (mF)	1.0	1.2	1.1	2.5	4.4
G_{dc_i} (U)	0.10	0.09	0.12	0.12	0.18
q_i (\$/kW ² h)	0.056	0.028	0.019	0.014	0.011
P_{ℓ_i} (kW)	10	12.5	13.5	16	25
$ V_i $ (V)	300.7	298.8	299.7	301.0	300.3
v_{dc}^* (kV)	1.0	0.9	0.8	1.2	1.5

**Figure 6.3:** Frequency regulation and optimal power injection after a step change in the local loads connected to the nodes 1, 3, and 5.

or parallel capacitors. Finally, observe that the load is shared among the sources with the ratios of $\{q_1^{-1}, \dots, q_5^{-1}\}$, which is in agreement with the proportional power sharing (6.25).

6.5 Conclusion

In this chapter, inverters with capacitors that emulate inertia, were investigated in two cases. First, the case of a single inverter connected to a constant load, and second, a network of inverters with local constant power loads. A control method including primary and secondary controllers was proposed, by which the stability


and frequency regulation are guaranteed. Finally, a numerical simulation illustrated that the method successfully regulates the frequency, and share the power between sources in an optimal fashion.

Chapter 7

Power Systems in Port-Hamiltonian Framework

“Space and time are the framework within which the mind is constrained to construct its experience of reality.”

– Immanuel Kant

 PORT-HAMILTONIAN (pH) modeling of physical systems has gained extensive attention in recent years. pH systems theory provides a systematic framework for modeling and analysis of physical systems and processes [140, 141]. In this chapter, we investigate modeling power systems in pH framework, and study their shifted passivity properties in two cases: (i) The control input acts on the *flow*; and (ii) The control input acts on the *power*.¹ (with constant structure and dissipation matrices)

7.1 Shifted passivity of port-Hamiltonian systems: Application to stability analysis of the 6th order model of synchronous generators

As mentioned in Chapter 2, showing shifted passivity for port-Hamiltonian systems with state-dependent dissipation and interconnection matrices is nontrivial. In this section, we examine the shifted passivity property of pH systems with strictly convex Hamiltonian, and derive conditions under which shifted passivity is guaranteed. In case the Hamiltonian is quadratic and state dependency appears in an affine manner in the dissipation and interconnection matrices, our conditions reduce to negative semidefiniteness of an appropriately constructed constant matrix. Moreover, we elaborate on how these conditions can be extended to the case when the shifted passivity property can be enforced via output feedback, thus paving the path for

¹Rate of change of the Hamiltonian

controller design. Stability of forced equilibria of the system is analyzed invoking the proposed passivity conditions. The utility and relevance of the results is illustrated with the application to the 6th order synchronous generator model.

7.1.1 Introduction

In this section, we study shifted passivity of port-Hamiltonian (pH) systems that, as is well-known, provide an attractive energy-based modeling framework for nonlinear physical systems [141, 142].² As mentioned in Chapter 2, the Hamiltonian readily serves as a storage function certifying passivity of a pH system, however, proving its shifted passivity is in general nontrivial. It was also shown that pH systems with convex Hamiltonian are shifted passive provided the input, dissipation and interconnection matrices are all constant. Conditions for shifted passivity of pH systems with state-dependent matrices have been reported in [82] and [49]. In the former case, quite conservative, *integrability conditions*, are imposed while the latter ones are too general and thus can be difficult to verify. The main contribution of this section is to give compact and easily verifiable conditions, *i.e.*, monotonicity of a suitably defined function, to ensure shifted passivity of pH systems with strictly convex Hamiltonian and *state-dependent* dissipation and interconnection matrices. Our candidate storage function is the shifted Hamiltonian.

Notably, for the case of affine pH systems with quadratic Hamiltonian, our conditions reduce to negative semidefiniteness of an appropriately constructed *constant* matrix. Such systems are relevant in applications such as synchronous generators as will be demonstrated by the case study. The proposed conditions are able to verify shifted passivity as well as stability of these systems in an efficient way, namely by checking whether a systematically constructed matrix is negative semidefinite. An additional contribution of our work is that the proposed conditions provide an estimate of the excess and shortage of passivity that serves as a tool for controller design; see, *e.g.*, [106].

The structure of the section is as follows. The problem formulation is provided in Subsection 7.1.2. The main results are given in Subsection 7.1.3, and are specialized to quadratic affine pH systems in Subsection 7.1.4. The results are illustrated with a synchronous generator in Subsection 7.1.5. The section closes with conclusions in Subsection 7.1.6.

²Throughout this section, unless explicitly specified, *shifted passivity* is referring to a *global* property, *i.e.*, $\mathcal{X} = \mathbb{R}^n$ in view of Definition 2 (Chapter 2).

7.1.2 Problem Formulation

Consider the pH system

$$\dot{x} = (J(x) - R(x))\nabla H(x) + Gu \quad (7.1a)$$

$$y = G^\top \nabla H(x), \quad (7.1b)$$

with state $x \in \mathbb{R}^n$, input $u \in \mathbb{R}^m$, and output $y \in \mathbb{R}^m$. The constant matrix $G \in \mathbb{R}^{n \times m}$ has full column rank, and $H : \mathbb{R}^n \rightarrow \mathbb{R}$ is the Hamiltonian of the system. The matrix J is skew-symmetric, i.e., $J(x) + J^\top(x) = 0$, and

$$R(x) \geq R^*, \quad \forall x \in \mathbb{R}^n \quad (7.2)$$

for some constant positive semidefinite matrix R^* .

Define the steady-state relation

$$\mathcal{E} := \{(x, u) \in \mathbb{R}^n \times \mathbb{R}^m \mid (J(x) - R(x))\nabla H(x) + Gu = 0\}.$$

Fix $(\bar{x}, \bar{u}) \in \mathcal{E}$ and the corresponding output $\bar{y} := G^\top \nabla \bar{H}$.³ We are interested in finding conditions under which the system (7.1) is shifted passive with respect to (\bar{x}, \bar{u}) .

7.1.3 Main Results

In this subsection, we provide our main results concerning shifted passivity, stability, and shifted feedback passivity of the pH system (7.1).

Shifted passivity

Here, we provide conditions under which the pH system (7.1) is shifted passive. Towards this end, we make two assumptions:

Assumption 7.1.1 [Strict convexity]

The Hamiltonian H is strictly convex.

Given the strictly convex function H , we define the *Legendre transform*, sometimes called Legendre-Fenchel transform, of H as the function

$$H^*(p) := \max_{x \in \mathbb{R}^n} \{x^\top p - H(x)\}, \quad (7.3)$$

where the domain of H^* is the set of all p for which the expression is well-defined (i.e., the maximum is attained). We list the following properties of the Legendre transform

³We denote $\nabla H(\bar{x})$ by $\nabla \bar{H}$; see Section 1.4.

H^* ; see, e.g., [7], [105].

1. The domain of H^* is equal to the convex range of ∇H .⁴
2. H^* is strictly convex.
3. $H^{**} = H$.⁵
4. $\nabla H^*(\nabla H(x)) = x$, for all x .
5. $\nabla H(\nabla H^*(p)) = p$, for all p in the convex range of ∇H .

Let $F(x) := J(x) - R(x)$. Leveraging the Legendre transform above, the function $F(x)$ can be restated in terms of co-energy variables $s := \nabla H(x)$ as

$$F(x) = F(\nabla H^*(s)) =: \mathcal{F}(s). \quad (7.4)$$

We denote the domain of H^* , which is equal to the range of ∇H , by S . Let $\bar{s} := \nabla \bar{H}$. We impose the following assumption on \mathcal{F} :

Assumption 7.1.2 [Monotonicity]

The mapping \mathcal{F} verifies

$$\nabla(\mathcal{F}(s)\bar{s}) + \nabla(\mathcal{F}(s)\bar{s})^\top - 2R^* \leq 0, \quad \forall s \in S. \quad (7.5)$$

Note that the choice of R^* is important in feasibility of (7.5), and it is best to choose the lower bound in (7.2) as tight as possible. Now, we have the main result of this section:

Proposition 7.1.3 [Shifted passivity]

Let Assumptions 7.1.1 and 7.1.2 hold. Then, the pH system (7.1) is shifted passive, namely

$$\dot{\mathcal{H}} \leq (u - \bar{u})^\top (y - \bar{y}) \quad (7.6)$$

is satisfied with \mathcal{H} being the shifted Hamiltonian

$$\mathcal{H}(x) := H(x) - (x - \bar{x})^\top \nabla \bar{H} - H(\bar{x}). \quad (7.7)$$

Proof. First, note that \mathcal{H} is nonnegative as the Hamiltonian H is (strictly) convex [20, 68]. Substituting (7.4) into (7.1) yields

$$\dot{x} = \mathcal{F}(s)s - \mathcal{F}(\bar{s})\bar{s} + G(u - \bar{u}),$$

⁴If p is not in the range of ∇H , then the maximum in (7.3) for such p does not exist.

⁵This means that the Legendre transform is an involution, namely the Legendre transform of the Legendre transform of H is equal to H itself.

where we have subtracted $0 = \mathcal{F}(\bar{s})\bar{s} + G\bar{u}$. Noting that $\nabla\mathcal{H}(x) = \nabla H(x) - \nabla\bar{H}$, the time derivative of $\mathcal{H}(x)$ is computed as

$$\begin{aligned}\dot{\mathcal{H}} &= (\nabla\mathcal{H})^\top \dot{x} = (s - \bar{s})^\top (\mathcal{F}(s)s - \mathcal{F}(\bar{s})\bar{s}) + (y - \bar{y})^\top (u - \bar{u}) \\ &= (s - \bar{s})^\top (\mathcal{F}(s) - \mathcal{F}(\bar{s}))\bar{s} \\ &\quad + (s - \bar{s})^\top F(x)(s - \bar{s}) + (y - \bar{y})^\top (u - \bar{u}) \\ &\leq (s - \bar{s})^\top (\mathcal{F}(s) - \mathcal{F}(\bar{s}))\bar{s} \\ &\quad - (s - \bar{s})^\top R^* (s - \bar{s}) + (y - \bar{y})^\top (u - \bar{u}),\end{aligned}\tag{7.8}$$

where we used (7.1b) in the first identity, added and subtracted the term $(s - \bar{s})^\top (\mathcal{F}(s)\bar{s})$ and used (7.4) to write the second equality, while the bound is obtained invoking (7.2). Now, let

$$\mathcal{M}(s) := \mathcal{F}(s)\bar{s} - R^*s.\tag{7.9}$$

Then $\dot{\mathcal{H}}$ can be written as

$$\dot{\mathcal{H}} = (s - \bar{s})^\top (\mathcal{M}(s) - \mathcal{M}(\bar{s})) + (y - \bar{y})^\top (u - \bar{u}).\tag{7.10}$$

By (7.5), we have that $\nabla\mathcal{M}(s) + (\nabla\mathcal{M}(s))^\top \leq 0$, for all $s \in S$, which ensures that the map $\mathcal{M}(\cdot)$ is monotone [115]. The proof is completed noting that by monotonicity

$$(s - \bar{s})^\top (\mathcal{M}(s) - \mathcal{M}(\bar{s})) \leq 0.$$

■

Remark 7.1.4 [Local shifted passivity]

By Assumptions 7.1.1 and 7.1.2, both the strict convexity and the monotonicity property must hold for the whole sets \mathbb{R}^n and S , respectively, which results in *global* shifted passivity of (7.1). For *local* shifted passivity,⁶ we can restrict to a subset $\mathcal{X} \subseteq \mathbb{R}^n$, with Assumptions 7.1.1 and 7.1.2 modified to

1. The Hamiltonian is strictly convex in $\mathcal{X} \subseteq \mathbb{R}^n$.
2. Inequality (7.5) holds for all $s \in \mathcal{S} := \{\nabla H(x) \mid x \in \mathcal{X}\}$,

while R^* is any matrix satisfying, instead of (7.2), $R(x) \geq R^*$, $\forall x \in \mathcal{X}$. □

We complete this subsection by considering the case where the condition (7.5) does not hold, which means that the system (7.1) may not be shifted passive, but it can be rendered shifted passive via output feedback.

⁶By “local” we mean that there exist open neighborhoods $\mathcal{X} \subseteq \mathbb{R}^n$ and $\mathcal{U} \subseteq \mathbb{R}^m$ of $(\bar{x}, \bar{u}) \in \mathcal{X} \times \mathcal{U}$ such that (7.6) holds for all $(x, u) \in \mathcal{X} \times \mathcal{U}$.

Proposition 7.1.5 [Shifted feedback passivity]

Consider the pH system (7.1) verifying Assumption 7.1.1 and such that

$$\nabla(\mathcal{F}(s)\bar{s}) + \nabla(\mathcal{F}(s)\bar{s})^\top - 2R^* \leq 2\gamma GG^\top,$$

for some $\gamma \in \mathbb{R}$. Then, the shifted Hamiltonian (7.25) satisfies the following dissipation inequality

$$\dot{\mathcal{H}} \leq (u - \bar{u})^\top (y - \bar{y}) + \gamma \|y - \bar{y}\|^2.$$

Proof. The proof is analogous to that of Proposition 7.1.3, by adding and subtracting the term $\gamma GG^\top (s - \bar{s})$ in (7.8), and modifying the map \mathcal{M} as

$$\tilde{\mathcal{M}}(s) := \mathcal{M}(s) - \gamma GG^\top s.$$

■

Note that a negative γ proves that the pH system is (output-strictly) shifted passive. On the other hand, a positive γ indicates the shortage of shifted passivity. Notice that the simple proportional controller

$$u = \bar{u} - K_P (y - \bar{y}) + v,$$

with $K_P \geq \gamma I$, ensures that the interconnected system is passive from the external input v to output $y - \bar{y}$. Analogously, Proposition 7.1.5 can be used to design dynamic passive controllers to stabilize the closed-loop system; see [106] for an application to control of permanent magnet synchronous motors.

Stability of the forced equilibria

Lyapunov stability of the equilibrium of (7.1) with $u = \bar{u}$, immediately follows from Proposition 7.1.3, with the Lyapunov function being the shifted Hamiltonian \mathcal{H} . Moreover, asymptotic stability follows by imposing the condition that $\dot{\mathcal{H}}$ is negative definite. As will be shown below, the case of state-dependent input matrix can also be accommodated in the stability analysis by imposing conditions analogous to (7.5). To this end, consider again the pH system (7.1a), where now $G = G(x)$. Let

$$G(x) = G(\nabla H^*(s)) =: \mathcal{G}(s).$$

Then, we have the following result:

Proposition 7.1.6 [Asymptotic stability]

Consider the pH system

$$\dot{x} = (J(x) - R(x))\nabla H(x) + G(x)\bar{u}, \quad (7.11)$$

with $(\bar{x}, \bar{u}) \in \mathcal{E}$. Then, we have

1. The equilibrium is asymptotically stable if $\nabla^2 H(\bar{x}) > 0$ and there exists $\epsilon > 0$ such that the inequality

$$\nabla(\mathcal{F}(s)\bar{s} + \mathcal{G}(s)\bar{u}) + \nabla(\mathcal{F}(s)\bar{s} + \mathcal{G}(s)\bar{u})^\top - 2R^* \leq -2\epsilon J_n, \quad (7.12)$$

holds at $s = \bar{s}$.⁷

2. The equilibrium is globally asymptotically stable if the Hamiltonian H is *strongly* convex and (7.12) holds for all $s \in \mathbb{R}^n$.

Proof. The proof of the first item follows analogously to Proposition 7.1.3 by modifying the map \mathcal{M} in (7.9) as $\mathcal{F}(s)\bar{s} - R^*s + \mathcal{G}(s)\bar{u}$, and noting that the function \mathcal{H} is locally nonnegative and is equal to zero whenever $x = \bar{x}$ [20, p. 205], [68, Prop. 2].

To prove the second statement, it suffices to show that S is radially unbounded. This follows from strong convexity of H noting that [104, Ch.2]

$$\mathcal{H}(x) = H(x) - (x - \bar{x})^\top \nabla \bar{H} - H(\bar{x}) \geq \mu \|x - \bar{x}\|^2,$$

for some $\mu \in \mathbb{R}^+$. ■

Remark 7.1.7 [Alternative for (7.12)]

The identity matrix in the right hand side of (7.12) can be replaced by a positive semidefinite matrix $C^\top C$, with $C \in \mathbb{R}^{m \times n}$, if the equilibrium is “observable” from the input-output pair $(\bar{u}, C\nabla \bar{H})$, namely if

$$\dot{x} = F(x)\nabla H + G(x)\bar{u}, \quad C\nabla H(x) = C\nabla \bar{H} \implies x = \bar{x}.$$

□

Remark 7.1.8 [Shifted passivity with state-dependent input matrix]

While the inequality (7.12) with $\epsilon = 0$ does not imply shifted passivity of the pH system with state-dependent input matrix, it ensures that the map $u - \bar{u}$ to the output y_m defined as

$$y_m := G^\top(x)\nabla \mathcal{H}(x) = G^\top(x)(\nabla H(x) - \nabla H(\bar{x}))$$

is passive. □

⁷This means that the Jacobian of $\mathcal{F}(s)\bar{s} + \mathcal{G}(s)\bar{u}$ in (7.12) has to be evaluated at $s = \bar{s}$.

7.1.4 Application to Quadratic Affine Systems

In this subsection we specialize our results to the case where

$$F(x) = F_0 + \sum_{i=1}^n F_i x_i, \quad (7.13)$$

with $F_j \in \mathbb{R}^{n \times n}$, $j = 0, \dots, n$, constant and

$$H(x) = \frac{1}{2} x^\top Q x, \quad (7.14)$$

with $Q \in \mathbb{R}^{n \times n}$ being positive definite. We call these systems *quadratic affine* pH systems.

In order to satisfy (7.2) and state the global version of our results, we need to assume that $R(x) = R_0$ for some constant matrix R_0 . This is due to the fact that in the affine case the inequality $R(x) \geq R^*$, for all $x \in \mathbb{R}^n$, implies that the matrix R is constant. In Remark 7.1.12, we elaborate on how this assumption is relaxed to obtain local results. Note that, with a constant dissipation matrix, $F_0 + F_0^\top = -2R_0 \leq 0$ and $F_j + F_j^\top = 0$ for each $j \geq 1$.

Proposition 7.1.9 [Shifted passivity of quadratic affine systems]

Consider the quadratic affine pH system (7.1) with (7.13) and (7.14). Fix $(\bar{x}, \bar{u}) \in \mathcal{E}$ and define the $n \times n$ constant matrix

$$B := \sum_{i=1}^n F_i Q \bar{x} e_i^\top Q^{-1}, \quad (7.15)$$

with $e_i \in \mathbb{R}$ the i -th element of the standard basis. Then we have

$$\dot{\mathcal{H}} \leq (y - \bar{y})^\top (u - \bar{u}), \quad (7.16)$$

where \mathcal{H} is the quadratic shifted Hamiltonian function $\mathcal{H}(x) := \frac{1}{2}(x - \bar{x})^\top Q(x - \bar{x})$, if and only if

$$B + B^\top - 2R_0 \leq 0. \quad (7.17)$$

Proof. The "if" part follows by verifying the conditions of Proposition 7.1.3. In this case, $H^*(p) = \frac{1}{2} p^\top Q^{-1} p$,

$$\nabla H^*(s) = Q^{-1} s, \quad s = Qx,$$

and

$$\mathcal{F}(s) = F_0 + \sum_{i=1}^n F_i (e_i^\top Q^{-1} s). \quad (7.18)$$

Hence,

$$\mathcal{F}(s)\bar{s} = (F_0 + \sum_{i=1}^n F_i(e_i^\top Q^{-1}s))Q\bar{x}.$$

Now, by rewriting the last expression in the equivalent form

$$\mathcal{F}(s)\bar{s} = F_0Q\bar{x} + \sum_{i=1}^n F_iQ\bar{x}e_i^\top Q^{-1}s,$$

we obtain that

$$\nabla(\mathcal{F}(s)\bar{s}) = \sum_{i=1}^n F_iQ\bar{x}e_i^\top Q^{-1}.$$

Finally, using (7.15), condition (7.5) takes the form

$$\nabla(\mathcal{F}(s)\bar{s}) + \nabla(\mathcal{F}(s)\bar{s})^\top - 2R_0 = B + B^\top - 2R_0 \leq 0.$$

To prove the “only if” part, suppose that (7.16) is satisfied. This implies that the pH system linearized around the equilibrium $x = \bar{x}$ is passive with the Hamiltonian $H(x) = \frac{1}{2}x^\top Qx$ serving as a storage function [142, Ch. 11.3]. It is easy to verify that the resulting linear time-invariant system admits the form

$$\dot{x} = (J(\bar{x}) - R_0)Qx + BQx + Gu \quad (7.19a)$$

$$y = G^\top Qx. \quad (7.19b)$$

Therefore, we obtain that [142, Ch. 4.1]

$$Q(J(\bar{x}) - R_0 + B)Q + Q(J(\bar{x}) - R_0 + B)^\top Q \leq 0,$$

which reduces to $Q(-2R_0 + B + B^\top)Q \leq 0$. Clearly, the latter inequality is equivalent to (7.17). \blacksquare

Remark 7.1.10 [Stability condition in terms of co-energy variables]

The stability condition in Proposition 7.1.9 can equivalently be stated in terms of the co-energy variables $s = \nabla H(x)$, which in certain cases decreases the computational effort. To this end, note that by (7.18), the function $\mathcal{F}(s)$ can be written in the affine form:

$$\mathcal{F}(s) = F_0 + \sum_{i=1}^n \mathcal{F}_i s_i,$$

where $\mathcal{F}_i := \sum_{j=1}^n F_j Q_{ij}^{-1}$. Hence, the matrix B in (7.15) can be equivalently written as

$$B := \sum_{i=1}^n \mathcal{F}_i Q\bar{x}e_i^\top = \sum_{i=1}^n \mathcal{F}_i \bar{s}e_i^\top.$$

\square

Since H is strongly convex and the condition (7.17) is state independent, Proposition 7.1.6 yields the following result:

Corollary 7.1.11 [GAS of quadratic affine systems]

Consider the quadratic affine pH system (7.1a) with (7.13) and (7.14) under some constant input $u = \bar{u}$, and let $(\bar{x}, \bar{u}) \in \mathcal{E}$. The equilibrium \bar{x} is globally asymptotically stable if (7.17) holds with strict inequality.

Remark 7.1.12 [Local shifted passivity and stability]

Analogous to the previous subsection, local variations of Proposition 7.1.9 and Corollary 7.1.11 can be obtained by restricting x in a domain $\mathcal{X} \in \mathbb{R}^n$ with $\bar{x} \in \mathcal{X}$. In that case, the matrix R_0 in (7.17) is replaced by R^* , where $R(x) \geq R^* \geq 0$ for all $x \in \mathcal{X}$. \square

7.1.5 Synchronous generator (6^{th} -order model) connected to a resistor

In this subsection, we apply the proposed method to the six-dimensional model of the synchronous generator. As introduced in Chapter 1, the state variables of this model comprise of the stator fluxes on the dq axes $\psi_d \in \mathbb{R}, \psi_q \in \mathbb{R}$, rotor fluxes $\psi_r \in \mathbb{R}^3$ (the first component of ψ_r corresponds to the field winding and the remaining two to the damper windings), and the angular momentum of the rotor p . The Hamiltonian H (total stored energy of the synchronous generator) is the sum of the magnetic energy of the generator and the kinetic energy of the rotating rotor. More precisely, the Hamiltonian takes the form $H(x) = \frac{1}{2}x^\top Qx$ with $x = [\psi_d \ \psi_q \ \psi_r \ p]^\top$ and

$$Q = \begin{bmatrix} L^{-1} & 0_{51} \\ 0_{15} & m^{-1} \end{bmatrix} > 0, \quad L = \begin{bmatrix} L_d & 0 & kL_{afd} & kL_{akd} & 0 \\ 0 & L_q & 0 & 0 & -kL_{akq} \\ kL_{afd} & 0 & L_{ffd} & L_{akd} & 0 \\ kL_{akd} & 0 & L_{akd} & L_{kkd} & 0 \\ 0 & -kL_{akq} & 0 & 0 & L_{kkq} \end{bmatrix},$$

where $m \in \mathbb{R}$ is the total moment of inertia of the turbine and the rotor. Note that the elements of the inductance matrix L are all constant parameters; see [50] for more details. The system dynamics is then given by the pH system [50]

$$\dot{x} = (J(x) - R)\nabla H(x) + G \begin{bmatrix} V_f \\ \tau \end{bmatrix},$$

with

$$J(x) = \begin{bmatrix} 0_{22} & 0_{23} & \begin{bmatrix} -\psi_q \\ \psi_d \end{bmatrix} \\ 0_{32} & 0_{33} & 0_{31} \\ [\psi_q & -\psi_d] & 0_{13} & 0 \end{bmatrix}, \quad R = \begin{bmatrix} \begin{bmatrix} r & 0 \\ 0 & r \end{bmatrix} & 0_{23} & 0_{21} \\ 0_{32} & \begin{bmatrix} R_f & 0 & 0 \\ 0 & R_{kd} & 0 \\ 0 & 0 & R_{kq} \end{bmatrix} & 0_{31} \\ 0_{12} & 0_{13} & d \end{bmatrix} > 0,$$

$$G = \begin{bmatrix} 0_{21} & 0_{21} \\ \begin{bmatrix} 1 \\ 0 \\ 0 \end{bmatrix} & 0_{31} \\ 0 & 1 \end{bmatrix},$$

where V_f represents the rotor field winding voltage, τ is the mechanical torque, r is the summation of the load and stator resistances, R_f, R_{kd}, R_{kq} denote the rotor resistances, and d corresponds to the mechanical friction. We can rewrite the system as

$$Q^{-1}\dot{s} = (\mathcal{J}(s) - R)s + G \begin{bmatrix} V_f \\ \tau \end{bmatrix}, \quad (7.20)$$

where $s = Qx = [I_d \ I_q \ I_r \ \omega]^\top$. Here $I_d \in \mathbb{R}, I_q \in \mathbb{R}$ are the components of the stator current on the dq axes, and $I_r \in \mathbb{R}^3$ and $\omega \in \mathbb{R}$ are the currents and angular velocity of the rotor, respectively. Note that

$$\mathcal{J}(s) = \begin{bmatrix} 0_{22} & 0_{23} & v_J(s) \\ 0_{32} & 0_{33} & 0_{31} \\ v_J^\top(s) & 0_{13} & 0 \end{bmatrix}, \quad v_J(s) := \begin{bmatrix} -L_q I_q + L_{akq} I_{kq} \\ L_d I_d + L_{afd} I_f + L_{akd} I_{kd} \end{bmatrix}.$$

Let $V_f = \bar{V}_f$ and $\tau = \bar{\tau}$, for some constant vectors \bar{V}_f and $\bar{\tau}$. Through straightforward calculations, and using Remark 7.1.10, the condition (7.17) reads as

$$\begin{bmatrix} -2r & \bar{\omega}(L_d - L_q) & 0 & 0 & k\bar{\omega}L_{akq} & -\bar{I}_q L_d \\ \bar{\omega}(L_d - L_q) & -2r & k\bar{\omega}L_{afd} & k\bar{\omega}L_{akd} & 0 & \bar{I}_d L_d \\ 0 & k\bar{\omega}L_{afd} & -2R_f & 0 & 0 & -\bar{I}_q L_{afd} \\ 0 & k\bar{\omega}L_{akd} & 0 & -2R_{kd} & 0 & -\bar{I}_q L_{akd} \\ k\bar{\omega}L_{akq} & 0 & 0 & 0 & -2R_{kq} & -\bar{I}_d L_{akq} \\ -\bar{I}_q L_d & \bar{I}_d L_d & -\bar{I}_q L_{afd} & -\bar{I}_q L_{akd} & -\bar{I}_d L_{akq} & -2d \end{bmatrix} \leq 0, \quad (7.21)$$

where $\bar{I}_d, \bar{I}_q, \bar{I}_r, \bar{\omega}$ are the associated values of s at the equilibrium of (7.20), *i.e.*,

$$(\mathcal{J}(\bar{s}) - R)\bar{s} + G \begin{bmatrix} \bar{V}_f \\ \bar{\tau} \end{bmatrix} = 0,$$

with $\bar{s} = [\bar{I}_d \ \bar{I}_q \ \bar{I}_r \ \bar{\omega}]^\top$. Hence, by Proposition 7.1.9, (7.20) is shifted passive if (7.21) holds. Moreover, by Corollary 7.1.11, if (7.21) holds with strict inequality, then the equilibrium $\bar{x} = Q^{-1}\bar{s}$ is globally asymptotically stable. The stability result is consistent with those of [23, 143].⁸

Note that the general method proposed in [82] is based on augmenting the Hamiltonian with an extra term which is a function of the input and the states. However, this method relies on integrability conditions that are not satisfied for $\bar{\tau} \neq 0$ [50], which is the case of interest in practice. Also note that Corollary 7.1.11 is valid for a general quadratic affine pH-system, and the condition (7.21) is obtained in a systematic manner here, namely by verifying the negative definiteness test in (7.17). Moreover, if (7.21) does not hold, then in view of Proposition 7.1.5, one can investigate the possibility of designing suitable proportional, PI, or more generally dynamic (input-strictly) passive controllers rendering the equilibrium globally asymptotically stable.

7.1.6 Conclusion

We have examined the shifted passivity property of pH systems with convex Hamiltonian by proposing conditions in terms of the monotonicity of suitably constructed functions, under which the property is verified. We have leveraged these conditions to study (global) asymptotic stability of forced equilibria of the system. As we observed, for quadratic affine pH system, shifted passivity and (global) asymptotic stability are guaranteed if an appropriately constructed constant matrix is negative semidefinite. We demonstrated the applicability of the results on the 6th order synchronous generator model.

⁸Notice that the condition (7.21) is identical with (30) in [143], however there is a typo there as the term $\bar{\omega}(L_d - L_q)$ is missing.

7.2 Shifted passivity of power-controlled Hamiltonian systems: Application to electrical systems with constant power loads

Here, we study a type of port-Hamiltonian system, in which the controller or disturbance is not applied to the flow variables, but to the systems power; a scenario that appears in many practical applications. A suitable framework is provided to model these systems and to investigate their shifted passivity properties, based on which, a stability analysis is carried out. The applicability of the results is illustrated with the important problem of stability analysis of electrical circuits with constant power loads.

7.2.1 Introduction

Typically, the external inputs (controls or disturbances) in pH systems act on the flow variables, *i.e.*, on the derivative of the energy storing coordinates. However, in some cases of practical interest, these external inputs act on the systems *power*, either as the control variable, or as a power that is extracted from (or injected to) the system. We refer to this kind of systems as *Power-controlled Hamiltonian* (P_wH) systems. P_wH systems cannot be modeled with constant dissipation matrices, which is the scenario considered in [68], and therefore analyzing their passivity properties is nontrivial. Furthermore, the conditions derived in the Section 7.1 are general, and in cases conservative.

An example of P_wH systems is electrical systems with instantaneous constant-power loads (CPLs), which model the behavior of some point-of-load converters that are widely used in modern electrical systems; see [81, 116] and references therein. It is well-known that CPLs introduce a destabilizing effect that gives rise to significant oscillations or to network collapse [47], and hence they are the most challenging component of the standard load model, referred to as ZIP model [37, 125]. Therefore, the investigating the *stability* of the equilibria of the systems with CPLs is a topic of utmost importance; see [9, 17, 77, 81] for an analysis of *existence* of equilibria.

In [125], sufficient conditions are derived for all operating points of purely resistive networks with CPLs to lie in a desirable set. Stability analysis has been carried out in [3, 9] using linearization methods; see also [81]. In [12], and recently in [26], Brayton-Moser potential theory [19] is employed, however, constraints on individual grid components are imposed. Moreover, as shown in [81], the estimate of the region of attraction (ROA) of the equilibria based on the Brayton-Moser potential is rather conservative.

In this section, we propose a framework to model P_wH systems, and provide sufficient conditions for shifted passivity and stability of their equilibria. We use the shifted Hamiltonian as the candidate Lyapunov function. This Lyapunov function is hence based on the physical energy of the system, and unlike the case of Brayton-Moser model, is trivially computed. Two immediate corollaries of the shifted passivity property are: (i) that their shifted equilibrium can be stabilized with simple PI controllers [68]; (ii) that in the uncontrolled case, when a constant input power or load is imposed, stability of this equilibrium can be established. In this section we concentrate on the latter issue, that was first studied in the standard pH systems framework in [82]. Interestingly, our framework allows us to give an analytic characterization of an estimate of the ROA, in the case of a quadratic Hamiltonian.

The remainder of this section is organized as follows. The proposed model for P_wH systems is introduced in Subsection 7.2.2. The main result, that is, the derivation of conditions for their shifted passivity, is provided in Subsection 7.2.3. The stability analysis is given in Subsection 7.2.4. The main result is then illustrated in Subsection 7.2.5 with its application to electrical systems with CPLs, and in Subsection 7.2.6, with the application to synchronous generators. Finally, some concluding remarks are provided in Subsection 7.2.7.

7.2.2 Model

Consider the pH system driven by the flow $f \in \mathbb{R}^m$ [140]

$$\begin{aligned}\dot{x} &= (J - R)\nabla H(x) + Bf \\ e &= B^\top \nabla H(x),\end{aligned}$$

where $x \in \mathbb{R}^n$ is the system state, $e \in \mathbb{R}^m$ is the effort, H is the system Hamiltonian (energy) function, and the $n \times n$ constant matrices $J = -J^\top$ and $R \geq 0$, are the structure and the dissipation matrices, respectively. Without loss of generality, we consider the constant matrix B defined as

$$B := \begin{bmatrix} J_m \\ 0_{(n-m) \times m} \end{bmatrix}. \quad (7.22)$$

To model the power control input/disturbance, we define the control (power) input $u \in \mathbb{R}^m$ as the element-wise product of effort and flow, i.e., $u := \langle e \rangle \langle f \rangle \mathbf{1}$. Hence we have $f = \langle e \rangle^{-1} u$. We decompose the vector ∇H into

$$\nabla H = \begin{bmatrix} \nabla_u H(x) \\ \nabla_0 H(x) \end{bmatrix},$$

where $\nabla_u H(x) \in \mathbb{R}^m$ is associated with the actuated states. We have

$$\begin{aligned} Bf &= B\langle e \rangle^{-1}u = B\langle B^\top \nabla H(x) \rangle^{-1}u \\ &= B\langle \nabla_u H(x) \rangle^{-1}u \\ &= G(x)u, \end{aligned}$$

where the (power) input matrix $G \in \mathbb{R}^{n \times m}$ is defined as

$$G(x) := \begin{bmatrix} \langle \nabla_u H(x) \rangle^{-1} \\ 0_{(n-m) \times m} \end{bmatrix}. \quad (7.23)$$

The input matrix $G(x)$ is well-defined in the set Ω^+ characterized as

$$\Omega^+ := \{x \in \mathbb{R}^n : \langle \nabla_u H(x) \rangle > 0\}.$$

Then the dynamics of the Power-controlled Hamiltonian (P_wH) system is given by

$$\dot{x} = (J - R)\nabla H(x) + G(x)u, \quad x \in \Omega^+, \quad (7.24)$$

with the first m components of x corresponding to the *power* controlled states. Note that the external input u of the system (7.24), acts *directly* on the power (rate of change of the Hamiltonian), *i.e.*,

$$\dot{H} = -\nabla H^\top(x) R \nabla H(x) + \mathbf{1}^\top u.$$

The natural output corresponding to the input u is given as the constant vector $\mathbf{1}$, in accordance with the fact that the total supplied power is $\mathbf{1}^\top u$. Since this output cannot be employed, *e.g.*, for a controller design, we will use a *shifted* output; see (7.28) later on.

Defining the steady-state relation

$$\mathcal{E} := \{(x, u) \in \mathbb{R}^n \times \mathbb{R}^m \mid (J - R)G(x)u = 0\},$$

we can write the *shifted* model for the system as:

Lemma 7.2.1 [Shifted model]

Fix $(\bar{x}, \bar{u}) \in \mathcal{E}$, then the system (7.24), with the input matrix G as defined in (7.23), can be rewritten as

$$\dot{x} = \left(J - (R + Z(x)) \right) \nabla \mathcal{H}(x) + G(x)(u - \bar{u}), \quad (7.25)$$

where

$$Z(x) := \bar{G}(\bar{u})G^\top(x), \quad (7.26)$$

and \mathcal{H} is the shifted Hamiltonian

$$\mathcal{H}(x) := H(x) - (x - \bar{x})^\top \nabla \bar{H} - \bar{H}. \quad (7.27)$$

Proof. Subtracting the steady-state equation from (7.24) gives

$$\dot{x} = (J - R)(\nabla H(x) - \nabla \bar{H}) + G(x)u - \bar{G}\bar{u} .$$

Bearing in mind that $\nabla \mathcal{H}(x) = \nabla H(x) - \nabla \bar{H}$, we have

$$\begin{aligned} \dot{x} &= (J - R)\nabla \mathcal{H}(x) + G(x)u - \bar{G}\bar{u} \\ &\quad - G(x)\bar{u} + G(x)\bar{u} \\ &= (J - R)\nabla \mathcal{H}(x) + G(x)(u - \bar{u}) \\ &\quad + (G(x) - \bar{G})\bar{u} \end{aligned}$$

Note that

$$\begin{aligned} (G(x) - \bar{G})\bar{u} &= -(\langle \nabla H(x) \rangle - \langle \nabla \bar{H} \rangle)\bar{G}G^\top(x)Bu \\ &= -\bar{G}\langle \bar{u} \rangle G^\top(x)(\nabla H(x) - \nabla \bar{H}) \\ &= -Z(x)\nabla \mathcal{H} , \end{aligned}$$

where we used the fact that for all $a, b \in \mathbb{R}^n$, we have $\langle a \rangle b = \langle b \rangle a$. Hence

$$\dot{x} = (J - (R + Z(x)))\nabla \mathcal{H}(x) + G(x)(u - \bar{u}) .$$

This completes the proof. ■

The natural (shifted) output of the dynamics (7.25) is defined as

$$y = G^\top(x)\nabla \mathcal{H}(x) . \tag{7.28}$$

In the next section we will investigate the shifted passivity properties of the P_wH system (7.24), (7.28).

7.2.3 Main Result: Shifted Passivity

To establish the shifted passivity property, we further restrict the trajectories to be inside the set

$$\bar{\Omega}_p := \{x \in \Omega^+ : R + Z(x) \geq 0\} ,$$

that is the closure of the open set

$$\Omega_p := \{x \in \Omega^+ : R + Z(x) > 0\} , \tag{7.29}$$

where we assume that Ω_p is non-empty.

Theorem 7.2.2 [Shifted passivity]

Consider the system (7.24), (7.28). For all trajectories $x \in \bar{\Omega}_p$ we have that

$$\dot{\mathcal{H}} \leq (y - \bar{y})^\top (u - \bar{u}) . \quad (7.30)$$

Moreover, if H is convex, the system is shifted passive.

Proof. Using Lemma 7.2.1 we can rewrite the system as in (7.25). Therefore, we have

$$\dot{\mathcal{H}} = -\nabla \mathcal{H}^\top (R + Z(x)) \nabla \mathcal{H} + y^\top (u - \bar{u}) .$$

Now, note that y given in (7.28) can be written as

$$y = G^\top(x) (\nabla H(x) - \nabla \bar{H}) ,$$

and hence $\bar{y} = 0$. The proof of (7.30) is completed restricting the trajectories to satisfy $x \in \bar{\Omega}_p$. To establish the passivity claim, note that since H is convex, $\mathcal{H}(x)$ has an isolated minimum at \bar{x} , and hence is (locally, around \bar{x}) non-negative; see [68]. ■

Remark 7.2.3 [Constant power sources]

In case the control input includes only power sources, i.e., $\langle \bar{u} \rangle \geq 0$, we see from (7.26) and the fact that $x \in \Omega^+$, that $Z(x) \geq 0$, and hence $\bar{\Omega}_p = \Omega^+$. Therefore, throughout this section, we investigate the cases where at least one control input element is acting as power load, i.e., $\langle \bar{u} \rangle \not\geq 0$. □

Remark 7.2.4 [Additional constant input]

Theorem 7.2.2 holds also for the systems with an additional constant input, i.e.,

$$\dot{x} = (J - R)\nabla H(x) + G(x)u + \bar{u}_c ,$$

since the constant input $\bar{u}_c \in \mathbb{R}^n$ disappears in the shifted model (7.25). □

7.2.4 Stability Analysis for Constant Inputs

Consider the system (7.24) with a constant input $u = \bar{u}$. Then the dynamics reads as

$$\dot{x} = (J - R)\nabla H(x) + G(x)\bar{u} . \quad (7.31)$$

In this section, we first investigate the local stability of the equilibria of the system (7.31), that is, points \bar{x} such that $(\bar{x}, \bar{u}) \in \mathcal{E}$. Then, we give an estimate of their region of attraction (ROA). To establish these results we impose the stronger assumption that $x \in \Omega_p$ and, naturally, restrict ourselves to equilibrium points $\bar{x} \in \Omega_p$.

Local stability

Using the result of Theorem 7.2.2, we have the following corollary:

Corollary 7.2.5 [Local Stability]

Consider the system (7.31) having a point $\bar{x} \in \Omega_p$ such that $(\bar{x}, \bar{u}) \in \mathcal{E}$ and $\nabla^2 H(\bar{x}) > 0$. Then, the equilibrium $x = \bar{x}$ of the system (7.31) is asymptotically stable.

Proof. Since $R + Z(\bar{x}) > 0$ and $\nabla^2 H(\bar{x}) > 0$, there exists a ball $\mathcal{B}(\bar{x})$, centered in \bar{x} , such that $\mathcal{H}(x) > 0$ and $R + Z(x) > 0$ for all $x \in \mathcal{B}(\bar{x})$. Moreover, \mathcal{H} satisfies

$$\dot{\mathcal{H}} = -\nabla \mathcal{H}^\top (R + Z(x)) \nabla \mathcal{H} < 0, \quad \forall x \in \mathcal{B}(\bar{x}), x \neq \bar{x},$$

making it a strict Lyapunov function. This completes the proof. \blacksquare

Note that the result of Corollary 7.2.5 applies also to an equilibrium point $x \in \bar{\Omega}_p$, if a *detectability* condition is satisfied, guaranteeing asymptotic stability by the use of LaSalle's Invariance principle; see [141, Ch. 8].

Characterizing an estimate of the ROA

As it is well-known, all bounded level sets of Lyapunov functions are invariant sets. However, our proof of asymptotic stability is restricted to the domain Ω_p . Consequently, to provide an estimate of the ROA of \bar{x} it is necessary to find a constant k such that the corresponding sublevel set of \mathcal{H}

$$\mathcal{L}_k := \{x \in \mathbb{R}^n \mid \mathcal{H}(x) < k, k \in \mathbb{R}_+\}, \quad (7.32)$$

is bounded and is contained in Ω_p . To solve this, otherwise daunting task, we make some assumptions on the system. First, we assume a positive definite dissipation matrix, that is, $R > 0$. Given this assumption, it is possible to construct a set, defined in terms of lower bounds on ∇H , that is strictly contained in Ω_p .

Lemma 7.2.6 [Lower Bounds on ∇H]

If the dissipation matrix R is positive definite, then the set Ω_Γ defined as

$$\Omega_\Gamma := \left\{ x \in \Omega^+ : \langle \nabla_u H(x) \rangle > -\frac{\langle \nabla_u \bar{H} \rangle^{-1} \langle \bar{u} \rangle}{\lambda_m\{R\}} \right\}, \quad (7.33)$$

is contained in Ω_p .

Proof. For all $x \in \Omega_\Gamma$ we have

$$\lambda_m\{R\}J_m + \langle \nabla_u \bar{\mathcal{H}} \rangle^{-1} \langle \bar{u} \rangle \langle \nabla_u \mathcal{H}(x) \rangle^{-1} > 0$$

Recall that $B = [J_m \quad 0_{(m)(n-m)}]^\top$. We have

$$\lambda_m\{R\}J_n + B \langle \nabla_u \bar{\mathcal{H}} \rangle^{-1} \langle \bar{u} \rangle \langle \nabla_u \mathcal{H}(x) \rangle^{-1} B^\top > 0,$$

where we used the fact that $\lambda_m\{R\} > 0$. Hence

$$\lambda_m\{R\}J_n + \bar{G} \langle \bar{u} \rangle G^\top(x) > 0,$$

The proof is completed noting that the second left-hand term above is $Z(x)$ and recalling that $R \geq \lambda_m\{R\}J_n$. \blacksquare

Our second assumption is that the Hamiltonian is quadratic of the form

$$H(x) = \frac{1}{2}x^\top \mathcal{M}x, \quad \mathcal{M} > 0, \quad (7.34)$$

In this case, the shifted Hamiltonian (7.27) reduces to

$$\mathcal{H}(x) = \frac{1}{2}(x - \bar{x})^\top \mathcal{M}(x - \bar{x}). \quad (7.35)$$

Notice that, now, all sublevel sets \mathcal{L}_k , given in (7.32), are *bounded*. Therefore, in view of Lemma 7.2.6, we only need to find a constant $k_c > 0$ such that $\mathcal{L}_{k_c} \subset \Omega_\Gamma$, and this sublevel set provides an estimate of the ROA of \bar{x} .

Theorem 7.2.7 [Estimate of the ROA]

Consider the system (7.31) with the quadratic Hamiltonian (7.34) and the dissipation matrix $R > 0$. Assume that $\bar{x} \in \Omega_\Gamma$ where Ω_Γ is given by (7.33). Define

$$k_c := \frac{1}{2\lambda_M\{\mathcal{M}\}} \min_{i=1,\dots,m} \left\{ \left(\gamma_i - (\mathcal{M}\bar{x})_i \right)^2 \right\},$$

with

$$\gamma_i := \max\left\{0, -\frac{\bar{u}_i}{\lambda_m\{R\}\nabla_u \bar{H}_i}\right\},$$

and $(\mathcal{M}\bar{x})_i$ being the i th element of the vector $\mathcal{M}\bar{x}$. Then, an estimate of the ROA of the equilibrium \bar{x} is the set \mathcal{L}_{k_c} as defined in (7.32) with $k = k_c$.

Proof. From (7.35) we have

$$\mathcal{H}(x) = \frac{1}{2}(\mathcal{M}x - \mathcal{M}\bar{x})^\top \mathcal{M}^{-1}(\mathcal{M}x - \mathcal{M}\bar{x}).$$

Hence,

$$\mathcal{H}(x) \geq \frac{|\mathcal{M}x - \mathcal{M}\bar{x}|^2}{2\lambda_M\{\mathcal{M}\}}$$

with $|\cdot|$ being the Euclidean norm. This bound, together with $\mathcal{H}(x) < k_c$, ensures that for all $i \in \{1, \dots, m\}$

$$((\mathcal{M}x)_i - (\mathcal{M}\bar{x})_i)^2 < (\gamma_i - (\mathcal{M}\bar{x})_i)^2.$$

Note that since $\bar{x} \in \Omega_\Gamma$ we have $(\mathcal{M}\bar{x})_i > \gamma_i$. Hence $\gamma_i - (\mathcal{M}\bar{x})_i < 0$. Consequently, for all $i \in \{1, \dots, m\}$ we have

$$\gamma_i - (\mathcal{M}\bar{x})_i < (\mathcal{M}x)_i - (\mathcal{M}\bar{x})_i < -\gamma_i + (\mathcal{M}\bar{x})_i.$$

The left hand side of the inequality above guarantees $(\mathcal{M}x)_i > \gamma_i$. Therefore, using Lemma 7.2.6, we have $R + Z(x) > 0$. The proof is completed noting that the latter ensures $\mathcal{H}(x)$ is a strict Lyapunov function of the system. ■

In the following corollary, we show that in cases where \mathcal{M} and R are diagonal, the largest k in (7.32), and hence the largest \mathcal{L}_k contained in Ω_p , can be constructed explicitly.

To streamline the presentation of the result we define the constants

$$\eta_i := -\frac{\bar{u}_i}{R_{ii}\nabla_u \bar{H}_i}, \quad (7.36)$$

and the constant vectors

$$\ell^i := \text{col}(\bar{x}_1, \bar{x}_2, \dots, \bar{x}_{i-1}, \frac{\eta_i}{\mathcal{M}_{ii}}, \bar{x}_{i+1}, \dots, \bar{x}_n). \quad (7.37)$$

Corollary 7.2.8 [Estimate of the ROA with diagonal \mathcal{M} and R]

Consider the system (7.31) with the quadratic Hamiltonian (7.34) with *diagonal* $R > 0$ and $M > 0$. Assume that $\bar{x} \in \Omega_p$. Define

$$k_d := \min_{i=1, \dots, m} \{\mathcal{H}(\ell^i)\},$$

with (7.36) and (7.37). Then, an estimate of the ROA of the equilibrium \bar{x} is the set \mathcal{L}_{k_d} as defined in (7.32) with $k = k_d$.

Proof. Since both Z and R are diagonal, we have $R + Z(x) > 0$ if and only if $R_{ii} + Z(x)_{ii} > 0$ for all $i \in \{1, \dots, n\}$. Therefore, Ω_p is computed as

$$\Omega_p = \{x \in \Omega^+ : R_{ii} + \bar{G}_{ii}\bar{u}_i G_{ii} > 0, \quad i = 1, \dots, m\},$$

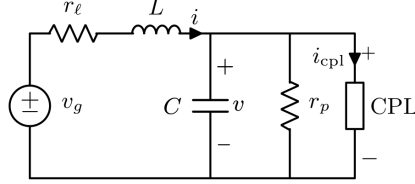


Figure 7.1: Single-Port DC circuit connected to a CPL.

where we used the fact that for all $i = m + 1, \dots, n$, $R_{ii} + Z_{ii} = R_{ii} > 0$. Hence, the set Ω_p can be defined in terms of lower bounds on ∇H , i.e.,

$$\Omega_p = \{x \in \Omega^+ : \nabla H(x)_i > -\frac{\bar{G}_{ii}\bar{u}_i}{R_{ii}}, i = 1, \dots, m\}. \quad (7.38)$$

The rest of the proof follows analogously to the proof of Theorem 7.2.7, and is hence, omitted. ■

Note that the set \mathcal{L}_{k_d} in this case is the ellipsoid

$$\left(\frac{x_1 - \bar{x}_1}{\sqrt{\frac{2k_d}{\mathcal{M}_{11}}}}\right)^2 + \left(\frac{x_2 - \bar{x}_2}{\sqrt{\frac{2k_d}{\mathcal{M}_{22}}}}\right)^2 + \dots + \left(\frac{x_n - \bar{x}_n}{\sqrt{\frac{2k_d}{\mathcal{M}_{nn}}}}\right)^2 < 1. \quad (7.39)$$

7.2.5 Application to DC Networks with Constant Power Loads (CPL)

In this section, we apply the proposed method to study the stability of equilibria of, single-port and multi-port, DC networks with CPLs.

Single-port system

A schematic representation of a DC network with a single CPL is shown in Figure 7.1. Observe that the combination of the resistive load r_p and the CPL, acts as a ZIP load connected to the capacitor C . In view of Remark 7.2.4, the current sink is omitted for brevity.

Define the state vector $x = \text{col}(q, \varphi)$, where q is the capacitor charge and φ is the inductor flux. Then the network can be modeled by

$$\dot{x} = (J - R)\nabla H(x) + G(x)u + u_c, \quad x \in \Omega^+, \quad (7.40)$$

with $H = \frac{1}{2}x^\top \mathcal{M}x$ and

$$\mathcal{M} = \begin{bmatrix} \frac{1}{C} & 0 \\ 0 & \frac{1}{L} \end{bmatrix}, \quad J = \begin{bmatrix} 0 & 1 \\ -1 & 0 \end{bmatrix}, \quad R = \begin{bmatrix} \frac{1}{r_p} & 0 \\ 0 & r_l \end{bmatrix}, \quad (7.41)$$

and $u_c = \text{col}(0, v_g)$, $u = -P$, where $P > 0$ is the power extracted by the CPL. The input matrix is

$$G(q, \varphi) = \begin{bmatrix} \frac{C}{q} \\ 0 \end{bmatrix},$$

which is well defined in the set

$$\Omega^+ = \{(q, \varphi) \in \mathbb{R}^2 \mid q > 0\}.$$

The equilibria of the system (7.40), (7.41) are computed in the following lemma.

Lemma 7.2.9 [Equilibria of the system (7.40)-(7.41)]

The system (7.40)-(7.41) admits two equilibria given by

$$\bar{q}_s = Cr_p \frac{v_g + \sqrt{\Delta}}{(r_\ell + r_p)}, \quad \bar{\varphi}_s = L \frac{r_p v_g - \sqrt{\Delta}}{r_\ell(r_\ell + r_p)}$$

and

$$\bar{q}_u = Cr_p \frac{v_g - \sqrt{\Delta}}{(r_\ell + r_p)}, \quad \bar{\varphi}_u = L \frac{r_p v_g + \sqrt{\Delta}}{r_\ell(r_\ell + r_p)},$$

where

$$\Delta := v_g^2 - 4 \frac{r_\ell(r_p + r_\ell)}{r_p} P.$$

The equilibrium points are real if and only if $\Delta \geq 0$ or equivalently

$$P \leq P_{\max}^e, \quad P_{\max}^e := \frac{r_p v_g^2}{4r_\ell(r_\ell + r_p)}. \quad (7.42)$$

Through straightforward computations, it can be shown that the Jacobian of the vector field in the right hand side of (7.40), has a positive eigenvalue at the equilibrium point $(\bar{q}_u, \bar{\varphi}_u)$ and hence it is unstable. Furthermore, it can be shown that for small values of the load power, the Jacobian is negative definite at the equilibrium point $(\bar{q}_s, \bar{\varphi}_s)$. \square

Considering the results of Lemma 7.2.9, we continue with the equilibrium $(\bar{q}_s, \bar{\varphi}_s)$ as the candidate for nonlinear stability analysis. To use the results of Corollary 7.2.5, we first compute

$$R + Z(q, \varphi) = \begin{bmatrix} \frac{1}{r_p} - \frac{C^2 P}{\bar{q}_s q} & 0 \\ 0 & r_\ell \end{bmatrix}. \quad (7.43)$$

Next, we observe that $R + Z(\bar{q}_s, \bar{\varphi}_s) > 0$ if and only if

$$P < P_{\max}^s, \quad P_{\max}^s := \frac{r_p v_g^2}{(r_p + 2r_\ell)^2}. \quad (7.44)$$

Hence, according to Corollary 7.2.5, if the condition (7.44) is satisfied, then the equilibrium $(\bar{q}_s, \bar{\varphi}_s)$ is asymptotically stable. Note that if $P < \min\{P_{\max}^e, P_{\max}^s\}$, then the existence of the asymptotically stable equilibrium point $(\bar{q}_s, \bar{\varphi}_s)$, is guaranteed.

Remark 7.2.10 [CPL as a negative resistor]

Let $\bar{v} := \frac{\bar{q}_s}{C}$ denote the voltage of the CPL at the equilibrium $(\bar{q}_s, \bar{\varphi}_s)$. Then the physical equivalent of the term $-\frac{C^2 P}{\bar{q}_s q}$ in (7.43), is the inverse of a nonlinear negative resistor with the resistance

$$r_{\text{CPL}}(v) := \left(\frac{C^2 P}{\bar{q}_s q} \right)^{-1} = \frac{\bar{v} v}{P}.$$

This resistor is in parallel with r_p , *i.e.*,

$$R + Z(q, \varphi) = \begin{bmatrix} \frac{1}{r_{\text{eq}}} & 0 \\ 0 & r_\ell \end{bmatrix},$$

where $r_{\text{eq}}(v) := \left(\frac{1}{r_p} - \frac{1}{r_{\text{CPL}}(v)} \right)^{-1}$ is the equivalent resistor. Interestingly, the physical interpretation of the condition (7.44) is that the equivalent resistance of the resistor r_p and the CPL, is positive (passive) at the equilibrium point, *i.e.*, $r_{\text{eq}}(\bar{v}) > 0$. \square

Next, using Corollary 7.2.8, we derive an estimate of the ROA of $(\bar{q}_s, \bar{\varphi}_s)$. Bearing in mind that the dissipative matrix R is diagonal, and using Lemma 7.2.6, we compute Ω_p as

$$\Omega_p = \{(q, \varphi) \in \mathbb{R}^2 : q > q_{\min}\},$$

where

$$q_{\min} := P r_p \frac{C^2}{\bar{q}_s} = \frac{P}{P_{\max}} \bar{q}_s > 0. \quad (7.45)$$

The interpretation of (7.45) is that the closer the load power to P_{\max} is, the smaller the ROA is.

Now assume that (7.44) holds. Using Corollary 7.2.8, the set \mathcal{L}_{k_d} with

$$k_d = \mathcal{H}(q_{\min}, \bar{\varphi}_s),$$

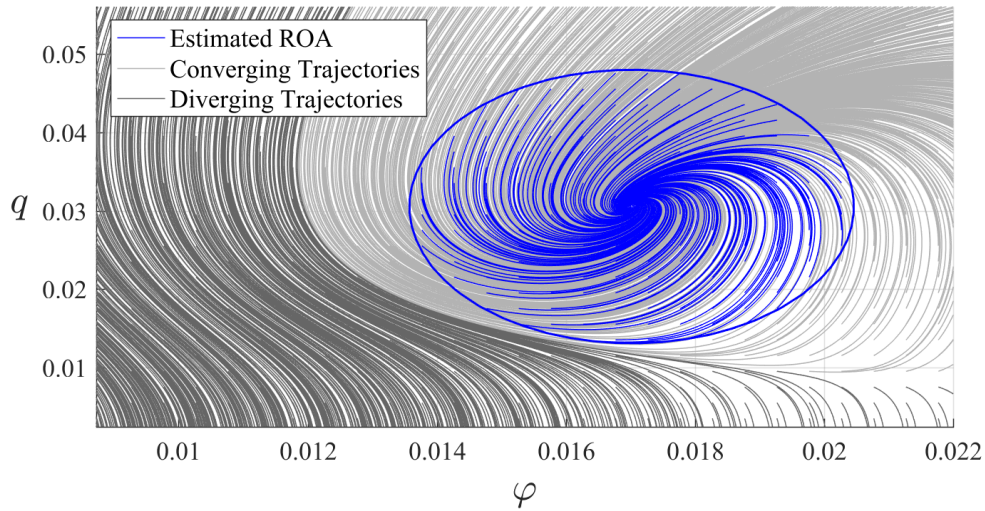
is an estimate of the ROA. Furthermore, using (7.39), we can rewrite this set as the oval

$$\left(\frac{q - \bar{q}_s}{\sqrt{2Ck_d}} \right)^2 + \left(\frac{\varphi - \bar{\varphi}_s}{\sqrt{2Lk_d}} \right)^2 < 1. \quad (7.46)$$

This set guarantees $q > q_{\min}$ for all solutions starting within the oval.

Table 7.1: Simulation Parameters of the Single-Port CPL

$v_g(\text{V})$	$r_\ell(\Omega)$	$r_p(\Omega)$	$L(\mu\text{H})$	$C(\text{mF})$	$P(\text{kW})$
24	0.04	0.1	78	2	1

**Figure 7.2:** Phase plane of the system (7.40)-(7.41) with the parameters given in Table 7.1.

We evaluate our results by a numerical example of the network shown in Fig. 7.1, with the parameters given by Table 7.1. The maximum power for existence of the equilibrium and its local stability are computed as $P_{\max}^e = 2.57 \text{ kW}$ and $P_{\max}^s = 2.33 \text{ kW}$, respectively. Note that the CPL satisfies the conditions (7.42) and (7.44), since

$$P < P_{\max}^s < P_{\max}^e.$$

Figure 7.2 shows the phase plane of the system (7.40)-(7.41). The estimate of the ROA (the oval (7.46)) is shown in blue, and all other converging solutions are shown in light gray. It is evident that the proposed method provides an appropriate estimate of the ROA, as the solutions just beneath this region (in dark gray), diverge from the equilibrium.

Multi-port networks

In this section, we investigate the stability of a complete multi-port DC network with CPLs. Let $i_M \in \mathbb{R}^l$ represent the currents of the inductors, and $v_C \in \mathbb{R}^c$ denote the voltages of the capacitors, where l and c are the number of inductors and capacitors. Then, the dynamics of the network can be described by [73]

$$\begin{bmatrix} \mathbb{C}\dot{v}_C \\ \mathcal{L}\dot{i}_M \end{bmatrix} = \begin{bmatrix} -\mathcal{Y} & -\Gamma^\top \\ \Gamma & -\mathcal{Z} \end{bmatrix} \begin{bmatrix} v_C \\ i_M \end{bmatrix} - \begin{bmatrix} \langle v_C \rangle^{-1} \\ 0_{lc} \end{bmatrix} P + u_c, \quad (7.47)$$

where $\mathbb{C} > 0 \in \mathbb{R}^{c \times c}$ and $\mathcal{L} > 0 \in \mathbb{R}^{l \times l}$ and are matrices associated with the magnitude of capacitors and inductors (and mutual inductances), $\mathcal{Y} \in \mathbb{R}^{c \times c}$ and $\mathcal{Z} \in \mathbb{R}^{l \times l}$ are positive definite matrices associated with the resistances, and $\Gamma \in \mathbb{R}^{l \times c}$ is the matrix associated with the network topology. Also, the power of the CPLs is denoted by $P = \text{col}(P_1, \dots, P_c)$. The vector $u_c \in \mathbb{R}^{c+l}$ is constant and its components are linear combinations of the voltages and currents of the sources in the network. We assume that the capacitors and the inductors are not ideal, *i.e.*, we consider that all the inductors have a resistance in series and the capacitors possess a resistor in parallel. Moreover, we assume that the constant power loads are connected to a capacitor in parallel. This feature amounts for the capacitive effect of the input filters for this type of loads; see [12, 26, 28].

With a little abuse of notation, define the state vector $x = \text{col}(q, \varphi) \in \mathbb{R}^{c+l}$ and the control vector $u = -P \in \mathbb{R}^c$, where $q \in \mathbb{R}^c$ denotes the electric charge of the capacitors, and $\varphi \in \mathbb{R}^l$ denotes the magnetic flux of the inductors. Then the network dynamics of the multi-port network given in (7.47) admits a Port-Hamiltonian representation given by

$$\dot{x} = (J - R)\nabla H(x) + G(x)u + u_c,$$

with $H = \frac{1}{2}x^\top \mathcal{M}x$ and

$$\mathcal{M} = \begin{bmatrix} \mathbb{C}^{-1} & 0 \\ 0 & \mathcal{L}^{-1} \end{bmatrix}, \quad J = \begin{bmatrix} 0 & -\Gamma^\top \\ \Gamma & 0 \end{bmatrix}, \quad R = \begin{bmatrix} \mathcal{Y} & 0 \\ 0 & \mathcal{Z} \end{bmatrix}.$$

Similar to the case of the single-port *RLC* circuit with a CPL, and using Theorem 7.2.7, an ellipsoid can be computed here as an estimate of the ROA.

7.2.6 Application to Synchronous Generators connected to a CPL

In this section, we apply the results to the case of a synchronous generator, modeled by the *improved swing equation*, connected to a CPL.⁹

$$\dot{p} = (J - R)\nabla H(p) + G(p)u + u_c, \quad (7.48)$$

with

$$\begin{aligned} p &= M\omega, \quad J = 0, \quad R = D_m + D_d, \quad G(p) = \frac{M}{p} = \omega^{-1} \\ H &= \frac{1}{2M}p^2, \quad u = -P_e, \quad u_c = \tau_m + D_d\omega^*, \end{aligned} \quad (7.49)$$

where $p \in \mathbb{R}_+$ is the angular momentum, $M > 0$ is the total moment of inertia of the turbine and generator rotor, $\omega \in \mathbb{R}_+$ is the rotor shaft velocity, $\omega^* > 0$ is the angular velocity associated with the nominal frequency of 50 Hz, $D_m > 0$ is the damping coefficient of the mechanical losses, $D_d > 0$ is the damping-torque coefficient of the damper windings, $\tau_m > 0$ is the constant mechanical torque (physical input), and P_e is the constant power load.

Assume that

$$P < \frac{(D_d\omega^* + \tau_m)^2}{4(D_d + D_m)}.$$

Then the dynamics (7.48), (7.49) has the following two equilibria

$$\bar{\omega}_s = \frac{D_d\omega^* + \tau_m + \sqrt{\Delta}}{2(D_d + D_m)}, \quad \bar{\omega}_u = \frac{D_d\omega^* + \tau_m - \sqrt{\Delta}}{2(D_d + D_m)},$$

with $\Delta := (D_d\omega^* + \tau_m)^2 - 4(D_d + D_m)P_e$. We have

$$R + Z(\omega) = D_d + D_m - \frac{P_e}{\bar{\omega}_s\omega}.$$

The equilibrium point $\omega = \bar{\omega}_s$ is asymptotically stable since

$$R + Z(\bar{\omega}_s) = \frac{\tau_m + D_d\omega^*}{\bar{\omega}_s} > 0.$$

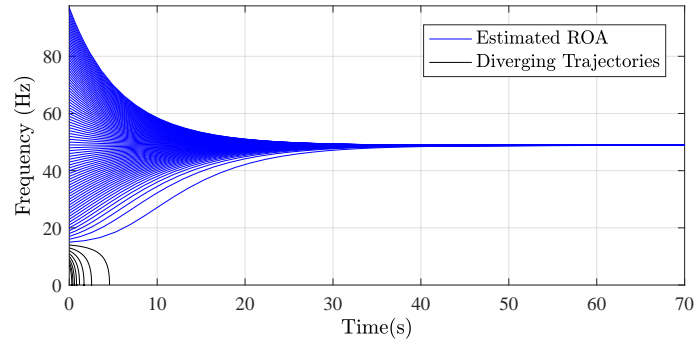
Through straightforward computations, it can be shown that the set Ω_p in (7.38) can be written as

$$\Omega_p = \{\omega \in \mathbb{R}_{>0} : \omega > \bar{\omega}_u\}. \quad (7.50)$$

⁹As studied in Chapter 6, an inverter with a capacitive inertia connected to a CPL can be modeled by similar dynamics.

Table 7.2: Simulation Parameters of the Synchronous Generator (p.u.)

M	D_m	D_d	P_e	τ_m
0.2	10^{-6}	10^{-4}	3	0.0027

**Figure 7.3:** Solutions of the system (7.48),(7.49) with different initial conditions.

In this set, the shifted Hamiltonian $H = \frac{1}{2}M(\omega - \bar{\omega}_s)^2$ is strictly decreasing. Therefore the solutions get closer to the equilibrium $\bar{\omega}_s$ and move away from the point $\bar{\omega}_u$ as time goes by. Consequently the set Ω_p in (7.50) is forward invariant and represents the estimate of the ROA. In fact, as shown in Chapter 5, this is not an estimate, but the *exact* region of attraction.

Figure 7.3 shows the trajectories of a number of solutions of the system (7.48)-(7.49), with the parameters given by Table 7.2, and with different initial conditions. It is clear that the proposed method successfully identifies a very precise estimate of the ROA (blue), as all the solutions starting from outside the ROA estimate (black) diverge from the equilibrium.

7.2.7 Conclusion

In this section, a class of pH systems was investigated, where the control input/disturbance acts on the power of the system. We refer to these systems as Power-controlled Hamiltonian (P_wH) systems. First, a model for such systems was proposed, and second, the condition on which the system is shifted passive was computed. Using these results, the stability of equilibria was investigated. Furthermore, an estimate of the region of attraction was derived for P_wH systems with quadratic Hamiltonian. The proposed modeling and conditions were derived and computed for two cases of interest in practice: A DC circuit and a synchronous generator, both


connected to constant power loads. Finally, the validity and utility of the proposed method was confirmed by numerical examples of these case studies.

Chapter 8

Conclusions

“A conclusion is simply the place where you got tired of thinking.”

– Dan Chaon, *Stay Awake*

 MICROGRIDS are sustainable and robust building blocks of the future power networks. In this thesis, we investigated the modeling and control of power systems in microgrids from different aspects. The main contributions of this dissertation, together with the points that can be considered for carrying forward the work of this thesis, are summarized in the following lines:

- We investigated how output impedances affect the inductivity and resistivity of the distribution lines, and proposed a metric to measure the inductivity of a (homogeneous) network with output impedances. The results show that the more connected the network is, the more output impedance diffuses into the network and the larger its effect will be. Examples showed that the impact of inductive output impedances on the network can be maximized in specific network topologies. Results of a comparison of our method with a phasor-based Kron reduction confirmed the validity and the effectiveness of the proposed metrics.

As an extension to these results, it is interesting to see that how the inductivity of a non-homogeneous network can be measured. Moreover, a relevant issue is to derive analytical solutions on maximizing the network inductivity/resistivity ratios. Although it was shown numerically, it is also of interest to investigate, analytically, the effect of network inductivity ratio on the performance of the droop-based methods.

- We proposed a master-slave microgrid architecture, where a synchronous generator is the master, and power converters act as the slaves. We showed that stability and frequency regulation can be achieved by using conventional PI controllers. Furthermore, we provided an implementation for the proposed

inverters. Numerical results confirmed that, without the need to any communication, the proposed network reaches frequency regulation and optimized power sharing.

In this work, we assumed that the phase locked loop is ideal. Therefore, a future possibility to extend these results, is to include the dynamics of the phase locked loop. Moreover, it is of interest to investigate how to relax the assumption of purely inductive lines, and to examine if reactive power sharing can be achieved using a similar method; based on voltage dynamics.

- We investigated the properties of an improved swing equation to model synchronous generators. We derived a set within which the system is shifted passive. Using this result, we designed an integral controller and showed that frequency regulation can be achieved for a system that consists of a synchronous generator connected to a constant power load. Furthermore, we looked into the case of a synchronous machine connected to an infinite bus, and provided an estimate of the region of attraction. Numerical results depicted that, in most cases, the behavior of the improved swing equation is different from the conventional swing equation.

In this work, we neglected the voltage dynamics, and hence a relevant issue is to investigate the stability with the dynamics including the improved swing equation together with synchronous generator voltage dynamics.

- We studied inverters with capacitors as the energy reservoirs, that emulate inertia of synchronous generators. We showed the stability of these inverters connected to constant power loads, and of a network of these inverters connected to each other. Aiming at frequency regulation, we designed a control method, and indicated that the stability and frequency regulation are guaranteed exploiting the proposed controllers.

We used the phasor notation for the analysis of the network. An open problem is a time-domain analysis using the third order model in [69]. Furthermore, it is of interest to extend the results to structure-preserving and differential algebraic models [14, 91, 111, 135].

- We derived conditions under which a pH system with a convex Hamiltonian is shifted passive. This result enabled us to study the (global) stability of forced equilibria of the pH systems. Interestingly, the aforementioned condition is independent of the states for quadratic affine pH systems. We showed the utility of the results on the sixth-order synchronous generator model.

Future works include attempting to reduce possible conservatism in the stability

conditions as well as deriving conditions for shifted passivity of the systems with a state dependent input matrix.

- Power-controlled Hamiltonian (P_wH) systems are a class of pH systems, where the control input/disturbance acts on the power of the system. We proposed a model for these systems and showed that, as long as the trajectories belong to a specific set, the system is shifted passive. Using these results, we derived conditions for asymptotic stability of the equilibrium, and characterized an estimate of the region of attraction for P_wH systems with quadratic Hamiltonian. The application of the results on two important physical systems (DC circuits and synchronous generators, connected to constant power loads), confirms the validity of the results.

A possible extension of this work is to design high-performance controllers with guaranteed stability domains. It is also of interest to extend the results to state-dependent structure and dissipation matrices, *e.g.*, the sixth-order model of the synchronous generator.

Bibliography

- [1] Akagi, H., Watanabe, E. H., and Aredes, M. (2017). *Instantaneous Power Theory and Applications to Power Conditioning*. John Wiley and Sons, Inc.
- [2] Alipoor, J., Miura, Y., and Ise, T. (2015). Power system stabilization using virtual synchronous generator with alternating moment of inertia. *IEEE Journal of Emerging and Selected Topics in Power Electronics*, 3(2):451–458.
- [3] Anand, S. and Fernandes, B. G. (2013). Reduced-order model and stability analysis of low-voltage DC microgrid. *IEEE Transactions on Industrial Electronics*, 60(11):5040–5049.
- [4] Andreasson, M., Dimarogonas, D. V., Sandberg, H., and Johansson, K. H. (2014). Distributed PI-control with applications to power systems frequency control. In *IEEE American Control Conference*, pages 3183–3188.
- [5] Arani, M. F. M. and El-Saadany, E. F. (2013). Implementing virtual inertia in DFIG-based wind power generation. *IEEE Transactions on Power Systems*, 28(2):1373–1384.
- [6] Arcak, M. (2007). Passivity as a design tool for group coordination. *IEEE Transactions on Automatic Control*, 52(8):1380–1390.
- [7] Arnol'd, V. I. (2013). *Mathematical Methods of Classical Mechanics*, volume 60. Springer Science & Business Media.
- [8] Bai, H., Arcak, M., and Wen, J. (2011). *Cooperative Control Design: A Systematic, Passivity-based Approach*. Springer, New York, NY.
- [9] Barabanov, N., Ortega, R., Griñó, R., and Polyak, B. (2016). On existence and stability of equilibria of linear time-invariant systems with constant power loads. *IEEE Transactions on Circuits and Systems I: Regular Papers*, 63(1):114–121.
- [10] Barabanov, N., Schiffer, J., Ortega, R., and Efimov, D. (2017). Conditions for almost global attractivity of a synchronous generator connected to an infinite bus. *IEEE Transactions on Automatic Control*, 62(10):4905–4916.

- [11] Beck, H. P. and Hesse, R. (2007). Virtual synchronous machine. In *9th International Conference on Electrical Power Quality and Utilisation*, pages 1–6.
- [12] Belkhat, M., Cooley, R., and Witulski, A. (1995). Large signal stability criteria for distributed systems with constant power loads. In *Power Electronics Specialists Conference, 1995. PESC '95 Record., 26th Annual IEEE*, volume 2, pages 1333–1338.
- [13] Benedito, E., del Puerto-Flores, D., Dòria-Cerezo, A., and Scherpen, J. M. (2017). Optimal power flow for resistive DC networks: a port-Hamiltonian approach. *IFAC-PapersOnLine*, 50(1):25–30.
- [14] Bergen, A. R. and Hill, D. J. (1981). A structure preserving model for power system stability analysis. *IEEE Transactions on Power Apparatus and Systems*, PAS-100(1):25–35.
- [15] Bevrani, H., Ise, T., and Miura, Y. (2014). Virtual synchronous generators: A survey and new perspectives. *International Journal of Electrical Power & Energy Systems*, 54:244–254.
- [16] Bollobás, B. (1998). *Modern graph theory*, volume 184. Springer Verlag.
- [17] Bolognani, S. and Zampieri, S. (2016). On the existence and linear approximation of the power flow solution in power distribution networks. *IEEE Transactions on Power Systems*, 31(1):163–172.
- [18] Brabandere, K. D., Bolsens, B., den Keybus, J. V., Woyte, A., Driesen, J., and Belmans, R. (2007). A voltage and frequency droop control method for parallel inverters. *IEEE Transactions on Power Electronics*, 22(4):1107–1115.
- [19] Brayton, R. K. and Moser, J. K. (1964). A theory of nonlinear networks–I. *Quarterly of Applied Mathematics*, 22:1–33.
- [20] Bregman, L. (1967). The relaxation method of finding the common point of convex sets and its application to the solution of problems in convex programming. *USSR Computational Mathematics and Mathematical Physics*, 7(3):200 – 217.
- [21] Bürger, M., Zelazo, D., and Allgöwer, F. (2014). Duality and network theory in passivity-based cooperative control. *Automatica*, 50(8):2051–2061.
- [22] Caliskan, S. Y. and Tabuada, P. (2012). Kron reduction of power networks with lossy and dynamic transmission lines. In *2012 IEEE 51st IEEE Conference on Decision and Control (CDC)*, pages 5554–5559.
- [23] Caliskan, S. Y. and Tabuada, P. (2014a). Compositional transient stability analysis of multimachine power networks. *IEEE Transactions on Control of Network Systems*, 1(1):4–14.
- [24] Caliskan, S. Y. and Tabuada, P. (2014b). Towards kron reduction of generalized electrical networks. *Automatica*, 50(10):2586 – 2590.

- [25] Caliskan, S. Y. and Tabuada, P. (2015). Uses and abuses of the swing equation model. In *2015 IEEE 54th Annual Conference on Decision and Control (CDC)*, pages 6662–6667.
- [26] Cavanagh, K., Belk, J. A., and Turitsyn, K. (2018). Transient stability guarantees for ad hoc DC microgrids. *IEEE Control Systems Letters*, 2(1):139–144.
- [27] Ceraolo, M. and Poli, D. (2014). *Fundamentals of electric power engineering: from electromagnetics to power systems*. John Wiley & Sons.
- [28] Cezar, G., Rajagopal, R., and Zhang, B. (2015). Stability of interconnected dc converters. In *IEEE 54th Annual Conference on Decision and Control (CDC)*, pages 9–14.
- [29] Chandorkar, M., Divan, D., and Adapa, R. (1993). Control of parallel connected inverters in standalone AC supply systems. *IEEE Transactions on Industry Applications*, 29(1):136–143.
- [30] Chen, J. and Chu, C. (1995). Combination voltage-controlled and current-controlled PWM inverters for UPS parallel operation. *IEEE Transactions on Power Electronics*, 10(5):547–558.
- [31] Chiang, S. J., Yen, C. Y., and Chang, K. T. (2001). A multimodule parallelable series-connected PWM voltage regulator. *IEEE Transactions on Industrial Electronics*, 48(3):506–516.
- [32] Colombino, M., Groß, D., and Dörfler, F. (2017). Global phase and voltage synchronization for power inverters: a decentralized consensus-inspired approach. In *2017 IEEE 56th Annual Conference on Decision and Control (CDC)*, pages 5690–5695.
- [33] Curi, S., Groß, D., and Dörfler, F. (2017). Control of low-inertia power grids: A model reduction approach. In *2017 IEEE 56th Annual Conference on Decision and Control (CDC)*, pages 5708–5713.
- [34] Cvetkovic, I., Boroyevich, D., Burgos, R., Li, C., and Mattavelli, P. (2015). Modeling and control of grid-connected voltage-source converters emulating isotropic and anisotropic synchronous machines. In *2015 IEEE 16th Workshop on Control and Modeling for Power Electronics (COMPEL)*, pages 1–5.
- [35] Dash, P. and Kazerani, M. (2011). Dynamic modeling and performance analysis of a grid-connected current-source inverter-based photovoltaic system. *Sustainable Energy, IEEE Transactions on*, 2(4):443–450.
- [36] De Abreu, N. M. M. (2007). Old and new results on algebraic connectivity of graphs. *Linear algebra and its applications*, 423(1):53–73.
- [37] De Persis, C., Weitenberg, E., and Dörfler, F. (2018). A power consensus algorithm for DC microgrids. *Automatica*, 89:364 – 375.
- [38] Desoer, C. A. and Vidyasagar, M. (2009). *Feedback Systems: Input-Output Properties*. SIAM.
- [39] Distribution System Analysis Subcommittee. IEEE 13 Node Test Feeder. *IEEE Power Engineering Society, Power System Analysis, Computing and Economics Committee*.

- [40] Dörfler, F. and Bullo, F. (2013). Kron reduction of graphs with applications to electrical networks. *IEEE Transactions on Circuits and Systems I: Regular Papers*, 60(1):150–163.
- [41] Dörfler, F., Simpson-Porco, J., and Bullo, F. (2014). Plug-and-play control and optimization in microgrids. In *Decision and Control (CDC), 2014 IEEE 53rd Annual Conference on*, pages 211–216.
- [42] Dörfler, F., Simpson-Porco, J. W., and Bullo, F. (2016). Breaking the hierarchy: Distributed control and economic optimality in microgrids. *IEEE Transactions on Control of Network Systems*, 3(3):241–253.
- [43] Dreidy, M., Mokhlis, H., and Mekhilef, S. (2017). Inertia response and frequency control techniques for renewable energy sources: A review. *Renewable and Sustainable Energy Reviews*, 69:144 – 155.
- [44] Du, Y. and Liao, Y. (2012). On-line estimation of transmission line parameters, temperature and sag using PMU measurements. *Electric Power Systems Research*, 93:39 – 45.
- [45] Duindam, V., Macchelli, A., and Stramigioli, S. (2009). *Modeling and control of complex physical systems: The port-Hamiltonian approach*. Springer Verlag.
- [46] Ekanayake, J. and Jenkins, N. (2004). Comparison of the response of doubly fed and fixed-speed induction generator wind turbines to changes in network frequency. *IEEE Transactions on Energy Conversion*, 19(4):800–802.
- [47] Emadi, A., Khaligh, A., Rivetta, C. H., and Williamson, G. A. (2006). Constant power loads and negative impedance instability in automotive systems: definition, modeling, stability, and control of power electronic converters and motor drives. *IEEE Transactions on Vehicular Technology*, 55(4):1112–1125.
- [48] European Network of Transmission System Operators for Electricity (ENTSOE) (2016). Frequency Stability Evaluation Criteria for the Synchronous Zone of Continental Europe - Requirements and impacting factors. *Distribution System Analysis Subcommittee*.
- [49] Ferguson, J., Middleton, R. H., and Donaire, A. (2015). Disturbance rejection via control by interconnection of port-Hamiltonian systems. In *2015 IEEE 54th Annual Conference on Decision and Control (CDC)*, pages 507–512.
- [50] Fiaz, S., Zonetti, D., Ortega, R., Scherpen, J., and van der Schaft, A. (2013). A port-Hamiltonian approach to power network modeling and analysis. *European Journal of Control*, 19(6):477 – 485.
- [51] Franceschelli, M., Gasparri, A., Giua, A., and Seatzu, C. (2009). Decentralized Laplacian eigenvalues estimation for networked multi-agent systems. In *Proceedings of the 48th IEEE Conference on Decision and Control, held jointly with the 28th Chinese Control Conference. CDC/CCC 2009.*, pages 2717–2722.

- [52] Godsil, C. and Royle, G. (2001). *Graphs*, volume 207. Springer, New York, NY.
- [53] Grainger, J. J., Stevenson, W. D., and Chang, G. W. (1994). *Power system analysis*, volume 621. McGraw-Hill New York.
- [54] Grigsby, L. L. (2016). *Power system stability and control*. CRC press.
- [55] Grone, R., Merris, R., and Sunder, V. S. (1990). The Laplacian spectrum of a graph. *SIAM Journal on Matrix Analysis and Applications*, 11(2):218–238.
- [56] Guerrero, J., Hang, L., and Uceda, J. (2008). Control of distributed uninterruptible power supply systems. *IEEE Transactions on Industrial Electronics*, 55(8):2845–2859.
- [57] Guerrero, J., Vasquez, J., Matas, J., Castilla, M., and de Vicuna, L. (2009). Control strategy for flexible microgrid based on parallel line-interactive UPS systems. *IEEE Transactions on Industrial Electronics*, 56(3):726–736.
- [58] Guerrero, J. M., Chandorkar, M., Lee, T., and Loh, P. C. (2013). Advanced control architectures for intelligent microgrids Part I: Decentralized and hierarchical control. *IEEE Transactions on Industrial Electronics*, 60(4):1254–1262.
- [59] Guerrero, J. M., De Vicuna, L. G., Matas, J., Castilla, M., and Miret, J. (2005). Output impedance design of parallel-connected UPS inverters with wireless load-sharing control. *IEEE Transactions on industrial electronics*, 52(4):1126–1135.
- [60] Guerrero, J. M., Matas, J., de Vicuna, L. G., Castilla, M., and Miret, J. (2007). Decentralized control for parallel operation of distributed generation inverters using resistive output impedance. *IEEE Transactions on industrial electronics*, 54(2):994–1004.
- [61] Guerrero, J. M., Matas, J., De Vicuna, L. G. D. V., Castilla, M., and Miret, J. (2006). Wireless-control strategy for parallel operation of distributed-generation inverters. *IEEE Transactions on Industrial Electronics*, 53(5):1461–1470.
- [62] Guerrero, J. M., Vasquez, J. C., Matas, J., de Vicuna, L. G., and Castilla, M. (2011). Hierarchical control of droop-controlled AC and DC microgrids; a general approach toward standardization. *IEEE Transactions on Industrial Electronics*, 58(1):158–172.
- [63] Hamzeh, M., Karimi, H., and Mokhtari, H. (2012). A new control strategy for a multi-bus mv microgrid under unbalanced conditions. *IEEE Transactions on Power Systems*, 27(4):2225–2232.
- [64] Hatziargyriou, N. (2014). *Microgrids: Architectures and Control*. Wiley.
- [65] He, J. and Li, Y. W. (2012). Generalized closed-loop control schemes with embedded virtual impedances for voltage source converters with LC or LCL filters. *IEEE Transactions on Power Electronics*, 27(4):1850–1861.

- [66] Hines, G. H., Arcak, M., and Packard, A. K. (2011). Equilibrium-independent passivity: A new definition and numerical certification. *Automatica*, 47(9):1949 – 1956.
- [67] Horn, R. A. and Johnson, C. R. (2012). *Matrix Analysis*. Cambridge university press.
- [68] Jayawardhana, B., Ortega, R., García-Canseco, E., and Castaños, F. (2007). Passivity of nonlinear incremental systems: Application to PI stabilization of nonlinear RLC circuits. *Systems & Control Letters*, 56(9):618–622.
- [69] Jouini, T., Arghir, C., and Dörfler, F. (2016). Grid-friendly matching of synchronous machines by tapping into the DC storage. *IFAC-PapersOnLine*, 49(22):192–197.
- [70] Khalil, H. (2002). *Nonlinear systems*, volume 3. Prentice hall Englewood Cliffs, NJ.
- [71] Kim, J., Guerrero, J. M., Rodriguez, P., Teodorescu, R., and Nam, K. (2011). Mode adaptive droop control with virtual output impedances for an inverter-based flexible AC microgrid. *IEEE Transactions on Power Electronics*, 26(3):689–701.
- [72] Kron, G. (1939). *Tensor Analysis of Networks*. New York: Wiley.
- [73] Kuh, E. S. and Rohrer, R. A. (1965). The state-variable approach to network analysis. *Proceedings of the IEEE*, 53(7):672–686.
- [74] Li, Y. W. and Kao, C. N. (2009). An accurate power control strategy for power-electronics-interfaced distributed generation units operating in a low-voltage multibus microgrid. *IEEE Transactions on Power Electronics*, 24(12):2977–2988.
- [75] Lorenzo, P. D. and Barbarossa, S. (2014). Distributed estimation and control of algebraic connectivity over random graphs. *IEEE Transactions on Signal Processing*, 62(21):5615–5628.
- [76] Lu, L. Y. and Chu, C. C. (2015). Consensus-based droop control synthesis for multiple dics in isolated micro-grids. *IEEE Transactions on Power Systems*, 30(5):2243–2256.
- [77] Machado, J. E., Griñó, R., Barabanov, N., Ortega, R., and Polyak, B. (2017). On existence of equilibria of multi-port linear AC networks with constant-power loads. *IEEE Transactions on Circuits and Systems I: Regular Papers*, 64(10):2772–2782.
- [78] Machowski, J., Bialek, J., and Bumby, J. (2008). *Power System Dynamics: Stability and Control*. Wiley, 2nd edition.
- [79] Mahmood, H., Michaelson, D., and Jiang, J. (2015). Accurate reactive power sharing in an islanded microgrid using adaptive virtual impedances. *IEEE Transactions on Power Electronics*, 30(3):1605–1617.
- [80] Majumder, R., Chaudhuri, B., Ghosh, A., Majumder, R., Ledwich, G., and Zare, F. (2010). Improvement of stability and load sharing in an autonomous microgrid using supplementary droop control loop. *IEEE Transactions on Power Systems*, 25(2):796–808.

- [81] Marx, D., Magne, P., Nahid-Mobarakeh, B., Pierfederici, S., and Davat, B. (2012). Large signal stability analysis tools in DC power systems with constant power loads and variable power loads; a review. *IEEE Transactions on Power Electronics*, 27(4):1773–1787.
- [82] Maschke, B., Ortega, R., and van der Schaft, A. J. (2000). Energy-based Lyapunov functions for forced Hamiltonian systems with dissipation. *IEEE Transactions on Automatic Control*, 45(8):1498–1502.
- [83] Maschke, B. and van der Schaft, A. (1992). Port-controlled Hamiltonian systems: Modeling origins and system-theoretic properties. In *IFAC symposium on nonlinear control systems*, pages 282–288, Bordeaux, France.
- [84] Matas, J., Castilla, M., d. Vicua, L. G., Miret, J., and Vasquez, J. C. (2010). Virtual impedance loop for droop-controlled single-phase parallel inverters using a second-order general-integrator scheme. *IEEE Transactions on Power Electronics*, 25(12):2993–3002.
- [85] Merikoski, J. K. and Kumar, R. (2004). Inequalities for spreads of matrix sums and products. In *Applied Mathematics E-Notes*, volume 4, pages 150–159.
- [86] Mesbahi, M. and Egerstedt, M. (2010). *Graph theoretic methods in multi-agent networks*. Princeton University Press.
- [87] Mohamed, Y. A. R. I. and El-Saadany, E. F. (2008). Adaptive decentralized droop controller to preserve power sharing stability of paralleled inverters in distributed generation microgrids. *IEEE Transactions on Power Electronics*, 23(6):2806–2816.
- [88] Mohar, B. (1992). Laplace eigenvalues of graphs - a survey. *Discrete Mathematics*, 109(13):171 – 183.
- [89] Monshizadeh, N., Monshizadeh, P., Ortega, R., and van der Schaft, A. (2017a). Conditions on shifted passivity of port-Hamiltonian systems. *System & Control Letters*. under review.
- [90] Monshizadeh, N. and Persis, C. D. (2015). Output agreement in networks with unmatched disturbances and algebraic constraints. In *2015 54th IEEE Conference on Decision and Control (CDC)*, pages 4196–4201.
- [91] Monshizadeh, N. and Persis, C. D. (2017). Agreeing in networks: Unmatched disturbances, algebraic constraints and optimality. *Automatica*, 75:63 – 74.
- [92] Monshizadeh, P., De Persis, C., Monshizadeh, N., and van der Schaft, A. (2016). A communication-free master-slave microgrid with power sharing. In *American Control Conference (ACC), 2016*, pages 3564–3569.
- [93] Monshizadeh, P., De Persis, C., Monshizadeh, N., and van der Schaft, A. (2016). Nonlinear analysis of an improved swing equation. In *IEEE 55th Conference on Decision and Control (CDC)*, pages 4116–4121.

- [94] Monshizadeh, P., E. Machado, J., Ortega, R., and van der Schaft, A. (2018a). Power-controlled Hamiltonian systems: Application to electrical systems with constant power loads. *Automatica*. under review.
- [95] Monshizadeh, P., Monshizadeh, N., De Persis, C., and van der Schaft, A. (2018b). Output impedance diffusion into lossy power lines. *IEEE Transactions on Power Systems*. provisionally accepted.
- [96] Monshizadeh, P., Persis, C. D., Stegink, T., Monshizadeh, N., and van der Schaft, A. (2017b). Stability and frequency regulation of inverters with capacitive inertia. In *2017 IEEE 56th Annual Conference on Decision and Control (CDC)*, pages 5696–5701.
- [97] Morren, J., Pierik, J., and de Haan, S. W. (2006). Inertial response of variable speed wind turbines. *Electric Power Systems Research*, 76(11):980 – 987.
- [98] Morstyn, T., Hredzak, B., and Agelidis, V. G. (2015). Distributed cooperative control of microgrid storage. *IEEE Transactions on Power Systems*, 30(5):2780–2789.
- [99] Moslemi, R., Mohammadpour, J., and Mesbahi, A. (2016). A modified droop control for reactive power sharing in large microgrids with meshed topology. In *2016 American Control Conference (ACC)*, pages 6779–6784.
- [100] Münz, U. and Metzger, M. (2014). Voltage and angle stability reserve of power systems with renewable generation. *IFAC Proceedings Volumes*, 47(3):9075–9080.
- [101] Natarajan, V. and Weiss, G. (2014a). Almost global asymptotic stability of a constant field current synchronous machine connected to an infinite bus. In *2014 IEEE 53rd Annual Conference on Decision and Control (CDC)*, pages 3272–3279.
- [102] Natarajan, V. and Weiss, G. (2014b). A method for proving the global stability of a synchronous generator connected to an infinite bus. In *Electrical Electronics Engineers in Israel (IEEEI), 2014 IEEE 28th Convention of*, pages 1–5.
- [103] Natarajan, V. and Weiss, G. (2017). Synchronverters with better stability due to virtual inductors, virtual capacitors, and anti-windup. *IEEE Transactions on Industrial Electronics*, 64(7):5994–6004.
- [104] Nesterov, Y. (2013). *Introductory Lectures on Convex Optimization: A Basic Course*, volume 87. Springer Science & Business Media.
- [105] Nielsen, F. (2010). *Legendre Transformation and Information Geometry*. CIG-MEMO2.
- [106] Ortega, R., Monshizadeh, N., Monshizadeh, P., Bazylev, D., and Pyrkin, A. (2018). Permanent magnet synchronous motors are globally asymptotically stabilizable with PI current control. *Automatica*. to appear.

- [107] Ortega, R., Perez, J. A. L., Nicklasson, P. J., and Sira-Ramirez, H. (2013). *Passivity-based Control of Euler-Lagrange Systems: Mechanical, Electrical and Electromechanical Applications*. Springer Science & Business Media.
- [108] Paquette, A., Reno, M., Harley, R., and Divan, D. (2014). Sharing transient loads : Causes of unequal transient load sharing in islanded microgrid operation. *Industry Applications Magazine, IEEE*, 20(2):23–34.
- [109] Pavlov, A. and Marconi, L. (2008). Incremental passivity and output regulation. *Systems & Control Letters*, 57(5):400–409.
- [110] Persis, C. D. and Monshizadeh, N. (2018). Bregman storage functions for microgrid control. *IEEE Transactions on Automatic Control*, 63(1):53–68.
- [111] Persis, C. D., Monshizadeh, N., Schiffer, J., and Dörfler, F. (2016). A Lyapunov approach to control of microgrids with a network-preserved differential-algebraic model. In *2016 IEEE 55th Conference on Decision and Control (CDC)*, pages 2595–2600.
- [112] Pogromsky, A. Y. (1998). Passivity based design of synchronizing systems. *International journal of Bifurcation and Chaos*, 8(02):295–319.
- [113] Reigosa, D., Arbolea, P., Gonzalez-Moran, C., and Gomez-Aleixandre, J. (2009). An improved control scheme based in droop characteristic control for microgrid converters. In *Electrical Machines and Systems, 2009. ICEMS 2009. International Conference on*, pages 1–6.
- [114] Rocabert, J., Luna, A., Blaabjerg, F., and Rodriguez, P. (2012). Control of power converters in AC microgrids. *Power Electronics, IEEE Transactions on*, 27(11):4734–4749.
- [115] Ryu, E. K. and Boyd, S. (2016). Primer on monotone operator methods. *Applied and Computational Mathematics*, 15(1):3–43.
- [116] Sanchez, S., Ortega, R., Griñó, R., Bergna, G., and Molinas, M. (2014). Conditions for existence of equilibria of systems with constant power loads. *IEEE Transactions on Circuits and Systems I: Regular Papers*, 61(7):2204–2211.
- [117] Schiffer, J., Fridman, E., Ortega, R., and Raisch, J. (2016a). Stability of a class of delayed port-Hamiltonian systems with application to microgrids with distributed rotational and electronic generation. *Automatica*, 74:71 – 79.
- [118] Schiffer, J., Ortega, R., Astolfi, A., Raisch, J., and Sezi, T. (2014). Conditions for stability of droop-controlled inverter-based microgrids. *Automatica*, 50(10):2457 – 2469.
- [119] Schiffer, J., Seel, T., Raisch, J., and Sezi, T. (2016b). Voltage stability and reactive power sharing in inverter-based microgrids with consensus-based distributed voltage control. *IEEE Transactions on Control Systems Technology*, 24(1):96–109.

- [120] Shahidehpour, M. and Khodayar, M. (2013). Cutting campus energy costs with hierarchical control: The economical and reliable operation of a microgrid. *Electrification Magazine, IEEE*, 1(1):40–56.
- [121] Shi, D., Tylavsky, D. J., Koellner, K. M., Logic, N., and Wheeler, D. E. (2011). Transmission line parameter identification using PMU measurements. *European Transactions on Electrical Power*, 21(4):1574–1588.
- [122] Shintai, T., Miura, Y., and Ise, T. (2014). Oscillation damping of a distributed generator using a virtual synchronous generator. *IEEE Transactions on Power Delivery*, 29(2):668–676.
- [123] Simpson-Porco, J. W. (2018). Equilibrium-independent dissipativity with quadratic supply rates. *IEEE Transactions on Automatic Control*.
- [124] Simpson-Porco, J. W., Dörfler, F., and Bullo, F. (2013). Synchronization and power sharing for droop-controlled inverters in islanded microgrids. *Automatica*, 49(9):2603 – 2611.
- [125] Simpson-Porco, J. W., Dörfler, F., and Bullo, F. (2015). On resistive networks of constant-power devices. *IEEE Transactions on Circuits and Systems II: Express Briefs*, 62(8):811–815.
- [126] Simpson-Porco, J. W., Dörfler, F., and Bullo, F. (2017). Voltage stabilization in microgrids via quadratic droop control. *IEEE Transactions on Automatic Control*, 62(3):1239–1253.
- [127] Sinha, M., Dörfler, F., Johnson, B. B., and Dhople, S. V. (2016). Synchronization of liénard-type oscillators in uniform electrical networks. In *American Control Conference (ACC), 2016*, pages 4311–4316.
- [128] Soni, N., Doolla, S., and Chandorkar, M. C. (2013). Improvement of transient response in microgrids using virtual inertia. *IEEE Transactions on Power Delivery*, 28(3):1830–1838.
- [129] Stan, G. and Sepulchre, R. (2007). Analysis of interconnected oscillators by dissipativity theory. *IEEE Transactions on Automatic Control*, 52(2):256–270.
- [130] Stegink, T., Persis, C. D., and van der Schaft, A. (2017). A unifying energy-based approach to stability of power grids with market dynamics. *IEEE Transactions on Automatic Control*, 62(6):2612–2622.
- [131] Susetyo, M. E., Hariyanto, N., Rizqiawan, A., and Sitompul, S. A. (2017). Droop control implementation on hybrid microgrid PV-diesel-battery. In *2017 International Conference on High Voltage Engineering and Power Systems (ICHVEPS)*, pages 295–300.
- [132] Teixeira, A., Paridari, K., Sandberg, H., and Johansson, K. H. (2015). Voltage control for interconnected microgrids under adversarial actions. In *2015 IEEE 20th Conference on Emerging Technologies & Factory Automation (ETFA)*, pages 1–8. IEEE.
- [133] Tielens, P. and Hertem, D. V. (2016). The relevance of inertia in power systems. *Renewable and Sustainable Energy Reviews*, 55:999 – 1009.

- [134] Trip, S., Bürger, M., and De Persis, C. (2016). An internal model approach to (optimal) frequency regulation in power grids with time-varying voltages. *Automatica*, 64:240–253.
- [135] Tsolas, N., Arapostathis, A., and Varaiya, P. (1985). A structure preserving energy function for power system transient stability analysis. *IEEE Transactions on Circuits and Systems*, 32(10):1041–1049.
- [136] Ulbig, A., Borsche, T. S., and Andersson, G. (2014). Impact of low rotational inertia on power system stability and operation. *IFAC Proceedings Volumes*, 47(3):7290–7297.
- [137] Van, T. V., Visscher, K., Diaz, J., Karapanos, V., Woyte, A., Albu, M., Bozelie, J., Loix, T., and Federenciuc, D. (2010). Virtual synchronous generator: An element of future grids. In *IEEE PES Innovative Smart Grid Technologies Conference Europe (ISGT Europe)*, pages 1–7.
- [138] van der Schaft, A. (2010). Characterization and partial synthesis of the behavior of resistive circuits at their terminals. *Systems & Control Letters*, 59(7):423 – 428.
- [139] van der Schaft, A. (2017). The flow equations of linear resistive electrical networks. *arXiv preprint arXiv:1712.10263*.
- [140] van der Schaft, A. (2017). *L₂-Gain and Passivity Techniques in Nonlinear Control*. 3rd Revised and Enlarged Edition (1st edition 1996, 2nd edition 2000), Springer Communications and Control Engineering series, Springer-International.
- [141] van der Schaft, A. and Jeltsema, D. (2014). *Port-Hamiltonian Systems Theory: An Introductory Overview*. Now Foundations and Trends.
- [142] van der Schaft, A. and Maschke, B. (2013). Port-Hamiltonian systems on graphs. *SIAM Journal on Control and Optimization*, 51(2):906–937.
- [143] van der Schaft, A. and Stegink, T. (2016). Perspectives in modeling for control of power networks. *Annual Reviews in Control*, 41:119–132.
- [144] van Wesenbeeck, M. P. N., de Haan, S. W. H., Varela, P., and Visscher, K. (2009). Grid tied converter with virtual kinetic storage. In *IEEE Bucharest PowerTech*, pages 1–7.
- [145] Vandoorn, T. L., De Kooning, J. D., Meersman, B., Guerrero, J. M., and Vandevelde, L. (2012a). Automatic power-sharing modification of p/v droop controllers in low-voltage resistive microgrids. *IEEE Transactions on Power Delivery*, 27(4):2318–2325.
- [146] Vandoorn, T. L., Meersman, B., Degroote, L., Renders, B., and Vandevelde, L. (2011). A control strategy for islanded microgrids with DC-link voltage control. *IEEE Transactions on Power Delivery*, 26(2):703–713.
- [147] Vandoorn, T. L., Meersman, B., Kooning, J. D. M. D., and Vandevelde, L. (2012b). Analogy between conventional grid control and islanded microgrid control based on a global DC-link voltage droop. *IEEE Transactions on Power Delivery*, 27(3):1405–1414.

- [148] Venezian, E. and Weiss, G. (2016). A warning about the use of reduced models of synchronous generators. In *Science of Electrical Engineering (ICSEE), IEEE International Conference on the*, pages 1–5.
- [149] Verriest, E. I. and Willems, J. C. (2010). The behavior of linear time invariant RLC circuits. In *49th IEEE Conference on Decision and Control (CDC)*, pages 7754–7758.
- [150] Vilathgamuwa, D. M., Loh, P. C., and Li, Y. (2006). Protection of microgrids during utility voltage sags. *IEEE Transactions on Industrial Electronics*, 53(5):1427–1436.
- [151] Washom, B., Dilliot, J., Weil, D., Kleissl, J., Balac, N., Torre, W., and Richter, C. (2013). Ivory tower of power: Microgrid implementation at the university of california, san diego. *IEEE Power and Energy Magazine*, 11(4):28–32.
- [152] Weiss, G. and Venezian, E. (2017). Stability analysis for coupled synchronous generators with virtual friction. In *Digital Signal Processing (DSP), 2017 22nd International Conference on*, pages 1–5.
- [153] Willems, J. (1972). Dissipative dynamical systems Part I : General Theory. *Archive for Rational Mechanics and Analysis*, 45:321–351.
- [154] Yao, W., Chen, M., Matas, J., Guerrero, J. M., and Qian, Z. M. (2011). Design and analysis of the droop control method for parallel inverters considering the impact of the complex impedance on the power sharing. *IEEE Transactions on Industrial Electronics*, 58(2):576–588.
- [155] Zhao, X., Zhou, H., Shi, D., Zhao, H., Jing, C., and Jones, C. (2015). On-line PMU-based transmission line parameter identification. *CSEE Journal of Power and Energy Systems*, 1(2):68–74.
- [156] Zhao, Z., Zheng, F., Gao, J., and Xu, L. (1995). A dynamic on-line parameter identification and full-scale system experimental verification for large synchronous machines. *IEEE Transactions on Energy Conversion*, 10(3):392–398.
- [157] Zhong, Q.-C. and Hornik, T. (2012). *Control of power inverters in renewable energy and smart grid integration*, volume 97. John Wiley & Sons.
- [158] Zhong, Q. C., Nguyen, P. L., Ma, Z., and Sheng, W. (2014). Self-synchronized synchronverters: Inverters without a dedicated synchronization unit. *IEEE Transactions on Power Electronics*, 29(2):617–630.
- [159] Zhong, Q. C. and Weiss, G. (2011). Synchronverters: Inverters that mimic synchronous generators. *IEEE Transactions on Industrial Electronics*, 58(4):1259–1267.
- [160] Zhou, J. and Ohsawa, Y. (2009). Improved swing equation and its properties in synchronous generators. *Circuits and Systems I: Regular Papers, IEEE Transactions on*, 56(1):200–209.

Summary

This thesis addresses several problems related to modeling and control of power systems in microgrids, as summarized in the following lines.

First, a method is established to measure the effect of the addition of output impedances on the inductivity of a (homogeneous) RL network. With this addition, the overall network is comprised of lines with different inductivity ratio $\frac{R}{L}$. We define a measure to evaluate the inductivity behavior of the overall network. Then we compute this measure for homogeneous networks with RL output impedances, and conclude that the more connected the network is, the more output impedances diffuse into the network. Numerical simulations show that optimizing the effect of output impedances, based on the proposed measure, can lead to a better performance of droop-controlled power converters.

Second, we propose a master-slave architecture for microgrids, in which the source with the highest generation capacity acts as the master. The master increases/decreases the generated frequency according to a decrease/increase in the load respectively. The rest of the sources measure this change in frequency, and proportionally inject power into the network. It is shown that this system is stable and remains synchronized for all times. In addition, power sharing can be achieved among the sources, without the need to any communication network.

Third, we aim at finding a model for synchronous generators which, compared to the swing equation, predicts better the behavior of the system, and yet it is easy to use. For this purpose, we eliminate a simplifying assumption, namely the assumption of constant angular momentum, in deriving the swing equation, and obtain an *improved swing* model. Incremental passivity properties of this model are shown, which paves the path for a controller design. The stability of a synchronous generator modeled with the improved swing equation is then shown in the cases where it is connected to a constant power load and an infinite bus.

As a fourth problem, we look into the problem of *lack of inertia* in networks with dominant renewable energies. First we model the power converters with large capacitors acting as inertia. Then we carry out stability and synchronization analysis for a network of these converters. We show that, by using appropriate controllers, frequency can be regulated to its nominal value.

Fifth, we investigate the *shifted* passivity property of port-Hamiltonian systems with strictly convex Hamiltonian. We establish conditions, in terms of monotonicity of suitably constructed

functions, under which the system is shifted passive. These conditions naturally guarantee stability of forced equilibria of pH systems. As a case study, we apply this results to the sixth-order model of a synchronous generator connected to a resistor.

Finally, a subclass of port-Hamiltonian systems is developed in this thesis that can be described as *power-controlled* Hamiltonian systems, where the control input or disturbance is acting on the *power* entering the system. Consequently, we investigate the shifted pasivity of such pH systems, and characterize a region of attraction for stability of the equilibrium. An interesting application of the proposed model is to verify stability of a DC circuit connected to a constant power load.

Samenvatting

In dit proefschrift worden verschillende problemen in de modelvorming en regeling van vermogenssystemen in microgrids bestudeerd.

Ten eerste is een methode verkregen waarmee het effect van het toevoegen van uitgangsimpedanties op de inductiviteit van een (homogeen) RL netwerk kan worden gemeten. Als gevolg van deze toevoeging ontstaan in het gehele netwerk transmissielijnen met verschillende inductiviteitsratio R/L . We hebben een maat gedefinieerd waarmee het inductieve gedrag van het gehele netwerk geëvalueerd kan worden. Vervolgens hebben we deze maat berekend voor homogene netwerken met RL uitgangsimpedanties, en concluderen dat hoe meer het netwerk verbonden is, hoe meer uitgangsimpedanties zich in het netwerk verspreiden. Numerieke simulaties tonen aan dat, gebaseerd op de voorgestelde maat, het optimaliseren van het effect van uitgangsimpedanties kan leiden tot een betere prestatie van *droop-controlled* vermogensomzetters.

Ten tweede wordt een master-slave architectuur voor microgrids voorgesteld waarin de bron met de hoogste generatiecapaciteit fungeert als de master. De master verhoogt/verlaagt de gegenereerde frequentie in overeenstemming met een toename/afname in de vermogenslast. De rest van de bronnen meten deze verandering in frequentie, en injecteren proportioneel aan deze verandering vermogen in het netwerk. Er wordt aangetoond dat dit systeem stabiel is en gesynchroniseerd blijft op ieder tijdstip. Daarbovenop kan vermogensdeling tussen de bronnen worden bereikt zonder dat daar een communicatienetwerk voor nodig is.

Ten derde hebben we getracht een model te vinden voor synchrone generatoren dat, vergeleken met de swing equation, het systeemgedrag beter voorspelt en tevens gemakkelijk in het gebruik is. Om dit te bereiken elimineren we een vereenvoudigende aanname, namelijk de aanname van constant impulsmoment, in het afleiden van de swing equation waarmee een verbeterd swing model wordt verkregen. Voor dit model worden verschoven passiviteits eigenschappen aangetoond, waarmee de weg is vrijgemaakt voor regelaarontwerp. Vervolgens wordt stabiliteit van een synchrone generator gemodelleerd met de verbeterde swing equation aangetoond voor situaties waarin deze verbonden is met een constante vermogenslast en een oneindige bus.

Het vierde probleem waarnaar we hebben gekeken is het gebrek aan traagheid in netwerken

met dominante renewable energies. Eerst modelleren we de vermogensomzeters met grote condensatoren die de rol van traagheid vervullen. Vervolgens voeren we een stabiliteits- en synchronisatie-analyse uit voor een netwerk van deze omzeters. We tonen aan dat door het gebruik van geschikte regelaars de frequentie kan worden geregeld naar de nominale waarde.

Ten vijfde hebben we de verschoven passiviteitseigenschap van poort-Hamiltonse (pH) systemen met een strikt convexe Hamiltoniaan onderzocht. We hebben voorwaarden verkregen waaronder het systeem verschoven apssief is in termen van monotoniciteit van passend geconstrueerde functies. Deze voorwaarden garanderen uit zichzelf stabiliteit van opgelegde evenwichten van pH systemen. In een case study passen we deze resultaten toe op een zesde-orde model van een synchrone generator verbonden met een weerstand.

Ten slotte is in dit proefschrift een sub-klasse van poort-Hamiltonse systemen ontwikkeld welke kan worden aangeduid als vermogens-geregelde Hamiltonse systemen. Hierbij grijpt de ingang van de regelaar of de verstoring aan op het ingaande vermogen van het systeem. Vervolgens hebben we de verschoven passiviteit van zulke pH systemen onderzocht, en een gebied van attractie gekarakteriseerd voor de stabiliteit van het evenwicht. Een interessante toepassing van het voorgestelde model is het verifiren van stabiliteit van een gelijkstroom elektrisch netwerk verbonden met een constante vermogenslast.